Distribution Mechanism of Solid Particles in Al-Based Composite by Severe Plastic Deformation

Al 基金属複合材料への巨大ひずみ加工に伴う固体粒子の分布機構

By

Duraisamy Sarath Babu

ドゥライサミ サラトゥ バブ

Supervisors

Prof. Yoshimi Watanabe

Assoc. Prof. Hisashi Sato

Thesis submitted for the degree of Doctor of Engineering,

Department of Physical Science and Engineering,

Graduate School of Engineering,

Nagoya Institute of Technology,

Nagoya, Japan.

2020

Declaration of Originality

I hereby declare that the research recorded in this thesis has been carried out by me and the thesis was accomplished and originated entirely by myself in the Graduate School of Engineering, Department of Physical Science and Engineering at Nagoya Institute of Technology.

Duraisamy Sarath Babu

Abstract

When the Al-based composite containing solid particles is deformed by severe plastic deformation (SPD) method, the shape, the size and the spatial distributions of solid particles in the composite changes drastically. However, the distribution mechanism of solid particle by SPD for the Al-based composite is not clear. This is because that previous studies concerning with SPD for metal-based composite have focused on grain refinement and its mechanical properties. In this thesis, fragmentation and distribution mechanisms of solid particles by SPD for the Al-based composite are investigated. Especially, as a model material of the Al-based composite, Al-Al_3Ti composite containing Al_3Ti intermetallic particles is used.

Initially, fragmentation mechanism of a platelet Al_3Ti particle in an Al-Al_3Ti composite during compression testing is investigated using 3-dimensional (3D) microstructural observation and crystallographic analysis. The Al-Al_3Ti composite comprises platelet Al_3Ti particles in an α-Al matrix is deformed by compression. To clarify the fragmentation process of a platelet Al_3Ti particle, the same area microstructural observation is performed. Based on the obtained results, it is found that the fracture surface of a platelet Al_3Ti particle is $\{112\}_{Al_3Ti}$. This means that cracks initiated in the platelet Al_3Ti particle are preferentially propagated along the twin boundary of $\{112\}_{Al_3Ti}$ after deformation twinning. It is concluded that the fragmentation of platelet Al_3Ti particle in the Al-Al_3Ti composite preferentially occurs at twin boundary after deformation twinning.

Furthermore, changes in the spatial distribution of the fragmented Al_3Ti particles

in an Al-Al_3Ti composite during equal-channel angular pressing (ECAP) are investigated by Morisita index, I_δ. ECAP is performed under the processing routes of A and B_c up to 8 passes and Al_3Ti particles size are gradually decreases as increasing the number of ECAP passes. The Al_3Ti particles in the specimen deformed using route A are aligned along the deformation axis, while particles in the specimens deformed with route B_c are formed into groups. Evaluation of the spatial distributions of Al_3Ti particles in the Al-Al_3Ti composite based on the I_δ results indicate that both processing routes generated aggregate distributions. After 5 passes using routes A and B_c, the homogeneity of the spatial distribution is increased. During 8 passes of ECAP under route B_c, the Al-Al_3Ti composite shows the more homogenous distribution than route A. These variations in the spatial distributions of the Al_3Ti particles can be explained by the occurrence of the material flow of the α-Al matrix during ECAP using routes A and B_c. Although, spatial distributions of spherical Al_3Ti particles in an Al-Al_3Ti composite by ECAP is investigated and spherical Al_3Ti particles are not fragmented by ECAP. It was found that changes in the spatial distributions of spherical Al_3Ti particles in an Al-Al_3Ti composite by ECAP depend on the particle size. In addition, stress concentration develops more easily for specimens with the smaller size particles compare to the specimens which have larger size particles. Hence, the spatial distributions and stress concentration are depending on the particles size of the spherical Al_3Ti particles in an Al-Al_3Ti composite.

Moreover, effects of particles shape on the fragmentation behavior and spatial distribution of Al_3Ti particles in ECAPed Al-Al_3Ti composite are investigated. The three different shape particles such as spherical, polyhedral and granular Al_3Ti particles in Al-Al_3Ti composite are used. Changes in the spatial distributions of fragmented spherical,

polyhedral and granular Al_3Ti particles in deformed Al-Al_3Ti composite depend on the particle size and spatial distribution of Al_3Ti particles is controlled by the material flow of the α-Al matrix. Finally, fragmentation of Al_3Ti particles occurs by stress concentration around the Al_3Ti particles and fragmentation behavior depends on the Al_3Ti particles shape.

Consequently, the fragmentation behavior of platelet Al_3Ti particles in Al-Al_3Ti composite by multi-directional forging (MDF), symmetric rolling (SR) and asymmetric rolling (ASR) are investigated. These SPD processes can be applied easily as industrial processing comparing with ECAP. The platelet Al_3Ti particles in Al-Al_3Ti composites are fragmented by MDF, SR and ASR. The results show that compression and rolling can be used to modify the distribution of platelet Al_3Ti particles in Al-Al_3Ti composite. It is found that ASR can modify the distribution of platelet Al_3Ti particles more severely as compare to SR and MDF. Distribution depending on the material flow of the α-Al matrix in the composites.

Grain refining performance of Al-Al_3Ti composite containing platelet Al_3Ti particles by SPD is investigated with the use of as-cast Al. It is well known that Al_3Ti particles in Al-Al_3Ti composite play the role of good heterogeneous nucleation sites for solidification of molten Al. Because of this, grain refinement of as-cast Al occurs by addition of the Al-Al_3Ti composites deformed by ECAP and MDF is studied. It is found that ECAP and MDF for the Al-Al_3Ti composite are an effective process to enhance the graining refining ability for the as-cast Al.

Table of Contents

Chapter 1

General introduction

1.1 Metal matrix composite

The matrix component is a metal in which the reinforcement is distributed such a composite material is called as metal matrix composite (MMC) [1-12]. MMCs are made by dispersion of reinforcements such as fibers, particles, whiskers into the base metal. The continuous or discontinuous reinforcement can be embedded into base metal. The most commonly used base metals are aluminum, titanium, magnesium, copper and their alloys. The dispersion of reinforcement particle into the metal matrix is shown in **Fig. 1**. The concept of MMC is first considered by scientists during the launch of satellite in 1957 [2]. Scientists are looking for spacecraft materials with lighter and stronger components than glass fiber reinforced polymers (GFRPs) at that time. The space race is mainly concentrated to fabricate MMCs with have the properties of light-weight, high strength, high-temperature resistance, stiffness and low coefficient of thermal expansion. However, MMCs found uses in variety of real-world applications such as aerospace, ground transportation, thermal management, industry, infrastructures and other numerous applications by the mid of 1990s.

The characteristic of MMCs are determined by three entities such as matrix, reinforcement and interface [4,5]. In addition, factors that influencing the characteristics of MMCs are matrix alloy composition, matrix-reinforcement interface, reinforcement volume fraction, orientation, geometric arrangement of reinforcement and heat treatment. The effective selection of reinforcements and matrix permits the development of MMCs with attractive physical and mechanical

properties. Generally, MMCs are fabricated by solid state (powder metallurgy and diffusion bonding), liquid state (casting, spray deposition and infiltration) and vapor deposition processes [2-12]. Recently, the majority of MMCs comprise discontinuous reinforcement with particles or whiskers in the metal matrix are fabricated [5-12]. Furthermore, the distribution of reinforcements in the matrix has been receiving significant attention [5,6]. The various factors affecting distribution of reinforcements in MMC are processing, microstructure and mechanical behavior of discontinuous reinforcement.

1.2 Severe plastic deformation of MMC

When the MMC comprises reinforcement, particles are undergoing severe plastic deformation (SPD), the shape, the size and the distribution of reinforcement particles changes drastically [3, 5-12]. This is because that the matrix around the reinforcement particles in the MMC is severely deformed by SPD. SPD is helpful to reduce or eliminate porosity, excellent particle-to-particle bonding, homogeneity of particles with in the composite and it leads to improve the mechanical and physical properties of MMC. SPD can introduce plastic strain higher than conventional methods. The investigation of microstructure of MMCs processed by SPD has been limited. MMCs exhibit outstanding high strength, high corrosion resistance and excellent mechanical properties compare with coarse grain materials. In addition, several methods have been developed to fabricate ultrafine-grain (UFG) materials using SPD [1,5-12]. Many different techniques based on the SPD principles are equal-channel angular pressing (ECAP), multi-directional forging (MDF), accumulative roll-bonding (ARB) and high-pressure

torsion (HPT) [5-12]. Among these processing methods, ECAP is the most popular SPD processing [3,5].

ECAP is a metal working technique that can achieve a high strain without any dimensional changes of the specimens. ECAP makes the grain to be finer with a required number of passes and the finial grain size of the specimen achieves sub-micrometer size. **Figure 1.2** shows a schematic illustration of the ECAP process. Sabirov *et al.* subjected ECAP on the Al6061-20%Al_2O_3 powder metallurgy MMC, they have reported that ECAP leads to an increase of the uniformity of the particle distribution [5]. Chang *et al.* have suggested that ECAP can provide relatively homogeneous microstructure and enhance mechanical properties of the MMCs [3]. Also, some researchers have found that MDF can increase structure homogeneity of MMC was reported [10, 12]. **Figure 1.3** shows a schematic illustration of the MDF process with the sequence of pass.

Jamaati and Toroghinejad studied that ARB process produces a better distribution of alumina particles in the aluminum matrix [8]. ARB is a roll-bonding process that cause accumulatively intense plastic straining into the specimen as shown in **Fig 1.4.** Alizadeh and paydar have developed aluminum matrix composite through ARB process [9], and it is found that mechanical properties of the composite increases by ARB process.

Aluminum based MMCs are gaining importance because of their excellent mechanical properties, good strength-to-weight ratios, high specific strength, stiffness and hardness. When the Al-based composite containing solid particles is deformed by SPD, distributions of solid particles are changes drastically. However, distribution mechanism of the solid particle by SPD for the Al-based composite is not clear. In this thesis, fragmentation and distribution

mechanisms of solid particles by SPD for the Al-based composite are studied. Especially, as a model material of the Al-based composite, Al-Al_3Ti composite comprises Al_3Ti intermetallic particles is used. In addition, grain refining performance of Al-Al_3Ti composite comprises Al_3Ti intermetallic particles by SPD is investigated with the use of as-case Al.

1.3 Thesis outline

This thesis is presented in seven chapters.

In chapter 1, previous researches concerning with SPD for metal-based composites are described. Based on this background, contents of this thesis are discussed.

In chapter 2, fragmentation mechanism of a platelet Al_3Ti particle in an Al-Al_3Ti composite during compression test is investigated using 3-dimensional (3D) microstructural observation and crystallographic analysis. To calrigy the fragmentation process of a platelet Al_3Ti particle, same area microstructural observation is performed. From obtained results, it is found that the fracture surface of a platelet Al_3Ti particle is $\{112\}_{Al_3Ti}$, and cracks are preferentially propagated along the twin boundary of $\{112\}_{Al_3Ti}$, after deformation twinning.

In chapter 3, changes in the spatial distribution of the fragmented Al_3Ti particles in an Al-Al_3Ti composite during ECAP are investigated by Morisita index, I_δ. ECAP is performed under the processing routes of A and B_c up to 8 passes and Al_3Ti particles are aligned along the deformation axis using route A, while particles in the specimens deformed with B_c are formed into groups. Spatial distribution of Al_3Ti particles based on the I_δ results indicate that both processing routes generated aggregated distributions. After 5 passes using routes A and B_c,

the homogeneity of the spatial distribution is increased. These variations in the spatial distributions of the Al_3Ti particles can be explained by the occurrence of the material flow of the α-Al matrix during ECAP using routes A and B_c. Although, spatial distributions of spherical Al_3Ti particles in an Al-Al_3Ti composite by ECAP is investigated and spherical Al_3Ti particles are not fragmented by ECAP. In addition, stress concentration develops more easily for specimens with smaller size particles compare to the specimens which have larger size particles.

In chapter 4, effects of Al_3Ti particles shape on the fragmentation behavior and spatial distribution of Al_3Ti particles in ECAPed Al-Al_3Ti composite are investigated. In this chapter, spherical, polyhedral and granular Al_3Ti particles are used. Changes in the spatial distributions of fragmented spherical, polyhedral and granular Al_3Ti particles depend on the particle size. Moreover, it is found that fragmentation of Al_3Ti particles occurs by stress concentration around Al_3Ti particle.

In chapter 5, the fragmentation behavior of platelet Al_3Ti particles in the Al-Al_3Ti composite by MDF, symmetric rolling (SR) and asymmetric rolling (ASR) are presented. This SPD processes can be applied easily as industrial processing comparing with ECAP. The obtained results show that the platelet Al_3Ti particles in the Al-Al_3Ti composites deformend by MDF, SR and ASR are also fragmented and distributed depending on material flow of α-Al matrix in the composites. Therefore, these SPD processing methods can be used to modify the distribution of platelet Al_3Ti particles in the Al-Al_3Ti composite.

In chapter 6, grain refining performance of Al-Al_3Ti composite comprises the platelet Al_3Ti particles deformed by SPD is investigated with the use of as-cast Al. It is well known that Al_3Ti particles in Al-Al_3Ti composite play a role of good

heterogeneous nucleation sites for solidification of molten Al. Because of this, grain refinement of as-cast Al occurs by addition of the Al-Al_3Ti composite into molten Al. In this chapter, grain refinement performance of Al-Al_3Ti composites deformed by ECAP and MDF is studied. As a result, it is found that both of ECAP and MDF for the Al-Al_3Ti composite Using the obtained results, the grain refining ability of the Al-Al_3Ti composite are an effective process to enhance its graining refining ability for the as-cast Al.

Finally, chapter 7 describes the summary and conclusion of all chapters in this study.

References

[1] A. Cibula, The mechanism of grain refinement of sand casting in aluminium alloys, J. Inst. Met., **76** (1949-1950) 321-60.

[2] S. Rawal, Metal-matrix composite for space applications, JOM, **53** (2001) 14-17.

[3] S-Y. Chang, K-S. Lee, S. K. Ryu, K. T. Park and D. H. Shin, Effect of equal channel angular pressing on the distribution of reinforcements in the discontinuous metal matrix composites, Mater. Trans., **43** (2002) 757-761.

[4] J. M. Torralba, C. E. D. Costa and F. Velasco, P/M aluminum matrix composites: an overview, J. Mater., **133** (2003) 203-206.

[5] I. Sabirov, O. Kolednik, R. Z. Valiev and R. Pippan, Equal channel angular pressing of metal matrix composites: effect on particle distribution and fracture toughness, Acta Mater., **53** (2005) 4919-4930.

[6] I. Sabirov, O. Kolednik and R. Pippan, Homogenization of metal matrix composites by high-pressure torsion, Metall. Mater. Trans. A, **36A** (2005) 2861-2870.

[7] R. Jamaati and M. R. Toroghinejad, Manufacturing of high-strength aluminum/alumina composite by accumulative roll bonding, Mater. Sci. Eng. A, **527** (2010) 4146-4151.

[8] R. Jamaati and M. R. Toroghinejad, High-strength and highly-uniform composite produced by anodizing and accumulative roll bonding processes, Mater. Des., **31** (2010) 4816-4822.

[9] M. Alizadeh and M. H. Paydar, Fabrication of nanostructure Al/SiC_p composite by accumulative roll bonding, J. Alloys Compd., **492** (2010) 231-235.

[10] Q. Zhu, L. Li, Z. Zhang, Z. Zhao, Y. Zuo and J. Cui, Microstructure evolution of AZ80 magnesium alloy during multi-directional forging process, Mater. Trans., **55** (2014) 270-274.

[11] M. Zha, Y. Li, R. H. Mathiesen, R. Bjorge and H. J. Roven, Microstructure evolution and mechanical behavior of a binary Al–7Mg alloy processed by equal-channel angular pressing, Acta Mater., **84** (2015) 42-54.

[12] O. Sitdikov, R. Garipova, E. Avtokratova, O. Mukhametdinova and M. Markushev, Effect of temperature of isothermal multidirectional forging on microstructure development in the Al-Mg alloy with nano-size aluminides of Sc and Zr, J. Alloys Compd., **746** (2018) 520-531.

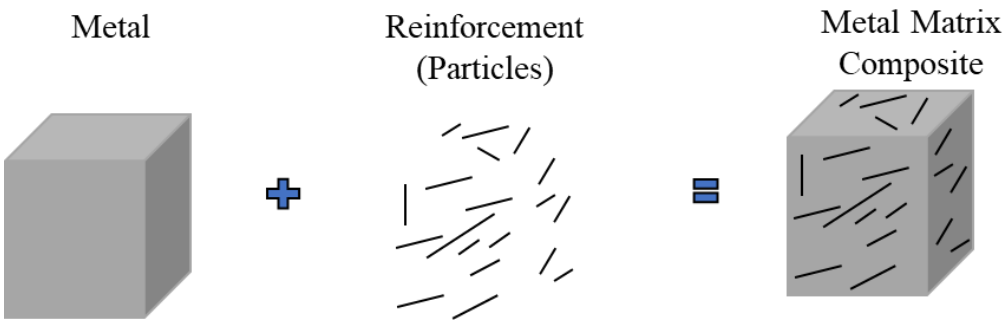

Fig. 1.1. Schematic representation of metal matrix composite

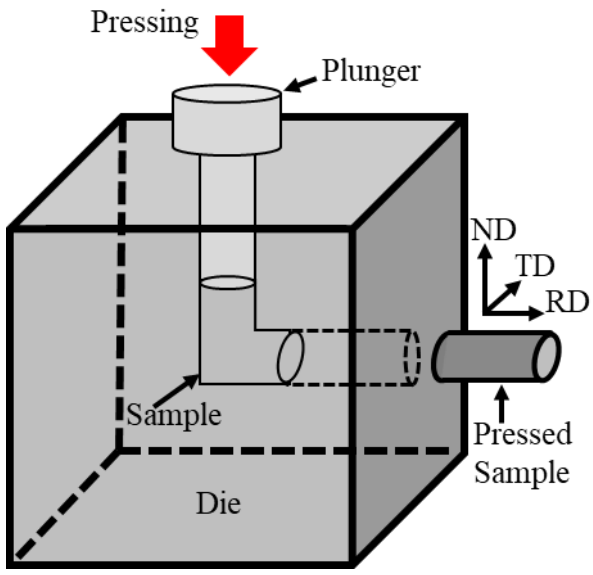

Fig. 1.2. Schematic illustration of the ECAP die.

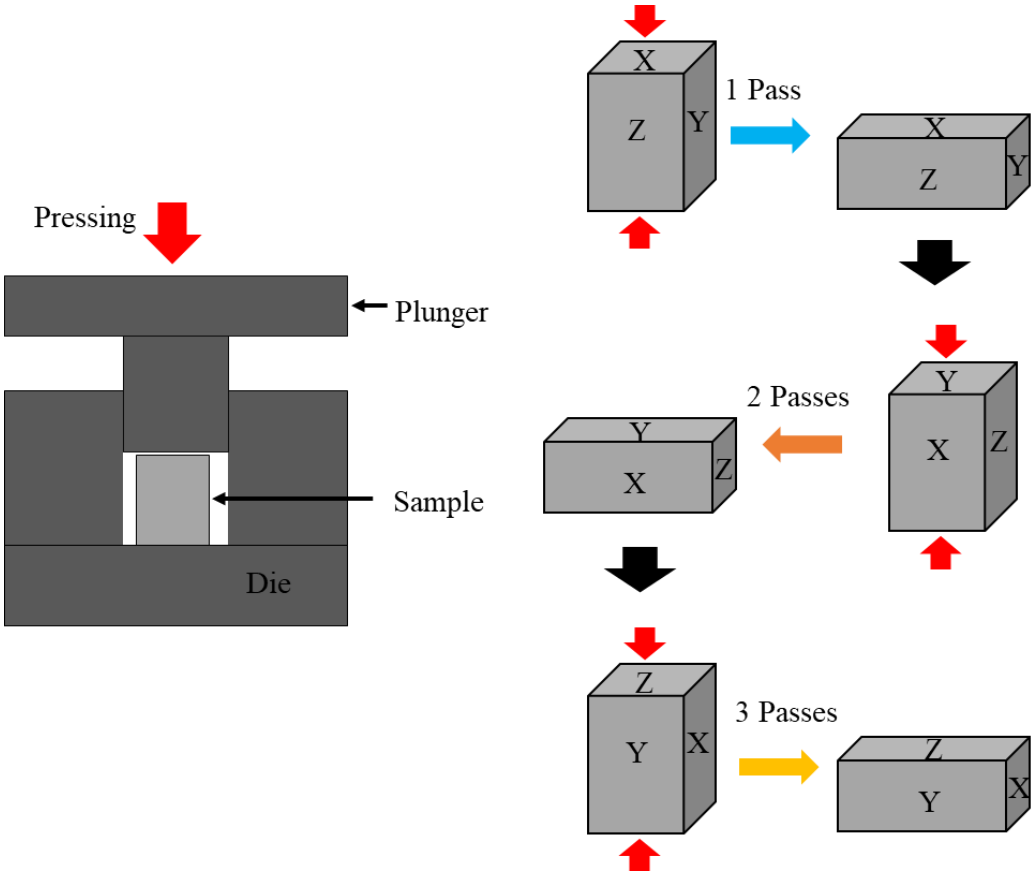

Fig. 1.3. Schematic illustration of the MDF process with the sequence of pass.

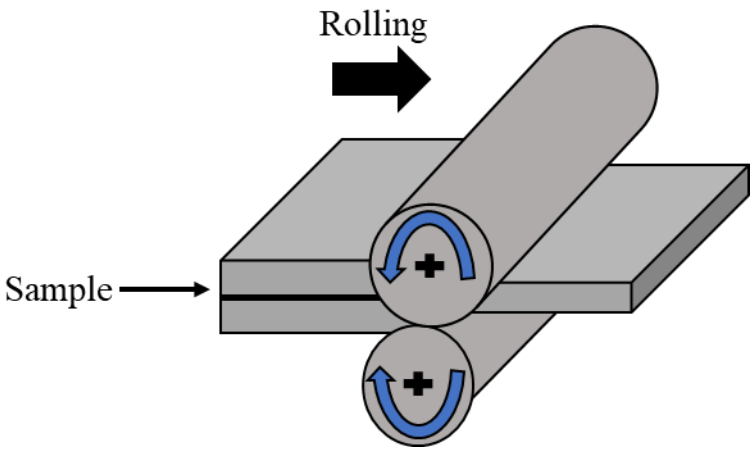

Fig. 1.4. Schematic illustration of the ARB process.

Chapter 2

Fragmentation mechanism of a platelet Al_3Ti particle in Al-based composite by compression test

2.1 Introduction

It is well known that the Al-Al_3Ti composite is an effective grain refiner for as-cast Al and its alloys [1-5]. This Al-Al_3Ti composite contains intermetallic platelet Al_3Ti particles with $D0_{22}$-type crystal structure in the α-Al matrix and Al_3Ti particles play the role of good heterogeneous nucleation sites for α-Al. In a previous study, the Al-Al_3Ti composite was subjected to severe plastic deformation (SPD) by equal-channel angular pressing (ECAP) and its grain refining ability for as-cast Al was investigated [3]. When the Al-Al_3Ti composite is deformed by ECAP, the number of Al_3Ti particles increased due to their fragmentation. Because of this, the Al-Al_3Ti composite deformed by ECAP had better grain refining ability compared with the undeformed Al-Al_3Ti composite. Similarly, it has been reported that the cold rolling for the Al-Al_3Ti composite enhances its grain refinement ability [4]. Therefore, it is important to understand the fragmentation process of platelet Al_3Ti particles by SPD for the Al-Al_3Ti composite as a method for enhancement of its grain refinement ability.

In addition, Al_3Ti has a good lattice matching with Al, and that this is one of the reasons why Al_3Ti provides a good heterogeneous nucleation site for α-Al [1-9]. Watanabe *et al*. have reported that the $\{112\}_{Al_3Ti}$ plane is the most effective nucleation site for Al because it can have good lattice matching with Al [5, 10]. Furthermore, they found that an Al_3Ti particle having $\{112\}_{Al_3Ti}$ on its surfaces is more effective as a nucleus for Al [5]. As a possible reason, if the platelet Al_3Ti

particles are preferentially fragmented on the $\{112\}_{Al_3Ti}$ trace by ECAP, this partly explains the high grain refinement ability of ECAP processed Al-Al_3Ti composite.

Sato *et al*. have reported that cracks in the platelet Al_3Ti particles preferentially propagate along $\{112\}_{Al_3Ti}$ when the Al_3Ti particle in Al-Al_3Ti composite is fragmented by ECAP [11]. However, the fragmentation of the platelet Al_3Ti particles in the Al-Al_3Ti composite is discussed by microstructural observation for the fragmented Al_3Ti particles in the deformed Al-Al_3Ti composite. Because of this, the fragmentation mechanism of the platelet Al_3Ti particles in the Al-Al_3Ti composite is not clear. In order to clarify the fragmentation process of Al_3Ti particles, it is important to perform the same area observation of the platelet Al_3Ti particle in the Al-Al_3Ti composite during deformation.

In this study, the fragmentation process of a platelet Al_3Ti particle in Al-Al_3Ti composite during compression testing was investigated with the repetition of microstructural observation on the same area. Moreover, the fragmentation process of platelet Al_3Ti particles in Al-Al_3Ti composite is discussed based on the results obtained by a combination of crystallographic analysis and 3-dimensional (3D) observation.

2.2 Experimental procedure

2.2.1 *Preparation of Al-Al_3Ti composite*

A commercial Al-5 mass% Ti alloy ingot was cast at 1073 K in an alumina crucible using an electrical resistance furnace under an argon gas atmosphere as shown in **Fig 2.1**. The as-cast ingot was cut and polished to obtain a specimen size of $5 \times 5 \times 5$ mm^3 for compression tests. This specimen contained platelet Al_3Ti particles with a volume fraction of 11% in an α-Al matrix. In

addition, the platelet Al_3Ti particle in the composite is single crystalline. Hereafter, the Al-5 mass% Ti alloy will be called as the Al-Al_3Ti composite. Using this composite, compression test was performed.

2.2.2 *2D microstructural observation of Al-Al_3Ti composite during compression*

The same area microstructural observation and compression testing were repeated to investigate the microstructural change of a platelet Al_3Ti particle in an Al-Al_3Ti composite during compression test. The specimen coordinate system for microstructural observation was defined as shown in **Fig 2.2**. Initial microstructure of the Al-Al_3Ti composite was observed by scanning electron microscopy (SEM) and electron backscatter diffraction (EBSD). Furthermore, compression test was performed up to a nominal strain of 5% at a strain rate of 10^{-3} /s. Subsequently, the microstructure of the platelet Al_3Ti particle was observed at the same position using EBSD. After that, the compression test was carried out up to the nominal strain of 8% using the same specimen, and then microstructural observation is performed again at the same position using EBSD. Moreover, EBSD measurement was performed with an SEM acceleration voltage of 15 kV and step sizes of 0.1 μm or 1.5 μm.

2.2.3 3D microstructural observation of Al_3Ti particle in Al-Al_3Ti composite after compression test

Three-dimensional (3D) microstructural observation of the platelet Al_3Ti particle in the Al-Al_3Ti composite deformed by the nominal strain of 8% was performed by the serial sectioning method to determine the crystal plane orientation on the crack surface of the fragmented Al_3Ti particle [12-14]. Serial images were obtained through repeated mechanical polishing and microstructural observation using an optical microscopy (OM). Initially, near to the observation

particles, two indentations were made by a micro-Vickers hardness tester and the serial images were obtained. The serial sectioning images are aligned and the sectioning distances are measured. The sectioned images in this study were approximately 10 μm thick. A 3D image of the platelet Al_3Ti particle was reconstructed using the commercial reconstruction software AMIRA ver. 6.0 from the serial sectioning images.

2.3 Results and discussion

2.3.1 Initial microstructure of Al-Al_3Ti composite

Figure 2.2 shows the initial microstructure of Al-Al_3Ti composite. From this photo, it is seen that the coarse platelet Al_3Ti particles are distributed in the α-Al matrix before compression test. In addition, the coarse platelet Al_3Ti particles are not aligned in the longitudinal direction and no platelet Al_3Ti particles has cracks. These microstructural characteristics of the Al-Al_3Ti composite are in agreement with the previous studies [3-6, 15-19]. Using this Al-Al_3Ti composite, the fragmentation process of the platelet Al_3Ti particles during compression test was investigated. This investigation was performed by the same area observation in the same area repeatedly.

2.3.2 Microstructural observation of Al_3Ti particle in Al-Al_3Ti composite during compression test

Figure 2.3 is a stress–strain curve of the Al-Al_3Ti composite obtained from the compression test. From the shape of this stress-strain curve, the Al-Al_3Ti composite is greatly deformed during compression test. Same-area microstructural

observations of a Al_3Ti particle in the Al-Al_3Ti composite were performed by stopping the compression test at nominal strains of ε= 5% and 8%.

Figure 2.4 (a) image quality (IQ) and inverse pole figure (IPF) maps of the Al-Al_3Ti composite obtained before compression testing using EBSD. As seen in this photograph, no crystal rotation or slip line was observed in the α-Al matrix. This indicates that the specimen not plastically deformed before the compression test. **Figures 2.4** (b) and (c) are IQ and IPF maps of the Al-Al_3Ti composite obtained using EBSD after compression testing up to nominal strains of ε=5% and 8%, respectively. It is seen that after compression tests, slip lines are observed in the α-Al matrix as shown in the IQ maps of **Figs. 2.4** (b) and (c). Especially, many slip lines are clearly visible at the nominal strain of ε=8% and these slip lines are heavily curled. In addition, a crack is generated in the Al_3Ti particle at a nominal strain of ε=5% and identified Al_3Ti particle shown by the rectangle formed dashed white lines. Moreover, when the specimen was compressed up to ε=8%, the same Al_3Ti particle was completely fragmented in **Fig. 2.4** (c).

The microstructure of the marked rectangles in **Figs. 2.4** was observed under higher magnification to investigate the fragmentation process of the platelet Al_3Ti particle in more detail. **Figures 2.5** (a) and (b) are highly magnified IQ maps of the Al-Al_3Ti composite compressed up to nominal strains of ε=5% and 8%, respectively. Trace analysis of $\{112\}_{Al3Ti}$ in platelet Al_3Ti particle was carried out and white lines in these figures are the traces of $\{112\}_{Al_3Ti}$. **Figure 2.5** (a) shows microstructure at the nominal strain of ε=5%. Some boundaries and crack generation are observed on the platelet Al_3Ti particle. Moreover, as seen in **Fig. 2.5** (a), it is seen that these boundaries are parallel to the trace of $\{112\}_{Al_3Ti}$. Yamaguchi *et al*. reported that Al_3Ti is fragmented after deformation twinning

with a twin boundary plane of $\{112\}_{Al_3Ti}$ [20]. Hence, it is considered that the boundary observed in **Fig. 2.5** (a) is a deformation twin boundary. Furthermore, increasing the nominal strain up to ε=8% cracks propagated along the boundary parallel to the $\{112\}_{Al_3Ti}$ trace, as shown in **Fig. 2.5** (b). Therefore, it can be expected that deformation twinning occurred in the platelet Al_3Ti particle during compression and subsequently the crack propagated along the twin boundary with $\{112\}_{Al_3Ti}$. Moreover, the crystal plane orientation of the cracked surface of a Al_3Ti particle was determined by 3D microstructural observation in this study.

2.3.3 3D microstructural observation and crystallographic analysis of fragmented Al_3Ti particle in Al-Al_3Ti composite

Figure 2.6 (a) is SEM micrograph of the fragmented Al_3Ti particle in the specimen deformed up to the nominal strain of 8%. Several cracks are observed in the fragmented Al_3Ti particle. In this study, the 3D shape of a fragmented Al_3Ti particle shown in **Fig. 2.6** (a) was visualized by serial sectioning. The reconstructed 3D image was shown in **Fig. 2.6** (b), which indicates the shape of a fragmented Al_3Ti particle clearly visible. This 3D image was used to determine the crystal plane orientation of the crack surface in the fragmented Al_3Ti particle by the following procedure. Initially, the angle (θ_{3D}) between the observation plane and crack surface was obtained by using the reconstructed 3D image. As a result, the measured θ_{3D} of a fragmented Al_3Ti particle was 89.7°. Furthermore, the angle (θ_{cal}) between the crystal plane orientation of the observation surface in the fragmented Al_3Ti particle and the predicted plane orientation of the crack surface were calculated. The predicted crystal plane orientations of the crack surface were $\{111\}_{Al_3Ti}$, $\{110\}_{Al_3Ti}$, $\{112\}_{Al_3Ti}$, or $(001)_{Al_3Ti}$ and the crystal plane orientation of

the observation plane was (5 2 -5). The θ_{cal} can be calculated by the following equation [21]:

$$\theta_{cal} = \cos^{-1}\left(\frac{h_1h_2 + k_1k_2 + \frac{1}{2}(h_1k_2 + k_1h_2) + \frac{3}{4}\left(\frac{a}{c}\right)^2 l_1l_2}{\sqrt{\left({h_1}^2 + {k_1}^2 + h_1k_1 + \frac{3}{4}\left(\frac{a}{c}\right)^2 {l_1}^2\right)\left({h_2}^2 + {k_2}^2 + h_2k_2 + \frac{3}{4}\left(\frac{a}{c}\right)^2 {l_2}^2\right)}}\right) \quad (2.\ 1)$$

where (h_1, k_1, l_1) is the crystal plane orientation of the observation surface, (h_2, k_2, l_2) is the predicted crystal plane orientation. a and c are the uniaxial lattice constant and the long axis lattice constant. In this study, the lattice constants of Al_3Ti with a $D0_{22}$-type structure are a = 0.3851 nm and c = 0.8608 nm [22, 23]. The calculated results for θ_{cal} are listed in Table 1. The θ_{cal} are compared with θ_{3D} (θ_{3D} = 89.7°). Furthermore, Table 1 shows that θ_{cal} is closest to θ_{3D} when the crystal plane orientation of the crack surface is $\{112\}_{Al_3Ti}$. This results that the crack surface of the fragmented Al_3Ti particle is $\{112\}_{Al_3Ti}$. As already discussed, the boundary plane of the deformation twin is $\{112\}_{Al_3Ti}$. Hence, it is clear that the crack of the fragmented Al_3Ti particle propagated along the twin boundary.

Somekawa *et al.* have reported that the formation of deformation twins in magnesium (Mg) alloy [24]. It is found that deformation twins occur near the crack tip when Mg alloy is deformed. Furthermore, they have investigated that twins form at the initial stage of the deformation process and crack propagation occurs along the twin boundaries [25]. This deformation process of the Mg alloy is similar the fragmentation process of the Al_3Ti particle. Therefore, it is reasonable that the crack in the Al_3Ti particle propagates along deformation twin boundary plane of $\{112\}_{Al_3Ti}$.

2.3.4 Fragmentation process of Al_3Ti particle in Al-Al_3Ti composite

In this section, the fragmentation process of platelet Al_3Ti particles in the Al-Al_3Ti alloy during compression was discussed. From previous studies, it was reported the deformation process of Al_3Ti [20] and the fragmentation process of the platelet Al_3Ti particles in the ECAP-processed Al-Al_3Ti composite [11]. As mentioned in **Section 2.3.2**, Yamaguchi *et al.* found that Al_3Ti particles are fragmented after twin deformation with twin boundary plane of $\{112\}_{Al_3Ti}$ [20]. In addition, some of the recent investigation of the formation process of the wear-induced layer by sliding wear for Al-Al_3Ti functionally graded materials (FGMs) [12]. That investigation observed many deformation twins in the fragmented Al_3Ti particles of the worn Al-Al_3Ti FGMs. In addition, Sato *et al.* have found that the fragmented Al_3Ti particles in the Al-Al_3Ti alloy deformed by ECAP consist of a crack surface with $\{112\}_{Al_3Ti}$ [11]. From those previous studies results that the platelet Al_3Ti particles are fragmented by crack propagation along twin boundaries after deformation twinning. Moreover, Wang *et al.* have studied that higher shear modulus of the particle provides the extra driven force for the interfacial cracking in Mg alloys [26]. However, the crack in the Al_3Ti particles propagates along the twin boundary plane rather than the interface between the matrix and the particle in the present study. This is because that bonding strength between Al_3Ti particle and α-Al matrix would be strong since the Al_3Ti has good lattice matching with the Al. Considering the above findings in mind, it was concluded that platelet Al_3Ti particles in the Al-Al_3Ti composite fragment by the following process shown in **Fig. 2.7** and described as follows:

(1) When Al-Al_3Ti composite is plastically deformed, shear stress is transmitted to the platelet Al_3Ti particles by shear deformation of the α-Al matrix.

(2) The platelet Al_3Ti particles are embedded in the α-Al matrix and the platelet Al_3Ti particles deform under a constrained state. Moreover, deformation twinning occurs in the Al_3Ti particles to relieve the stress around them (**Fig. 2.7** (b)). Deformation twinning formed in particle may create shear stress concentrations at the boundary.

(3)Furthermore, increasing shear stress around the platelet Al_3Ti particles. The cracks are initiate in the twin-deformed particles and preferentially propagate along the twin boundary of $\{112\}_{Al3Ti}$ (**Fig. 2.7** (c)). Finally, because a relatively large hole is formed between fragmented Al_3Ti particles, ductile fracture of the α-Al matrix would be enhanced.

2.4 Conclusions

The fragmentation process of platelet Al_3Ti particles in Al-Al_3Ti composite during compression was investigated by the combination of EBSD and 3D microstructural evaluation with crystallographic analysis. Same-area observation of a platelet Al_3Ti particle in the Al-Al_3Ti alloy during compression deformation was performed. The obtained main results are as follows:

(1) The Al-Al_3Ti composite containing platelet Al_3Ti particles was deformed by compression. The platelet Al_3Ti particle in the Al-Al_3Ti composite was compressed up to a nominal strain of 5%, and a twin boundary parallel to a $\{112\}_{Al3Ti}$ trace was observed and it was found that the platelet Al_3Ti particle is

first deformed by deformation twinning and in a direction parallel to the $\{112\}_{Al_3Ti}$ trace.

(2) Increasing the nominal strain up to 8%, cracks were generated in the same platelet Al_3Ti particle. The cracks generated along with the twin boundary-initiated fragmentation in the platelet Al_3Ti particle.

(3) The crystallographic analysis was performed on the fracture surface of the fragmented platelet Al_3Ti particle with 3D microstructural observation. The combination of EBSD and 3D microstructural observation indicated that the crystal plane orientation of the fracture surface in the platelet Al_3Ti particle was $\{112\}_{Al_3Ti.}$. The fragmentation of the Al_3Ti particle occurred along the $\{112\}_{Al_3Ti}$ plane. From these results, it is suggested that cracks initiated in the platelet Al_3Ti particles preferentially propagate along the twin boundary of $\{112\}_{Al_3Ti}$ after deformation twinning. The fragmentation of platelet Al_3Ti particles in Al-Al_3Ti composite preferentially occurs at twin boundary after deformation twinning.

References

[1] A. Cibula, The mechanism of grain refinement of sand casting in aluminium alloys, J. Inst. Met., **76** (1949-1950) 321-60.
[2] A. Kamio, J. Jpn. Inst. Light Met., **56** (2006) 496-500 (in Japanese).
[3] Z. Zhang, S. Hosoda, I-S. Kim and Y. Watanabe, Grain refining performance for Al and Al-Si alloy casts by addition of equal-channel angular presses Al-5 mass% Ti alloy, Mater. Sci. Eng A, **425 (**2006) 55-63.
[4] H. Sato, K. Ota, M. Furukawa, M. Azuma, Y. Watanabe, Z. Zhang and K. Tsuzaki, Grain refinement of as-cast pure Al by cold-rolled Al-Ti alloy refiner, Mater. Trans., **54** (2013)1554-1561.
[5] Y. Watanabe and H. Sato, Grain refinement of aluminum casting alloy by heterogeneous nucleation sites with smaller lattice disregistry, Keikinzoku, **64** (2014) 157-163 (in Japanese).
[6] K. Yamauchi, T. Kunimine, H. Sato and Y. Watanabe, Grain refinement of Al_3Ti dispersed aluminum matrix composites by reaction centrifugal mixed-powder method, Mater. Trans., **56** (2015) 99-107.
[7] M. X. Zhang, P. M. Kelly, M. A. Easton and J. A. Taylor, Crystallographic study of grain refinement in aluminum alloys using the edge-to-edge matching model, Acta Mater., **53** (2005)1427-1438.
[8] M. Easton and D. St. John, Grain refinement of aluminium alloys: part 1. The nucleation and solute paradigms-a review of the literature, Metall. Mater. Trans. A, **30A** (1999) 1613-1623.
[9] W. Ding, T. Xia and W. Zhao, Performance comparison of Al-Ti master alloys with different microstructure in grain refinement of commercial purity in aluminium, Materials, **7** (2014) 3663-3676.
[10] Y. Watanabe, P. D. Sequeira, H. Sato, T. Inamura and H. Hosoda, Aluminium matrix texture in Al-Al_3Ti functionally graded materials analyzed by electron back-scattering diffraction, Jpn. J. Appl. Phys., **55** (2016) 01AG03.
[11] H. Sato and Y. Watanabe, Three-dimensional microstructural analysis of fragmentation behavior of platelet Al_3Ti particles in Al-Al_3Ti composite deformed by equal channel angular pressing, Mater. Charact., **144** (2018) 305-15.
[12] H. Sato, Y. Noda and Y. Watanabe, 3-dimensional microstructure evaluation of wear-induced layer in Al-Al_3Ti functionally graded materials by serial sectioning, Mater. Trans., **54** (2013) 1274-1280.
[13] F. Wang, D. Eskin, J. Mi, T. Connnnolley, J. Lindsay and M. Mounib, A refining mechanism of primary Al_3Ti intermetallic particles by ultrasonic treatment in the liquid state, Acta Mater., **116** (2016) 354-63.
[14] K. Yamashita, C. Watanabe, S. Kumai, M. Kato, A. Sato and Y. Watanabe, Cyclic deformation and development of dislocation structures in a centrifugally cast Al-Al_3Ti of functionally graded material, Mater. Trans., **41** (2000) 1322-1328.
[15] C. Tijun, L. Jian and H. Yuan, Microstructures and corrosion properties of casting in-situ Al_3Ti-Al composites, Rare Metals, **29** (2010) 78.
[16] S. El-Hadad, H. Sato and Y. Watanabe, Investigation of wear anisotropy in a severely deformed Al-Al_3Ti composite, Metall. Mater. Trans. A, **43A** (2012) 3249-3256.
[17] H. Sato, T. Hishikawa, Y. Makino, T. Kunimine and Y. Watanabe, 3-dimensional microstructure of Al-Al_3Ti alloy severely deformed by ECAP, Proceedings of 13th International Conference on Aluminum Alloys (ICAA13), (2012) 1575-1580.

[18] S. B. Duraisamy, H. Sato, T. Chiba and Y. Watanabe, Fragmentation process of platelet Al_3Ti particles in compressed Al-Al_3Ti alloy observed by serial sectioning and EBSD analysis, Mater. Res. Express, **6** (2019) 096575.
[19] H. Sato, A. Mori, M. Kitagawa, S. B. Duraisamy, T. Chiba and Y. Watanabe, Three-dimensional analysis of fragmentation process of Al_3Ti platelet particles in Al-Al_3Timultiphase alloy deformed by asymmetric rolling, JOM, **72** (2020) 57-64.
[20] M. Yamaguchi, Y. Umakoshi and T. Yamane Plastic deformation of the intermetallic compound Al_3Ti, Philos. Mag. A, **57** (1987) 301-15.
[21] W. F. Hosford, The Mechanics of Crystals and Textured Polycrystals oxford science publications 1993.
[22] JCPDS No. 26-0039.
[23] Y. Watanabe, Q. Zhou, H. Sato, T. Fujii and T. Inamura, Microstructures of Al-Al_3Ti functionally graded materials fabricated by centrifugal solid-particle method and centrifugal in situ method, Jpn. J. Appl. Phys., **56** (2017) 01AG01.
[24] H. Somekawa, A. Singh and T. Mukai, Fracture mechanism of a coarse-grained magnesium alloy during fracture toughness testing, Philos. Mag. Lett., **89** (2009) 2-10.
[25] H. Somekawa, K. Nakajima, A. Singh and T. Mukai, Ductile fracture mechanism in fine-grained magnesium alloy, Philos. Mag. Lett., **11** (2010) 831-839.
[26] Y. N. Wang, C. Xie, Q. H. Fang, X. Liu, M. H. Zhang, Y. W. Liu and L. X. Li, Toughening effect of the nanoscale twinning induced by particle/matrix interfacial fracture on fine-grained Mg alloys, Int J Solids Struct, **102-103** (2016) 230-237.

Table 2.1. Predicted crystal plane orientation and calculated angle of crack surface.

Predicted crystal plane orientation	Calculated angle (θ_{cal})	Measured angle (θ_{3d})
$\{111\}_{Al_3Ti}$	83.8°	89.7°
$\{110\}_{Al_3Ti}$	22.0°	
$\{112\}_{Al_3Ti}$	90.0°	
$(001)_{Al_3Ti}$	107.2°	

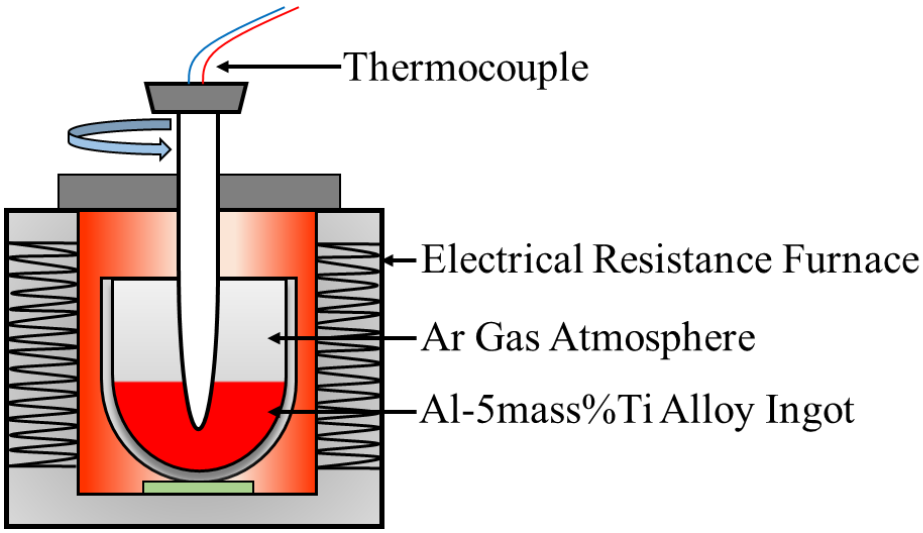

Fig. 2.1. Schematic illustration of casting process.

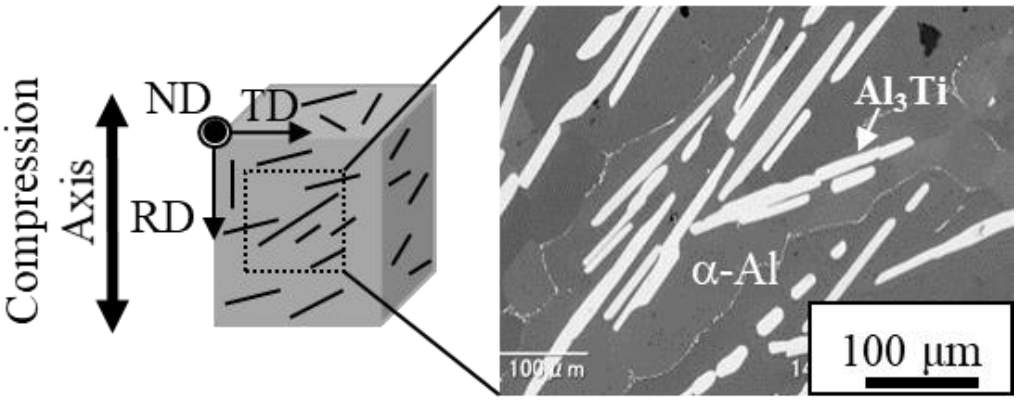

Fig. 2.2. SEM photograph showing microstructure of Al-Al_3Ti composite before compression together with specimen coordinates for microstructural observation.

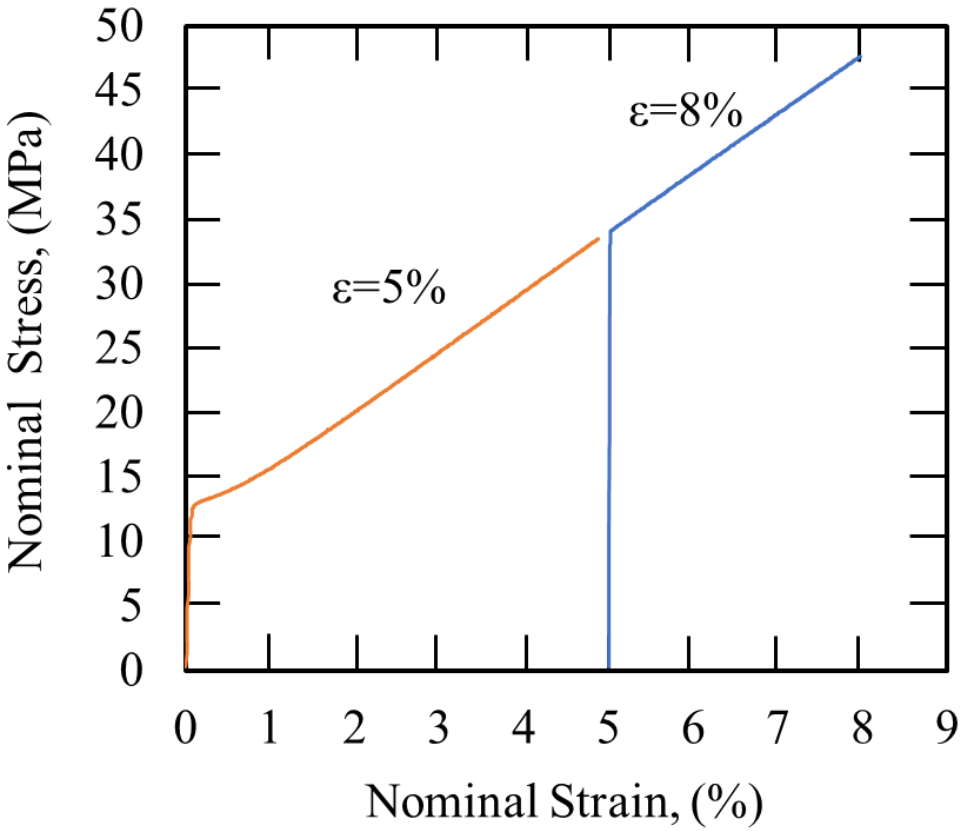

Fig. 2.3. A stress-strain curve of the Al-Al_3Ti composite obtained by compression test.

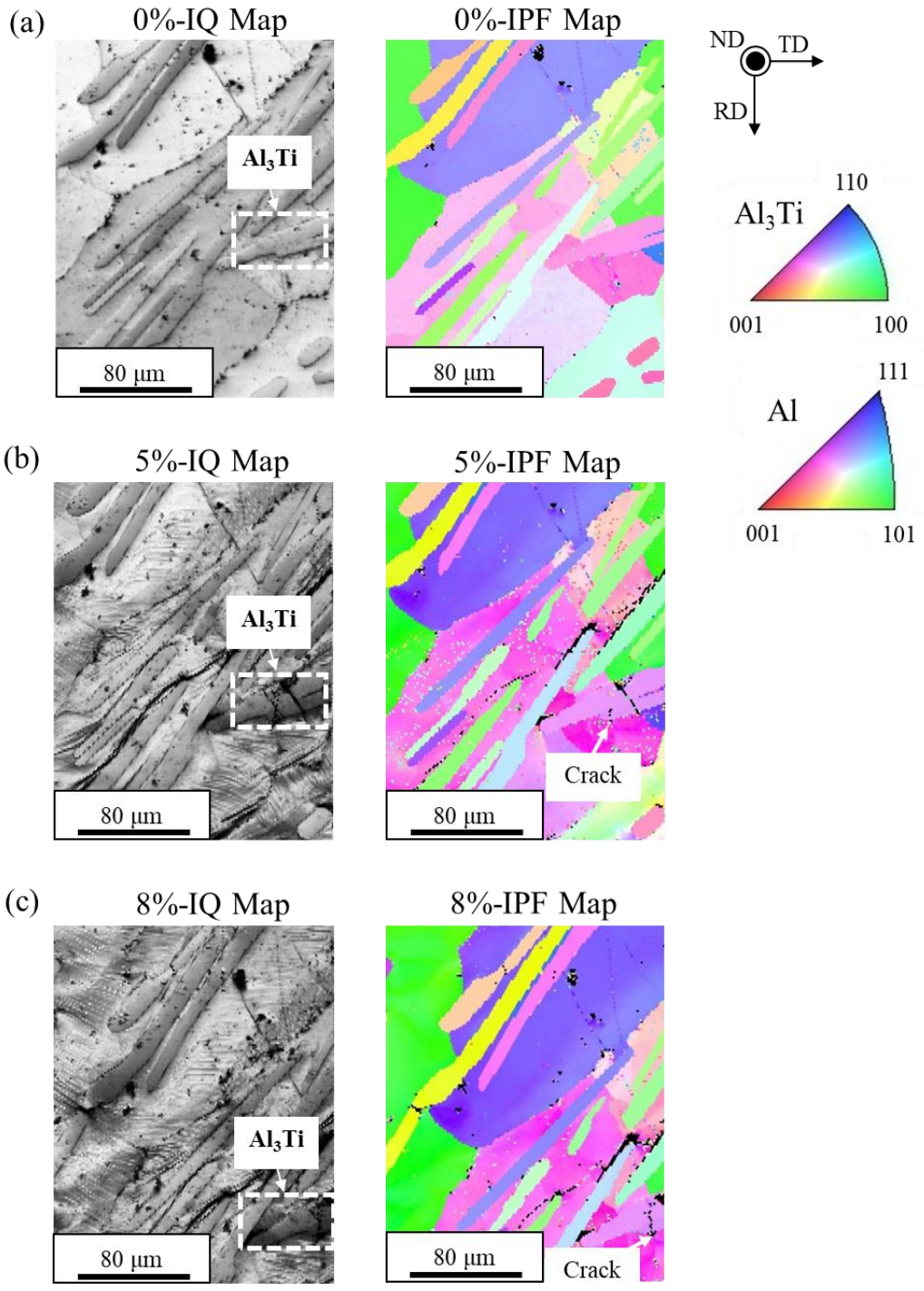

Fig. 2.4. (left) IQ and (right) IPF maps of the Al-Al_3Ti composite (a) before compression test and after compression tests up to nominal strains of (b) ε = 5% and (c) ε = 8%.

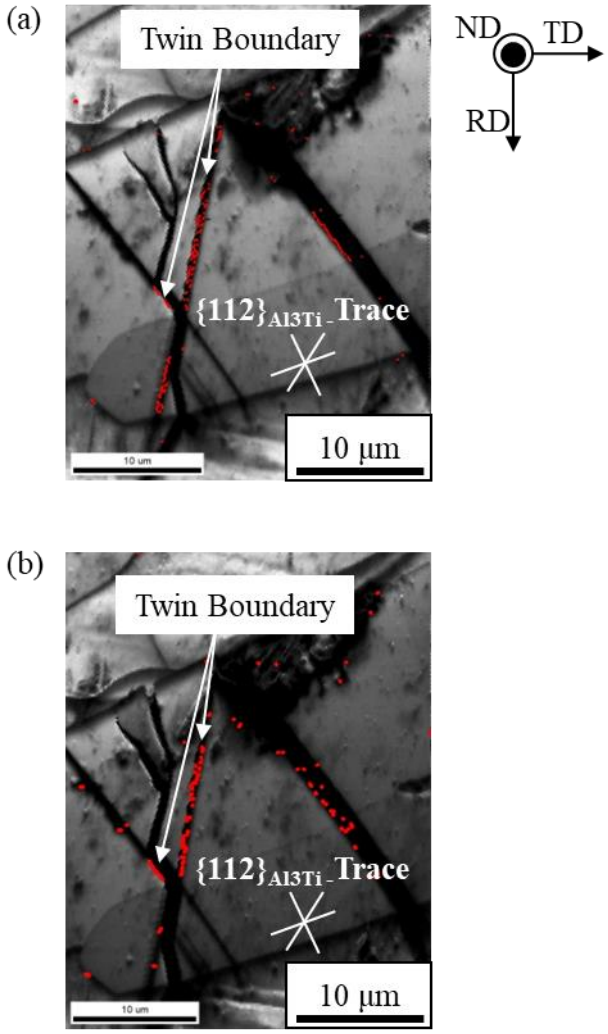

Fig. 2.5. Highly magnified IQ maps of the Al-Al_3Ti composite compressed up to nominal strains of (a) ε=5% and (b) 8% together with $\{112\}_{Al_3Ti}$ trace analysis.

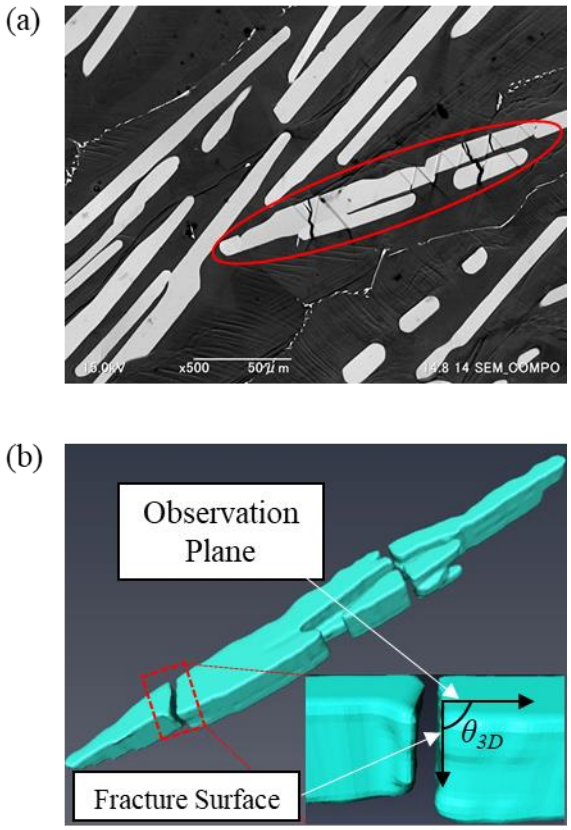

Fig. 2.6. (a) SEM photograph and (b) 3D image showing the fragmented platelet Al_3Ti particle at nominal strain of ε = 8%. Angle between the observation plane and the fracture surface (θ_{3d}) was measured with 3D image.

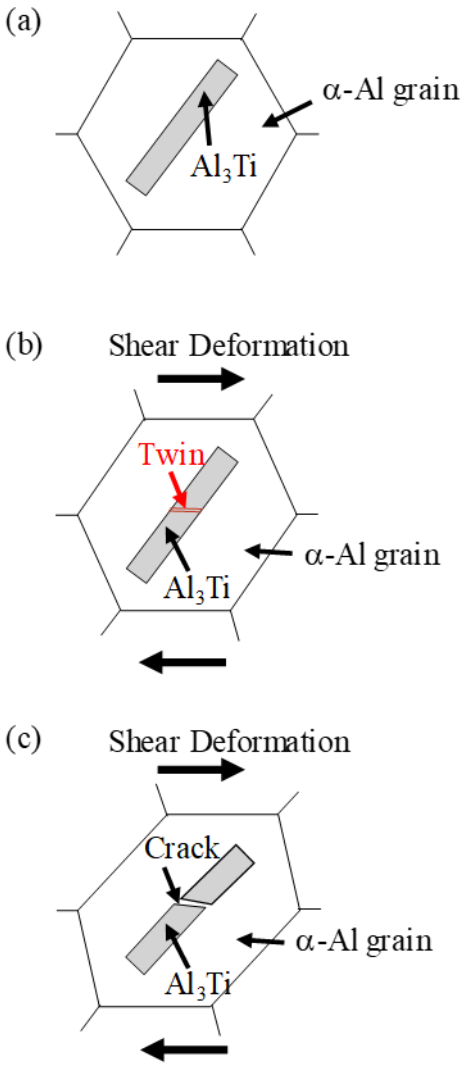

Fig. 2.7. Schematic representations showing the fragmentation process of the platelet Al_3Ti particle in the Al-Al_3Ti composite under compression test: (a) before deformation, (b) at the beginning of deformation and (c) after deformation.

Chapter 3

Controlling factor for solid particles fragmentation in Al-based composite by equal-channel angular pressing

3.1 Introduction

Recent years there has been an increasing interest to manufacture of ultrafine-grain (UFG) materials, due to the unique properties [1-3]. In addition, this UFG contains sub micrometer of grain size compare with other conventional materials. Severe plastic deformation (SPD) processing is an innovative group of metalworking techniques that can be used to produce bulk UFG materials [4]. SPD can impose extremely high strains without any significant changes in the overall dimensions of the materials and results in plastic deformation of materials. High-pressure torsion (HPT) [5-7], equal-channel angular pressing (ECAP) [8-23], multi-directional forging (MDF) [24-26], accumulative roll-bonding (ARB) [27-29] and constrained groove pressing (CGP) [30] methods are few techniques works based on the SPD principles. Among them, HPT and ECAP are effective techniques to produce UFGs structure.

Figure 3.1 is a schematic illustration of ECAP die together with the shearing patterns introduced during each ECAP pass. A rod or bar shaped billet is repeatedly pressed through ECAP die with two channels that intersect at the bend and ECAP technique induce large shear strain into the billet. The equivalent strain (ε) accumulated by each ECAP passage can be calculated based on the angle between the two parts of the channel (ϕ) and the outer curvature angle where the two parts intersect (ψ). The value of ε is calculated using the equation [9, 10].

$$\varepsilon = \frac{N}{\sqrt{3}}\left[2cot\left\{\left(\frac{\phi}{2}\right)+\left(\frac{\psi}{2}\right)\right\}+\psi\text{cosec}\left\{\left(\frac{\phi}{2}\right)+\left(\frac{\psi}{2}\right)\right\}\right] \qquad (3.1)$$

where *N* is the number of ECAP passes through the billet. Furthermore, the strain induced by each ECAP passage can be modified by varying the processing route. Moreover, several processing routes have been proposed for ECAP such as routes A, B_A, B_c and C. During route A, the biller is pressed repetitively without rotation and so shear deformation occurs in two directions. In contrast, route B_A and B_c involves rotating the billet 90° in the alternative and same direction during each ECAP passage, respectively. While route C, the billet is rotated 180° in the same direction. In this study, most commonly used ECAP processing such as route A and B_c are performed. Route B_c impose a homogeneous strain following 4 passes as shown in **Fig. 3.1** and the final microstructure depends on the ECAP processing route [8, 10].

Some of the previous studies investigated the microstructural changes induced in metal-based composite by ECAP [12, 14]. Chang *et al.* reported that ECAPed 6061 Al-10vol% SiC_w composites produce a uniform distribution of SiC_w clusters and ECAP enhance the mechanical properties of the material [12]. Sabirov *et al.* investigated that ECAPed Al6061-20%Al_2O_3 powder metallurgy metal-based composite produce the homogeneity of the solid particles in the composite [14]. In addition, Tan and Zhang reported that the secondary processing of composites containing solid particles larger than a critical size can enhance the homogeneous distribution of such particles [31]. From those previous studies, it is found that the composites containing solid particles can enhance the homogeneous distribution of these particles after ECAP processing.

Watanabe *et al.* studied the effects of processing routes A and B_c on microstructure and texture development in Al-Al_3Ti composite by ECAP [32]. Their results show that route A produces a highly anisotropic distribution of

fragmented Al_3Ti particles in the α-Al matrix, while route B_c results in a homogeneous distribution of the fragmented Al_3Ti particles.

Sato and Watanabe investigated the fragmentation behavior of platelet Al_3Ti particles in severely deformed Al-Al_3Ti composite by ECAP using routes A, B_c and C [33]. It is found that the distribution difference of Al_3Ti particles in the Al-Al_3Ti composite by ECAP is controlled by plastic deformation of the α-Al matrix. However, changes in the spatial distributions of platelet Al_3Ti particles in Al-Al_3Ti composite during ECAP have never been evaluated quantitatively. To evaluate the spatial distribution of platelet Al_3Ti particles the Morisita index, I_δ, would be suitable method [26, 34-38] and this I_δ has been applied to the analysis of spatial distributions of Al_3Ti particles in Al-Al_3Ti composite deformed by MDF [26]. The spatial distribution of Al_3Ti particles in the Al-Al_3Ti composite deformed by ECAP has never been evaluated using I_δ.

In this study, the spatial distributions change of Al_3Ti particles in the Al-Al_3Ti composite during ECAP are investigated. Variations in the spatial distributions of these particles in the Al-Al_3Ti composite by ECAP were quantitatively evaluated using I_δ. First, the Al-Al_3Ti composite contains platelet Al_3Ti particles are prepared by casting and ECAP is performed up to 8 passes using routes A and B_c. On the other hand, the effects of particles sizes in the spatial distribution of spherical Al_3Ti particles in the Al-Al_3Ti composite during ECAP is studied and this Al-Al_3Ti composite is prepared by spark plasma sintering (SPS). Based on the obtained results, the distribution mechanism of Al_3Ti particles in Al-Al_3Ti composite during ECAP are discussed.

3.2 Experimental procedure

3.2.1 Specimen preparation of Al-Al_3Ti composites

First, one type of Al-Al_3Ti composite was prepared by casting process. A commercial Al-5mass%Ti alloy ingot was used as the starting material for the ECAP. This alloy ingot contained platelet Al_3Ti particles with volume fraction of 11vol% in an α-Al matrix [39-40]. The ingot was melted at 1073 K then the melt was poured into a steel mold containing a hole with 15 mm in diameter and 180 mm in length. After that, lathe machining was carried out to obtain required ECAP specimen size with 10 mm in diameter and 60 mm in length. Subsequently, each specimen was homogenized at 773 K for 1 h by heating and then air cooled. These specimens are used to perform ECAP process.

The other type of Al-Al_3Ti composite was prepared by SPS. **Figure 3.1** was schematic illustration showing the fabrication process of Al-Al_3Ti composite using SPS. At first, the spherical Al_3Ti particles were prepared by gas atomization method as shown in **Fig. 3.1** (a). Macrostructure of obtained spherical Al_3Ti particles was shown in **Fig. 3.2** and this spherical Al_3Ti particle was polycrystalline. After that, the gas-atomized spherical Al_3Ti particles are sieved to obtain three kinds of Al_3Ti particle sizes with different particle sizes. The particle diameters of the sieved Al_3Ti particles are below 75 μm, 75-150 μm and 150-250 μm. Subsequently, using three-dimensional motion mixer (Turbula mixer), these sieved Al_3Ti particles are mixed with Al particles (99.9%) with 106-180 μm in diameter. In addition, to minimize the powder particles aggregation while mixing stearic acid was added as a process control agent. The volume fraction of the Al_3Ti particles in the mixed-powder was 11 vol%. These mixed-powders were sintered using the spark plasma sintering (SPS, SPS-515S Syntax Inc.) apparatus. The

sintering was performed at 550 °C for 15 min under the applied pressure of 45 MPa. The SPSed Al-Al_3Ti composite was cut to obtain the required size of ECAP specimens with 10 mm in diameter and 30 mm in length. Finally, three kinds of Al-Al_3Ti composites containing Al_3Ti particles with different diameter were obtained. Specimen 1 which contains below 75 μm Al_3Ti particles in the Al-Al_3Ti composite, specimen 2 contains 75-150 μm Al_3Ti particles and specimen 3 contains 150-250 μm Al_3Ti particles in the Al-Al_3Ti composites.

3.2.2 ECAP processing of Al-Al_3Ti composites

The ECAP die was constructed with an intersecting angle of $\phi = 90°$ and an outer angle of curvature of $\Psi = 20°$ between the two channels as shown in **Fig. 3.3**. During each pass of ECAP, this die subjected the test specimens to a nominal equivalent strain of 1.01. The pressing speed of each ECAP specimen was 5 mm/min and a graphite oil were used as the lubricant. Each specimen was subjected to up to 8 passes under route A or B_c at ambient temperature. Thus, the total nominal equivalent strain induced in each specimen by the ECAP processing over 8 passes was approximately 8.08. ECAP for the SPSed Al-Al_3Ti composite was subjected up to 1 pass.

3.2.3 Microstructural observations of Al-Al_3Ti composites

The Al-Al_3Ti composite was cut down the middle along the deformation axis and then mechanically and chemically polished in preparation for microstructural observations. Microstructures of the Al-Al_3Ti composites before and after ECAP were examined by scanning electron microscopy (SEM) and optical microscopy (OM). During such assessments, the direction of microstructural observation was important, and **Fig. 3.4** provides the coordinate

system applied to each specimen. The sizes and spatial distributions of the Al_3Ti particles were analyzed based on the SEM and OM images. Phase identification was carried out by an X-ray diffractometer (XRD) analysis. Electron backscatter diffraction (EBSD) analysis was also used to determine the crystal orientation distributions of the Al_3Ti particles. EBSD analysis were acquired at an acceleration voltage of 15 kV and using a step size of 0.5 μm. The average diameter of the Al_3Ti particles in each specimen was determined employing the Motic Image Plus software package.

The spatial distributions of the Al_3Ti particles in the Al-Al_3Ti composite before and after ECAP were evaluated on the basis of I_δ values [26, 34-38]. The center of gravity of each Al_3Ti particle in each observation area was initially used to mark the particle position. The observation area was then divided into quadrats (q), and the number of marked positions were counted in each area. In these analyses, the observation area was divided into a total of 64 quadrats when determining I_δ and the Al_3Ti particles inside these quadrats were employed as the sampling units. In addition, in order to evaluate strain distribution around Al/Al_3Ti interface in Al matrix for the SPSed Al-Al_3Ti composite. Hencky equivalent strains of Al matrix were calculated based on the shape of Al-matrix grain.

3.3 Results and discussion

3.3.1 Initial microstructure of Al-Al_3Ti composite prepared by casting

Figure 3.5 is an SEM photograph showing the initial microstructure of an Al-Al_3Ti composite prepared by casing and before ECAP process this composite contained randomly distributed platelet Al_3Ti particles in the α-Al matrix. The average length of platelet Al_3Ti particles was approximately 210 μm inside the

observation area and these particles have no crack. This microstructure is in agreement with previous studies [32-33, 39-41]. Using such Al-Al_3Ti composites, ECAP was performed up to 8 passes under route A or B_c.

3.3.2 Microstructural changes induced in Al-Al_3Ti composites by ECAP

Figure 3.6 provides a set of photographic images showing the rod-shaped Al-Al_3Ti composite before and after ECAP up to 8 passes using route A or B_c. In **Fig. 3.6**(b), several small cracks are visible on the specimen surface following 8 passes using route A. In contrast, the Al-Al_3Ti composite subjected up to 8 passes using route B_c exits large cracks, as shown in **Fig. 3.6**(c). **Figures 3.7**(a)-(h) is a set of SEM microstructures of Al-Al_3Ti composites after ECAP up to 8 passes under route A. When 1 pass of ECAP is performed to the Al-Al_3Ti composite, severe cracking is observed in coarse platelet Al_3Ti particles as shown in **Fig. 3.7**(a). It is found that the Al_3Ti particles fragmented during 1 pass are aligned along the deformation axis compared to the initial particles shown in **Fig. 3.5**. In addition, fragmentation of particles observed at center of the specimen and around the specimens are different along the deformation axes. After 2 passes as shown in **Fig. 3.7**(b), the Al_3Ti particles are seen to be smaller compared to those in the specimen after 1 pass. Furthermore, increment in the number of passes greatly increased the degree of fragmentation of the Al_3Ti particles along with the number of cracks in the Al_3Ti particles. In addition, the fragmented Al_3Ti particles became more closely aligned along the deformation axis with increases in the number of ECAP passes. It was suggesting that the fragmented Al_3Ti particles were forced to migrate towards the shear plane. This is because route A induces unidirectional shear deformation of the specimen. When ECAP was subjected up to 8 passes under route A, the fine fragmented Al_3Ti particle were uniformly distributed in the

Al-Al_3Ti composite as shown in **Fig. 3.7**(h). **Figures 3.8**(a)-(h) is a set of high-magnification SEM microphotographs presents fragmented Al_3Ti particles after up to 8 passes using route A. **Figure 3.8**(a) shows that the Al_3Ti particles after 1 pass maintained their platelet shape, and that each fragment was separately dispersed in the Al-Al_3Ti composite. The fragmented Al_3Ti particles in the Al-Al_3Ti composite after 8 passes under route A show a granular shape and this morphological change is attributed to the shear deformation induced by ECAP.

Microstructures of Al-Al_3Ti composites by ECAP processing under route B_c up to 8 passes was shown in **Fig. 3.9**(a)-(h). When the ECAP was subjected more than 2 passes, it shows fragmented platelet Al_3Ti particles that are not aligned along the deformation axis. In contrast, these particles also appear to aggregate to produce several groups of particles. Watanabe *et al.* reported that Al-Al_3Ti composites subjected to ECAP under routes A or B_c show two different microstructures, such that the latter route generates a homogeneous distribution of the fragmented Al_3Ti particles in the α-Al matrix [32]. This phenomenon occurs because route B_c induces multidirectional shear deformation of the specimen. In this study, fragmented Al_3Ti particles under route A were observed to be aligned along the deformation axis. In contrast, route B_c produced several groups of the Al_3Ti particles. Thus, the spatial distribution of fragmented Al_3Ti particles in the Al-Al_3Ti composite after ECAP process varied depending on the processing route. **Figures 3.10**(a)-(h) is a set of high magnification SEM microphotographs of fragmented Al_3Ti particles in specimens subjected ECAP under route B_c up to 8 passes. As discussed above, these fragmented Al_3Ti particles aggregated to form several groups. Compared to route A, applying 8 passes under route B_c resulted in finer fragments in the α-Al matrix. In addition, the average lengths of the

fragmented Al_3Ti particles in Al-Al_3Ti composites groups obtained using route B_c after 4 passes and 8 passes were 256 μm and 248 μm, respectively. This average length of the fragmented Al_3Ti particles group were similar to the initial average length of platelet Al_3Ti particles in the undeformed Al-Al_3Ti composite before ECAP. The shape of the Al_3Ti particles after ECAP using routes A and B_c at 8 passes were found to transition from platelet to granular. Therefore, the microstructural evolution of the Al_3Ti particles in the Al-Al_3Ti composite was dependents on the ECAP processing route.

Figures 3.11 were a set of histograms shows the summarizing of diameter distributions of the Al_3Ti particles in Al-Al_3Ti composites before and after ECAP up to 8 passes using routes A and B_c. These diameters of the Al_3Ti particles were calculated based on their areas, assuming that the particles were circular in shape [33]. **Figure 3.11**(a) shows that before ECAP, the diameter of platelet Al_3Ti particles were relatively large. However, the particle size was decreased with increases the number of ECAP passes. Because of this, the number density of Al_3Ti particles was also increased by ECAP. **Figure 3.12** was a graph showing the average diameters of the Al_3Ti particles based on the histograms results. These graph results that the average diameter decreased gradually with increasing number of ECAP passes. However, the size reduction behavior is different between processing routes A and B_c, such that the Al-Al_3Ti composite subjected to 8 passes using route B_c had much smaller Al_3Ti particles. This was because of the route B_c attributed to the greater number of shear planes and shear directions at 8 passes comparing to route A.

Figures 3.13(a) and **3.13**(b) shows inverse pole figure (IPF), phase and kernel average misorientation (KAM) maps of the Al-Al_3Ti composites after 8

passes under routes A and B_c, respectively. The IPF maps present the crystal plane orientations of Al-Al_3Ti composites observed at ND plane. The α-Al matrix was seen to contain fine grains after 8 passes of ECAP. Watanabe *et al*. studied the orientation relationship between Al_3Ti particles and an Al matrix in Al-Al_3Ti functionally graded materials (FGMs) fabricated by centrifugal casting using EBSD [42-43]. In addition, authors have reported that the plane-normal direction of the platelet Al_3Ti particles corresponded to the $[001]_{Al_3Ti}$. KAM analysis was a useful means of characterizing local misorientation [44-47] and KAM values are readily obtained from EBSD analysis. **Figure 3.13** shows the KAM analyses with 5° threshold angle of α-Al matrix after 8 passes of ECAP under routes A and B_c. From this images, it was confirms that the KAM values were lower in the Al-Al_3Ti composite after ECAP under route A. Ashby established that, when a two-phase alloy is deformed, the dislocations induced in the crystal lattice allow compatible deformation of two phases via geometrically necessary dislocations (GNDs) and determined that KAM values are correlated with these GNDs [45]. The relationship between indentation size and the density of GNDs was studied using EBSD [46]. In this study, dynamic recrystallization was observed in the Al-Al_3Ti composite after ECAP using both processing routes. In addition, the density of GNDs in the α-Al matrix around the Al_3Ti particles decreased due to this recrystallization, and fragmentation of Al_3Ti particles are severely occurs. However, the extent of fragmentation of Al_3Ti particles in Al-Al_3Ti composites was found to vary depending on the number of ECAP passes for both routes A and B_c.

3.3.3 Spatial distribution of Al_3Ti particles in the Al-Al_3Ti composite

In a previous study, spatial distribution of Al_3Ti particles in an Al-Al_3Ti composite were investigated up to 4 passes by ECAP using the 3D microstructural analysis [33]. However, the spatial distributions have never been evaluated quantitatively. In this study, spatial distribution of Al_3Ti particles calculated quantitatively using the Morisita index, I_δ, by dividing the observation area into small regions or quadrats of equal size [26, 34-38]. The value of I_δ is defined by the equation

$$I_\delta = q \cdot \delta \qquad (3.\ 2)$$

where q is the number of quadrats in the total observation area and δ is calculated as

$$\delta = \frac{\sum_{i=1}^{q} n_i(n_i-1)}{N(N-1)} \qquad (3.\ 3)$$

where n_i (i=1, 2, 3...q) is the number of the individual particles found in each quadrat and N is the total number of individual particles inside the observation area. This value is defined as

$$N = \sum_{i=1}^{q} n_i \qquad (3.\ 4)$$

Substituting the expression for δ into Eq. (3. 2) gives

$$I_\delta = q.\frac{\sum_{i=1}^{q} n_i(n_i-1)}{N(N-1)} \qquad (3.\ 5)$$

I_δ can be calculated from SEM images using Eq. (3. 5). Schematic illustrations of I_δ and of various distributions are shown in **Fig. 3.14**. The particle

distribution can be classified into three types such as Poisson's (random), uniform (regular) and aggregate distribution. When the calculated I_δ value become 1 and it indicates a Poisson distribution in which the particles are homogeneously distributed throughout the matrix, uniform and aggregate distributions obtained while I_δ values of less than and greater than 1.

In previous study, the spatial distributions of Al_3Ti particles in Al-Al_3Ti specimens deformed by MDF has been investigated using I_δ [26]. In addition, Watanabe *et al.* investigated the spatial distributions of $Al_{2.7}Fe_{0.3}Ti$ particles in refiners fabricated by powder metal route on the basis of an I_δ analysis [38]. Therefore, I_δ is evidently an effective means of assessing the distribution of the Al_3Ti particles following ECAP specimens in this study.

Figure 3.15 shows I_δ values of the Al_3Ti particles in the ECAPed Al-Al_3Ti composites up to 8 passes under routes A and B_c as a function of the number of quadrats. It is found that the I_δ values were close to 1 before ECAP. However, the Al_3Ti particles are fragmented and dispersed in the matrix and so the I_δ values were increased after 1 pass. ECAP under both routes up to 4 passes, the fragmented particles were increasingly dispersed and the I_δ remained above 1 as shown in **Fig. 3.15**. Particularly, the I_δ value of the ECAPed Al-Al_3Ti composites using route B_c increased after 3 passes and then decreased after 4 passes, while that of the specimen ECAP processed under route A decreased after 2 passes. Furthermore, after 5 passes, the I_δ values obtained using both processing routes decreased and approached 1 with increases in the number of ECAP passes. This result indicates that the fragmented Al_3Ti particles were start to disperse homogeneously in the matrix after 5 passes. Therefore, I_δ values of the Al_3Ti particles in the Al-Al_3Ti composites ECAP processed up to 8 passes under routes A and B_c, associated with

aggregate distribution. It means that the size of each aggregate is small, and the particles have a Poisson's mode as shown in **Fig. 3.14**. However, the spatial distribution obtained from each pass is different between routes A and B_c. Moreover, this difference in spatial distribution of the Al_3Ti particles can be seen more clearly at the maximum number of quadrats (q=64). Because of this, the changes in the spatial distribution of Al_3Ti particles in the Al-Al_3Ti composites was discussed at the maximum number of quadrats in this study.

Figure 3.16 presents the changes in the I_δ values at the maximum number of quadrats (q=64) as a function of the number of ECAP passes. The I_δ values of the specimens after ECAP using route A are seen to decrease with increases in the number of ECAP passes. On the other hand, route B_c shows increase or decrease in the I_δ values with increasing the number of ECAP passes. Furthermore, the I_δ values for specimens ECAP processed using route B_c after 3 and 4 passes are higher than those for route A specimens. This result is attributed to the tendency of the route B_c to form groups of fragmented Al_3Ti particles. After 5 passes both processing routes increased the particle homogeneity although, after 8 passes using route B_c, the specimens showed more homogenous distributions than those processed with route A. Summarizes variations in the shape of cubic elements induced by both ECAP processing routes was shown in **Fig. 3.17**. During ECAP is performed under route A, the cubic elements undergo continuous change only in the TD and RD planes, as shown in **Fig. 3.17**(a). These particles are fragmented by unidirectional shear deformation because of this, the fragmented Al_3Ti particles are distributed along the deformation axis. In contrast, **Fig. 3.17**(b) shows that the route B_c induces changes in the TD, RD and ND planes. However, during ECAP under route B_c the cubic element recovers its original shape after 4 passes and 8

passes. Because of this, the fragmented Al_3Ti particles form into groups. The calculated I_δ values for Al_3Ti particles in the deformed Al-Al_3Ti composite suggest that the spatial distributions various according to plastic flow of the α-Al matrix by ECAP. Sato and Watanabe studied that the distribution of fragmented Al_3Ti particles in Al-Al_3Ti composites during ECAP up to 4 passes appears to indicate plastic flow of the α-Al matrix and this phenomenon is in agreement with previous studies [33].

3.3.4 Controlling factor for Al_3Ti particles fragmentation

Tan and Zhang predicted the degree of homogeneity of granular SiC particle distributions obtained the standard secondary processing of an AA8090 metal-based composite [31]. Their study determined that during extrusion or rolling process of an AA8090 metal-based composite, the granular SiC particles and matrix were deformed together and the particle distribution became more homogenous. In addition, it was found that a uniform distribution of particles was obtained when the particle size was larger than a critical value. However, the similar deformation in the metal-based composites is obtained by secondary processing even at the high reduction ratios. Because of this, the solid particle distributions in composites by secondary processing are limited.

As discussed in **Sections 3.3.2** and **3.3.3**, large platelet Al_3Ti particles were distributed in the Al-Al_3Ti specimen before deformation. When the Al-Al_3Ti composites deformed using route A exhibited a consistent reduction in Al_3Ti particle size with increasing the number of ECAP passes. In addition, the fragmented Al_3Ti particles were distributed along the deformation because of the uniaxial shear. On the other hand, the fragmented Al_3Ti particles returned to their initial positions after 4 and 8 passes under route B_c and it did not result in consistent

reduction of the Al_3Ti particle size and. Furthermore, 8 passes of ECAP under route B_c produced a more homogenous distribution of Al_3Ti particles compared to route A because of the greater number of shearing directions. This results clearly reports that movement of the fragmented Al_3Ti particles was similar to that expected from material flow of the α-Al matrix. The distribution of Al_3Ti particles is determined by the appearance of material flow of the α-Al matrix after ECAP and distribution becomes significantly more homogeneous with increasing number of passes. Therefore, changes in the spatial distribution of the Al_3Ti particles in the Al-Al_3Ti composite depend on the material flow of the α-Al matrix during ECAP. In addition, fragmentation of the Al_3Ti particles can be controlled by the ECAP processing routes.

3.3.5 Initial microstructure of Al-Al_3Ti composite prepared by SPS

SEM micrographs showing initial microstructure of Al-Al_3Ti composites fabricated by SPS are shown in **Fig. 3.18**. **Figures 3.18** (a-c) are Al-Al_3Ti composites containing spherical Al_3Ti particles in the range of below 75 µm, 75-150 µm and 150-250 µm, respectively. As shown in **Fig. 3.18**, spherical Al_3Ti particles in all of specimens are uniformly distributed in the Al matrix. **Figures 3. 19** (a-c) are size distributions of the Al_3Ti particles in the Al-Al_3Ti composites containing spherical Al_3Ti particles in the range of below 75 µm, 75-150 µm and 150-250 µm, respectively. Furthermore, average diameters of the Al_3Ti particles obtained from **Fig. 3.19** are presented in **Table 3.1**. Average diameter of spherical Al_3Ti particles increases when the diameter of Al_3Ti particles increases. **Figure 3.20** shows the XRD of the Al-Al_3Ti composites which contain three different size spherical Al_3Ti particles. XRD traces of the Al-Al_3Ti composites for all the

specimens indicates the peak pattern of the Al_3Ti with $D0_{22}$ structure and Al with fcc structure. It is concluded that Al-Al_3Ti composite which contains spherical Al_3Ti particles with $D0_{22}$ structure was successfully fabricated by the SPS technique. Using this Al-Al_3Ti composites ECAP is carried out.

3.3.6 Microstructural changes of spherical Al_3Ti particles in the Al-Al_3Ti composites by ECAP

Figures 3.21 (a-c) are SEM photographs showing microstructure of Al-Al_3Ti composites containing spherical Al_3Ti particles in the range of below 75 μm, 75-150 μm and 150-250 μm, respectively after ECAP. As seen in **Fig. 3.21**, no cracks are observed on Al_3Ti particles in all of ECAPed Al-Al_3Ti composites. Moreover, Al_3Ti particles in ECAPed Al-Al_3Ti composites are not plastically deformed regardless of ECAP. This means that the spherical Al_3Ti particles in the Al-Al_3Ti composites are hardly fragmented by SPD. In previous studies, it is found reported that platelet Al_3Ti particles in the Al-Al_3Ti composites are fragmented by compression and ECAP processes [33, 41]. It is found that cracks generated along with the twin boundary-initiated fragmentation in the platelet Al_3Ti particles. According to those studies, cracks in the Al_3Ti particles are generated at deformation twin and propagate along with the twin boundary. Therefore, it is seen that the fragmentation behavior of Al_3Ti particles in the Al-Al_3Ti composite by SPD is different depending on the shape of Al_3Ti particles.

3.3.7 Spatial distribution of spherical Al_3Ti particles by ECAP

Using the Eq. (3. 5) and SEM micrographs, the spatial distributions of the Al_3Ti particles in ECAPed Al-Al_3Ti composites is evaluated. **Figure 3.22** (a) show the I_δ curves of Al_3Ti particles in Al-Al_3Ti composites by ECAPed Al-Al_3Ti

composites containing Al_3Ti particles with below 75 μm diameter respectively. Before deformation, the I_δ value is near to 1. When ECAP is performed for the Al-Al_3Ti composite, the Al_3Ti particles are aggregated in the Al matrix and the calculated I_δ value becomes higher than before deformation. **Figure 3.22** (b) is the I_δ curves of the Al-Al_3Ti composites containing Al_3Ti particles with 75-150 μm in diameter deformed by ECAP. From **Fig. 3.22** (b), difference of the I_δ caused by ECAP is not observed. It is seen that the Al-Al_3Ti composite with relatively higher Al_3Ti particles has homogenous distribution. **Figure 3.22** (c) shows the I_δ curves of 150-250 μm Al_3Ti particles in Al-Al_3Ti composites by ECAP. Before ECAP, the larger size Al_3Ti particles results the calculated I_δ less than 1. When ECAP is performed at 1 pass, the Al_3Ti particles in Al-Al_3Ti composite are aggregated in the Al matrix and the I_δ becomes more than 1.

When the particle size is smaller or larger to the matrix size the spatial distribution becomes aggregated distribution after SPD. However, when the particle is similar to the matrix size the spatial distribution arrangements becomes uniform distribution. Therefore, the change in the spatial distribution of spherical Al_3Ti particles in the Al-Al_3Ti composites depends on the particle size. In addition, the difference in the spatial distribution of the Al_3Ti particles in the deformed Al-Al_3Ti composite is controlled by the material flow of the matrix by ECAP.

3.3.8 Hencky equivalent strain of the SPS fabricated Al-Al_3Ti composites by ECAP

As discussed in the above section, the change in the spatial distribution of spherical Al_3Ti particles depends on the particle size in the Al-Al_3Ti composites. To clarify this reason, strain distribution of the Al-Al_3Ti composites deformed by ECAP is investigated. To compare the SPD caused by two different processing

techniques, logarithmic strain or true strain must be used [48-51]. Onaka has suggested that Hencky strain is suitable to present huge strain induced by SPD processing [50]. **Figure 3.23** (a) is a schematic representation of the simple shear deformation caused by ECAP. When an equiaxed grain with diameter *d* is deformed by simple shear deformation, equiaxed grain changes into an ellipsoidal grain with thickness *c* as shown in **Fig. 3.23** (a). At this time, Hencky equivalent strain (h_{equiv}) induced by this simple shear deformation can be derived as

$$h_{equiv} = \frac{1}{\sqrt{3}} \ln\left\{\frac{\left(2+\gamma^2+\gamma\sqrt{4+\gamma^2}\right)}{2}\right\} \quad (3.\ 6)$$

$$\gamma = \left(\frac{d}{c}\right) \quad (3.\ 7)$$

where γ is a nominal shear strain. *d* values measured form **Fig. 3.24** are presented in **Table 3.1**. The measured *c* values for the Al-Al_3Ti composites contain below 75 µm Al_3Ti particles, 75-150 µm Al_3Ti particles and 150-250 µm Al_3Ti particles are 36.7 µm, 27.4 µm and 24.8 µm, respectively. Using the Eq. (3. 6), h_{equiv} is calculated. **Figure 3.25** (a) presents the distribution of h_{equiv} as a function of Al_3Ti particles diameter. The h_{equiv} distribution of the Al-Al_3Ti composite contains below 75 µm spherical Al_3Ti particles is less compare to other the Al-Al_3Ti composites which contain large size spherical Al_3Ti particles. However, h_{equiv} distribution of the Al-Al_3Ti composites increases with the increase in Al_3Ti particles size. Moreover, the h_{equiv} distribution indicates that the higher simple shear deformation is measured in the Al-Al_3Ti composite which contains 150-250 µm spherical Al_3Ti particles as shown in **Fig. 3.25** (a). It clearly indicates that larger simple shear deformation occurs when the specimen has the large particle size among all the specimens.

3.3.9 The effect of Al_3Ti particles size on the stress concentration by ECAP

In previous studies, stress concentration developed by the particle was investigated [52-54]. When the simple shear deformation develops the internal stress σ in the Al_3Ti particle by ECAP. Stress concentration around the Al_3Ti particle is as same as the σ. Mori *et al.* have derived internal stress σ [52].

$$\sigma = A(c/r)\,\mu\beta^{*} \tag{3. 8}$$

$$A = \pi\,(2-\nu)/\,\{4(1-\nu)\} \tag{3. 9}$$

ν and μ are Poisson ratio and shear modulus of the particle, respectively. The particle with radius r and grain boundary thickness $2c$ is shown in **Fig. 3.26 (a)**. In this study, ECAP die introduces the nominal strain β^{*} of 1.01 per pass and the average Al_3Ti particles are shown in **Table 1**. Stress concentration as a function of the average diameter of Al_3Ti particles is shown in **Fig. 3.26 (b).** Stress concentration around the particles has notable change when the particle size changes. This indicates that stress concentration depends more strongly on the particle size during plastic deformation. In addition, the specimen with the smaller particle size have greater stress concentration. However, when the particle size increases there is a notable decrease in the stress concentration. Onaka *et al.* have reported that stress concentration develops more easily for smaller particles in the Cu-GeO_2 alloy [53]. Therefore, it is found that stress concentration develops more easily for the Al-Al_3Ti composite which has smaller Al_3Ti particles.

3.4 Conclusions

The microstructures and spatial distributions of Al_3Ti particles in an Al-Al_3Ti composite during ECAP were investigated. Specially, variations in the spatial distributions of Al_3Ti particles in the Al-Al_3Ti composite by ECAP using routes A and B_c up to 8 passes were examined. In addition, the stress concentration around the Al_3Ti particles in the Al-Al_3Ti composite were studied. The most important results can be summarized as follows:

(1) An Al-Al_3Ti composite containing large platelet Al_3Ti particles in an α-Al matrix was deformed by ECAP using routes A and B_c. The large platelet Al_3Ti particles were increasingly fragmented with increases in the number of ECAP passes.

(2) The fragmented particles produced via routes A and B_c were found to have different spatial distributions. The Al_3Ti particles in the specimen deformed using route A were aligned along the deformation axis, while particles in the specimens deformed with route B_c are formed into groups, and had relatively homogenous distributions.

(3) Increasing the number of ECAP passes, changed the Al_3Ti particle shape from platelet to granular. Due to particle fragmentation, the particle size decreased while the number density increased using routes A and B_c. Moreover, the average diameter of the Al_3Ti particles gradually decreased as the number of ECAP passes increased. In addition, ECAP at 8 passes using route B_c generated much smaller Al_3Ti particles size compared to route A. Because route B_c involved a greater number of shear planes and shear directions.

(4) Evaluation of the spatial distributions of Al_3Ti particles in the Al-Al_3Ti alloy based on I_δ values showed the aggregate distributions for both routes A and B_c.

After 5 passes using routes A and B_c, the homogeneity of the spatial distribution was increased. Moreover, 8 passes with route B_c produced a more homogeneous distribution compare to route A. Therefore, it is concluded that changes in the spatial distributions of Al_3Ti particles are dependent on the occurrence of material flow of the α-Al matrix during ECAP with routes A and B_c.

(5) The spherical Al_3Ti particles in the Al-Al_3Ti composite were not fragmented by ECAP. It is found that the spatial distributions of Al_3Ti particles in the Al- Al_3Ti composite deformed by ECAP results the aggregated distribution. The change in spatial distributions of spherical Al_3Ti particles depends on the particle size. Uniform distribution of spherical Al_3Ti particles in the Al-Al_3Ti composite obtained when the particles size was larger than critical size.

(6) Distribution of Hencky equivalent strain, h_{equiv}, indicates that the highest simple shear deformation occurs in the specimen which had the larger particle size by ECAP. It was found that stress concentration develops more easily for specimens with the smaller size particles compare to the specimens which have larger size particles. This means that the specimen with larger particles size were deformed more compare to the specimens which have smaller particle size.

References

[1] Y. Huang and T. G. Langdon, Advances in ultrafine grained materials, Mater. Today, **16** (2013) 85-93.

[2] T. G. Langdon, Twenty-five years of ultrafine-grained materials: achieving exceptional properties through grain refinement, Acta Mater., **61** (2013) 7035-7059.

[3] R. Z. Valiev, A. P. Zhilyaev and T. G. Langdon, Bulk nanostructured materials: fundamentals and applications, John Wiley & Sons, New Jersey, 1st ed. (2014) pp. 6.

[4] V. V. Stolyarov, Y. T. Zhu, I. V. Alexandrov, T. C. Lowe and R. Z. Valiev, Influence of ECAP routes on the microstructure and properties of pure Ti, Mater. Sci. Eng. A, **299** (2001) 59-67.

[5] W. J. B. Filho, J. B. Fogagnolo, C. A. D. Rogdrigues, C. S.Kiminami, C. Bolfarini and A. R. Yavari, Consolidation of partially amorphous aluminium alloy powders by severe plastic deformation, Mater. Sci. Eng. A, **375** (2004) 936-941.

[6] I. Sabirov, O. Kolednik and R. Pippan, Homogenization of metal matrix composites by high-pressure torsion, Metall. Mater. Trans. A, **36A** (2005) 2861-2870.

[7]S-H. Joo, S. C. Yoon, C. S. Lee, D. H. Nam, S. H. Hong and H. S. Kim, Microstructure and tensile behavior of Al and Al-matrix carbon nanotube composites processed by high pressure torsion of the powders, J. Mater. Sci., **45** (2010) 4652-4658.

[8] M. Furukawa, Y. Iwahashi, Z. Horita, M. Nemoto and T. G. Langdon, The shearing characteristics associated with equal-channel angular pressing, Mater. Sci. Eng. A, **257** (1992) 328-332.

[9] Y. Iwahashi, J. Wang, Z. Horita, M. Nemoto and T. G. Langdon, Principle of equal-channel angular pressing for the processing of ultrafine-grained materials, Scr. Mater., **35** (1996) 143-146.

[10] K. Nakashima, Z. Horita, M. Nemoto and T. G. Langdon, Influence of channel angle on the development of ultrafine grains in equal-channel angular pressing, Acta Mater., **46** (1998) 1589-1599.

[11] M. Murayama, Z. Horita and K. Hono, Microstructure of two-phase Al–1.7 at% Cu alloy deformed by equal-channel angular pressing, Acta Mater., **49** (2001) 21–29.

[12] S-Y. Chang, K-S. Lee, S. K. Ryu, K. T. Park and D. H. Shin, Effect of equal channel angular pressing on the distribution of reinforcements in the discontinuous metal matrix composites, Mater. Trans., **43** (2002) 757-761.

[13] C. Xu, M. Furukawa, Z. Horita and T. G. Langdon, The evolution of homogeneity and grain refinement during equal-channel angular pressing: a model for grain refinement in ECAP, Mater. Sci. Eng. A, **398** (2005) 66-76.

[14] I. Sabirov, O. Keolednik, R. Z. Valiev and R. Pippan, Equal channel angular pressing of metal matrix composites: effect on particle distribution and fracture toughness, Acta Mater., **53** (2005) 4919-4930.

[15] Z. Zhang, Y. Watanabe, I. S. Kim, X. Liu and X. Bian, Microstructure and refining performance of an Al-5Ti-0.25C refiner before and after equal-channel angular pressing, Metall. Mater. Trans. A, **36A** (2005) 837-844.

[16] Z. Zhang, S. Hosoda, I. S. Kim and Y. Watanabe, Grain refining performance for Al and Al-Si alloy casts by addition of equal-channel angular pressed Al-5mass%Ti alloy, Mater. Sci. Eng. A, **425** (2006) 55-63.

[17] R. Z. Valiev and T. G. Langdon, Principles of equal-channel angular pressing as a processing tool for grain refinement, Prog. Mater. Sci., **51** (2006) 881-981.
[18] C. Xu and T. G. Langdon, The development of hardness homogeneity in aluminum and an aluminum alloy processed by ECAP, J. Mater. Sci., **42** (2007) 1542-1550.
[19] M. Reihanian, R. Ebrahimi, M. M. Moshksar, D. Terada and N. Tsuji, Microstructure quantification and correlation with flow stress of ultrafine grained commercially pure Al fabricated by equal channel angular pressing (ECAP), Mater. Charact., **9** (2008), 1312-1323.
[20] O. Sitdikov, T. Sakai, E. Avtokratova, R. Kaibyshev, K. Tsuzaki and Y. Watanabe, Microstructure behavior of Al-Mg-Sc alloy processed by ECAP at elevated temperature, Acta Mater., **56** (2008) 821-834.
[21] M. Zha, Y. Li, R. H. Mathiesen, R. Bjorge and H. J. Roven, Microstructure evolution and mechanical behavior of a binary Al–7Mg alloy processed by equal-channel angular pressing, Acta Mater., **84** (2015) 42-54.
[22] M. Howeyze, H. Arabi, A. R. Eivani and H. R. Jafarian, Strengthening of AA5052 aluminum alloy by equal channel angular pressing followed by softening at room temperature, Mater. Sci. Eng. A, **720** (2018) 160-168.
[23] A. Esmaeili, M. H. Shaeri, M. T. Noghani and A. Razaghian, Fatigue behavior of AA7075 aluminium alloy severely deformed by equal channel angular pressing, J. Alloy. Comp., **757** (2018) 324-332.
[24] H. Miura, Y. Nakao and T. Sakai, Enhanced grain refinement by mechanical twinning in a bulk Cu-30 mass%Zn during multi-directional forging, Mater. Trans., **48** (2007) 2539-2541.
[25] Q. Zhu, L. Li, Z. Zhang, Z. Zhao, Y. Zuo and J. Cui, Microstructure evolution of AZ80 magnesium alloy during multi-directional forging process, Mater. Trans., **55** (2014) 270-274.
[26] H. Sato, F. Teshima and Y. Watanabe, Effects of forging temperature on Al_3Ti particle distribution in Al-Al_3Ti multi-phase materials deformed by multi-directional forging, J. J. I. L. M., **68** (2018) 2-8 (in Japanese).
[27] S.H. Leea, Y. Saitoa, N. Tsujib, H. Utsunomiyaa and T. Sakai, Role of shear strain in ultra-grain refinement by accumulative roll-bonding (ARB) process, Scr. Mater., **46** (2002) 281-285.
[28] M. Eizadjou, H. D. Manesh and K. Janghorban, Microstructure and mechanical properties of ultra-fine grains (UFGs) aluminum strips produced by ARB process, J. Alloy. Comp., **474** (2009) 406-415.
[29] R. Jamaati and M. R. Toroghinejad, Manufacturing of high-strength aluminum/alumina composite by accumulative roll bonding, Mater. Sci. Eng. A, **527** (2010) 4146-4151.
[30] M. Shantharaj, Mechanical behaviour of pure aluminum processed by constrained groove pressing, J. Material. Sci. Eng., **2** (2013) 125-130.
[31] M. J. Tan and X. Zhang, Powder metal matrix composites: selection and processing, Mater. Sci. Eng. A, **244** (1998) 80-85.
[32] Y. Watanabe, P. D. Sequeira, O. Sitdikov, H. Sato and Z. Zhang, I. S. Kim, Effect of processing route on microstructure and texture development in ECAP of Al-Ti alloy, Mat. Sci. Forum., **561** (2007) 251-254.
[33] H. Sato and Y. Watanabe, Three-dimensional microstructural analysis of fragmentation behavior of platelet Al_3Ti particles in Al-Al_3Ti composite deformed by equal-channel angular pressing, Mater. Charact., **144** (2018) 305-315.
[34] M. Morisita, Measuring of the dispersion and analysis of distribution patterns,

Mem. Fac. Kyushu Univ., E **2**, (1959) 215-235.
[35] M. Morisita, I_δ-index, A measure of dispersion of individuals, Res. Popul. Ecol., **4** (1962) 1-7.
[36] M. Morisita, Composition of the I_δ-index, Res. Popul. Ecol., **13** (1971) 1-27.
[37] M. K. Amaral, S. N. Pellico, C. Lingnau and A. F. Figueiredo, Evaluation of the morisita index for determination of the spatial distribution of species in a fragment of aracuaria forest, Appl. Ecol. Envir. Res., **13** (2014) 361-371.
[38] Y. Watanabe, S. Taniai and H. Sato, Fabrication of grain refiners with a high-volume fraction of $Al_{2.7}Fe_{0.3}Ti$ heterogeneous nucleation site particles by spark plasma sintering, Jpn. J. Appl. Phys., **58** (2019) SAA0C4(9 pages).
[39] Y. Watanabe, N. Yamanaka and Y. Fukui, Wear behavior of Al-Al_3Ti composite manufactured by centrifugal method, Metall. Mater. Trans. A, **30A** (1999), 3253-3261.
[40] Y. Watanabe, H. Eryu and K. Matsuura, Evaluation of three-dimensional orientation of Al_3Ti platelet in Al based FGMs fabricated by a centrifugal casting technique, Acta Mater., **49** (2001) 775-783.
[41] S. B. Duraisamy, H. Sato, T. Chiba and Y. Watanabe, Fragmentation process of platelet Al_3Ti particles in compressed Al-Al_3Ti alloy observed by serial sectioning and EBSD analysis, Mater. Res. Express, **6** (2019) 096575 1-8.
[42] Y. Watanabe, P. D. Sequeira, H. Sato, T. Inamura and H. Hosoda, Aluminum matrix texture in Al-Al_3Ti functionally graded materials analyzed by electron back-scattering diffraction, Jpn. J. Appl. Phys., **55** (2016) 01AG03(7 pages).
[43] Y. Watanabe, Q. Zhou, H. Sato, T. Fujii and T. Inamura, Microstructure of Al-Al_3Ti functionally graded materials fabricated by centrifugal solid-particle method and centrifugal in situ method, Jpn J. Appl. Phys., **56** (2017) 01AG01(11 pages).
[44] C. Moussa, M. Bernacki, R. Besnard and N. Bozzolo, About quantitative EBSD analysis of deformation and recovery substructures in pure tantalum, Mater. Sci. Eng., **89** (2015) 1-7.
[45] M. F. Ashby, The deformation of plastically non-homogeneous materials, Philos. Mag., **21** (1969) 399-424.
[46] E. Demir, D. Raabe, N. Zaafarani and S. Zaefferer, Investigation of the indentation size effect through the measurement of the geometrically necessary dislocations beneath small indents of different depths using EBSD tomography, Acta Mater., **57** (2009) 559-569.
[47] S. Wronski, J. Tarasiuk, B. Bacroix, K. Wierzbanowski and H. Paul, Microstructre heterogeneity after the ECAP process and its influence on recrystallization in aluminium, Mater. Charact., **78** (2013) 60-68.
[48] H. Hencky and Z. Tech. Phys., **9** (1928) 214-247 (in German).
[49] J. H. Dautzenberg and J. H. Zaat, Quantitative determination of deformation by sliding wear, Wear, **23** (1973) 9-19.
[50] S. Onaka, Equivalent strain in simple shear deformation described by using the Hencky strain, Philos. Mag. Lett., **90** (2010) 633-639.
[51] V. M. Segal, Equivalent and effective strains during severe plastic deformation (SPD), Philos. Mag. Lett., **98** (2019) 511-520.
[52] T. Mori, M. Koda and R. Monzen, Particle blocking in grain boundary sliding and associated internal friction, Acta Metall., **31** (1983) 275-283.
[53] S. Onaka, M. Kato and R. Tanaka, Intermediate temperature embrittlement of dispersion hardened Cu-GeO_2 polycrystals, Trans. J. I. M., **28** (1987) 32-40.
[54] S. Bidhar, O. Kuwazuru, Y. Shiihara, Y. Hangai, T. Utsunomiya, I. Watanabe

and N. Yoshikawa, Practical application of empirical formulation of the stress concentration factor around equally sized dual spherical cavities to aluminum die cast, Appl. Math. Model., **39** (2015) 881-893.

Table 3.1. The average diameters of spherical Al_3Ti particles and mean grain size of Al-Al_3Ti composites.

Specimen	Average diameter of spherical Al_3Ti particles	Mean grain size
Al-Al_3Ti composite contains below 75 μm Al_3Ti particles	19.6 μm	46.9 μm
Al-Al_3Ti composite contains 75-150 μm Al_3Ti particles	72.5 μm	46.7 μm
Al-Al_3Ti composite contains 150-250 μm Al_3Ti particles	152.1 μm	48.4 μm

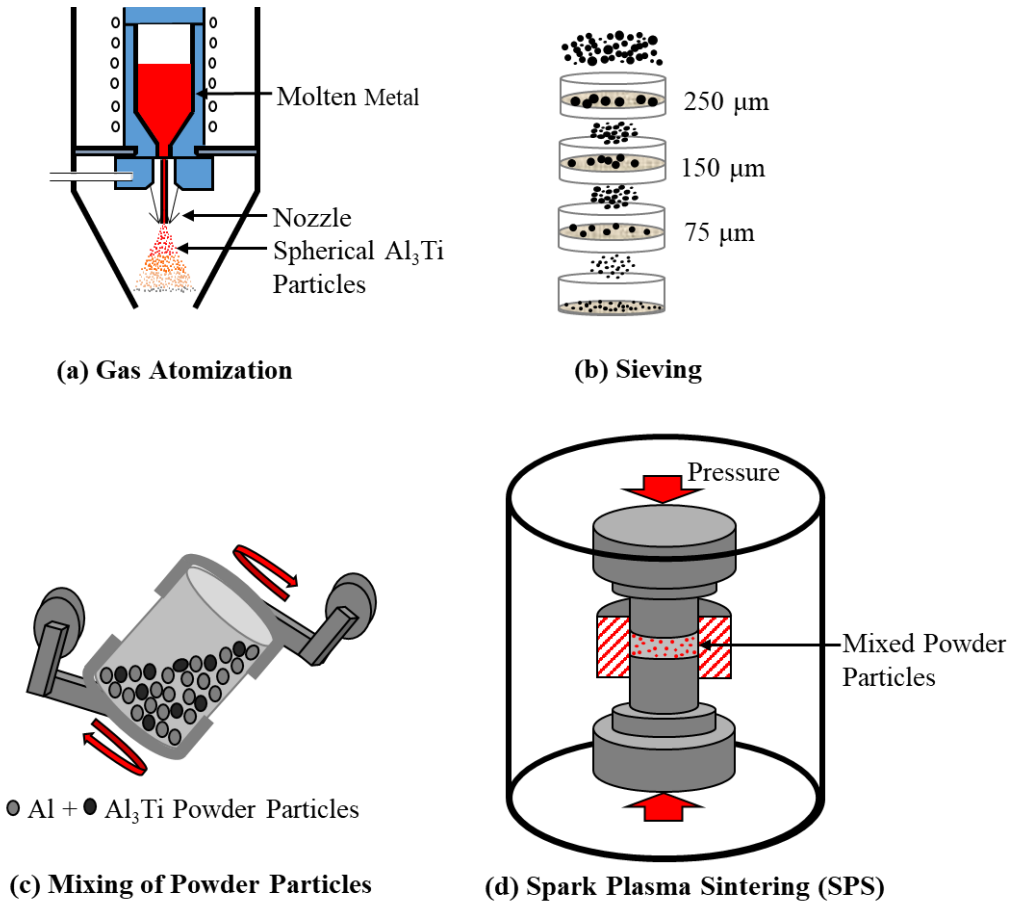

Fig. 3.1. Schematic illustration showing step by step fabrication procedure of Al-Al_3Ti composite.

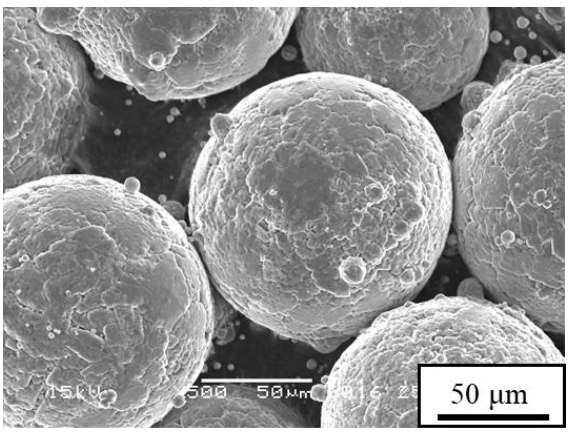

Fig. 3.2. SEM image of spherical Al_3Ti particles fabricated by gas atomization.

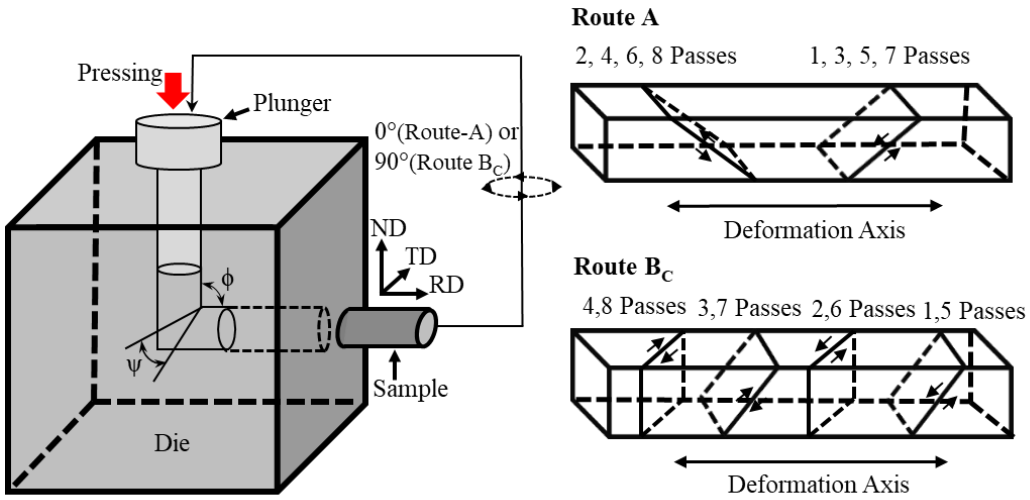

Fig. 3.3. Schematic representations of the ECAP die and the shearing patterns generated during ECAP routes A and B_c.

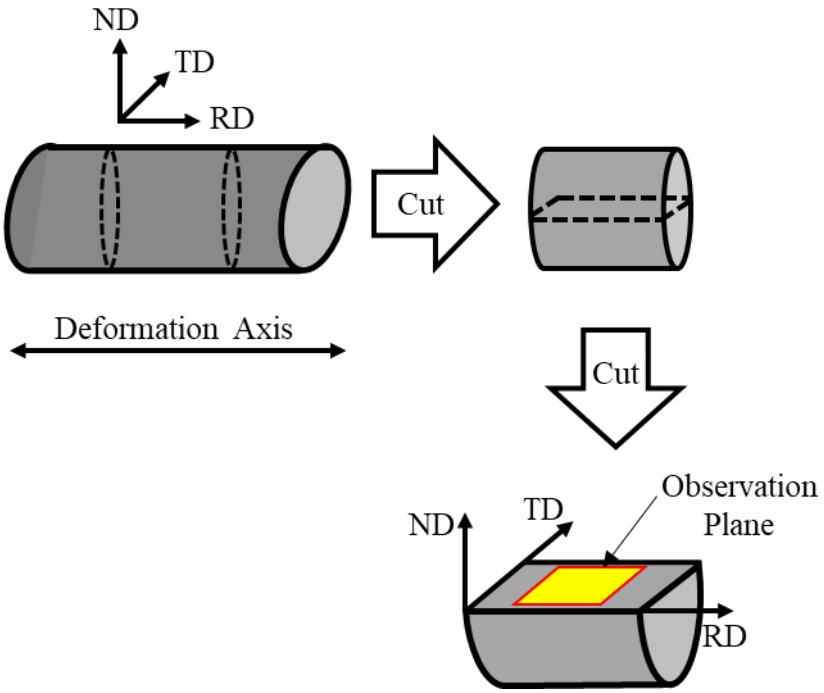

Fig. 3.4. The specimen coordinate system for microstructural observations of the Al-Al_3Ti composites during ECAP.

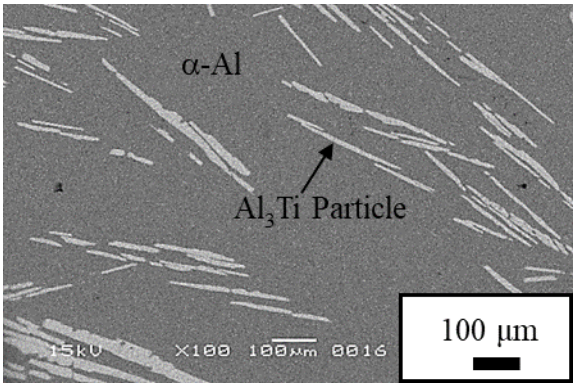

Fig. 3.5. An SEM photograph showing the microstructure of an Al-Al_3Ti composite that before ECAP.

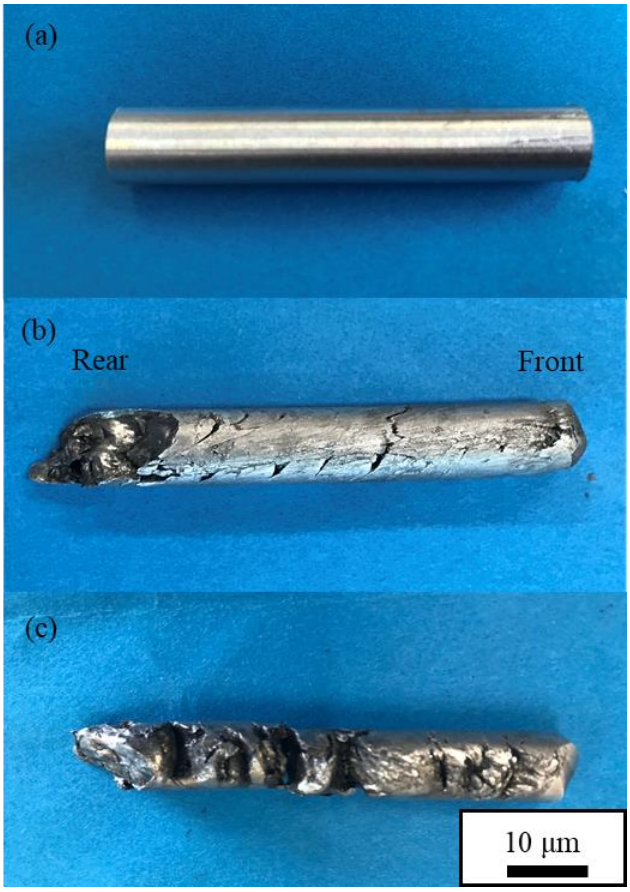

Fig. 3.6. The rod-shaped Al-Al_3Ti specimens used for ECAP- (a) before processing and after eight passes employing routes (b) A and (c) B_c.

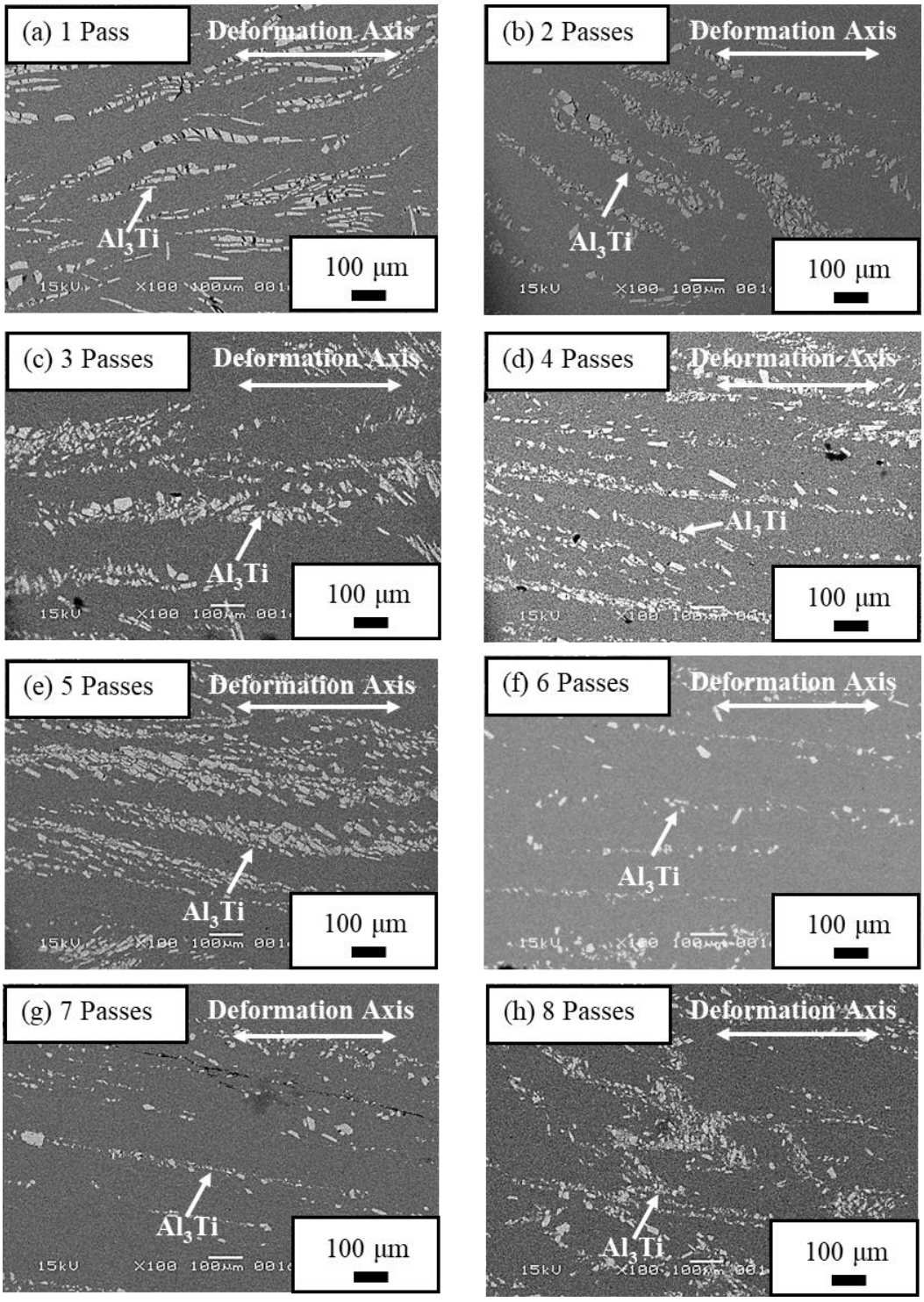

Fig. 3.7. SEM photographs showing the microstructures of Al-Al_3Ti composites by ECAP under route A (a) 1 pass, (b) 2 passes, (c) 3 passes, (d) 4 passes, (e) 5 passes, (f) 6 passes, (g) 7 passes and (h) 8 passes.

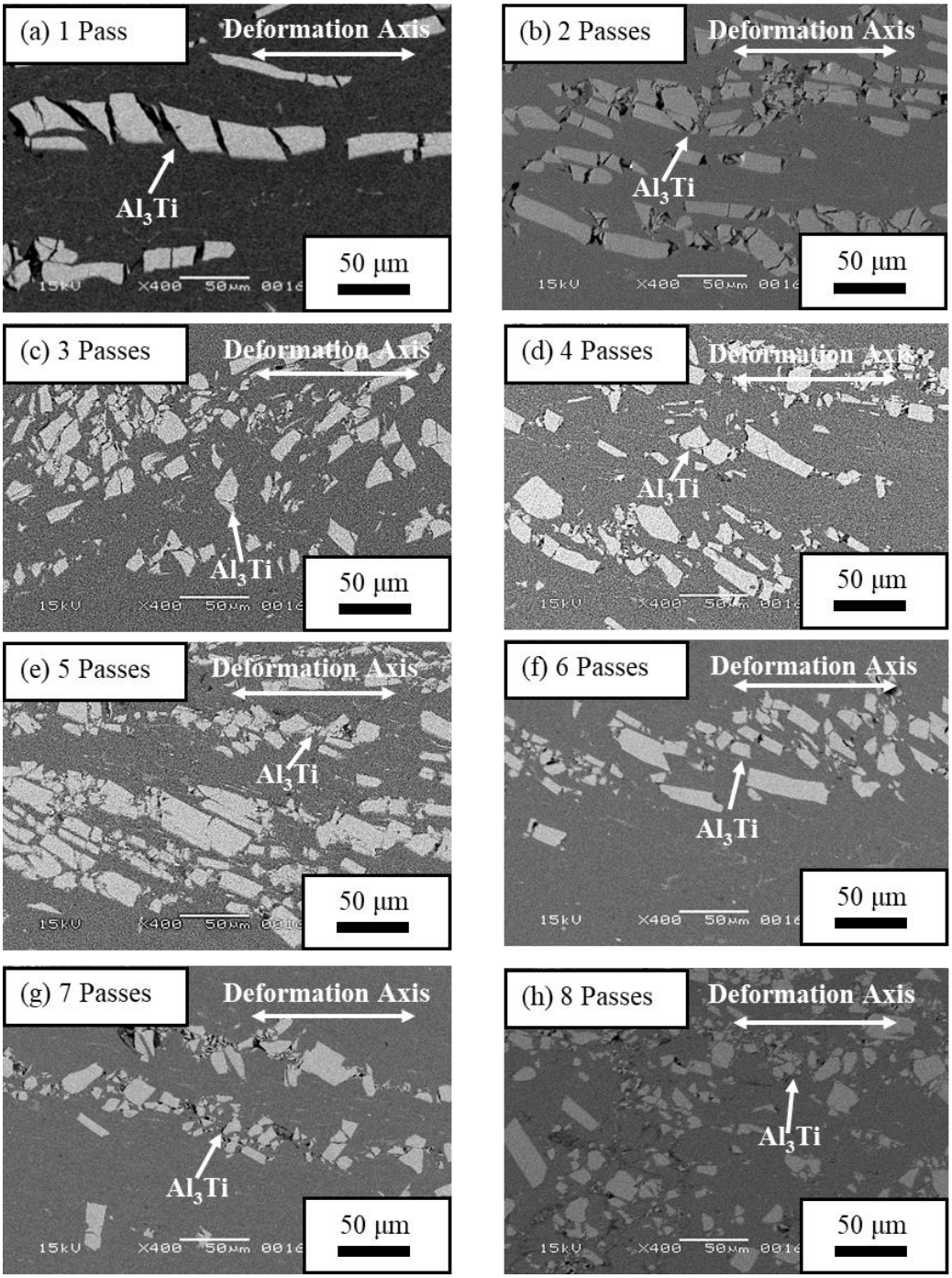

Fig. 3.8. High-magnification SEM photographs showing the microstructures of Al-Al_3Ti composites by ECAP under route A (a) 1 pass, (b) 2 passes, (c) 3 passes, (d) 4 passes, (e) 5 passes, (f) 6 asses, (g) 7 passes and (h) 8 passes.

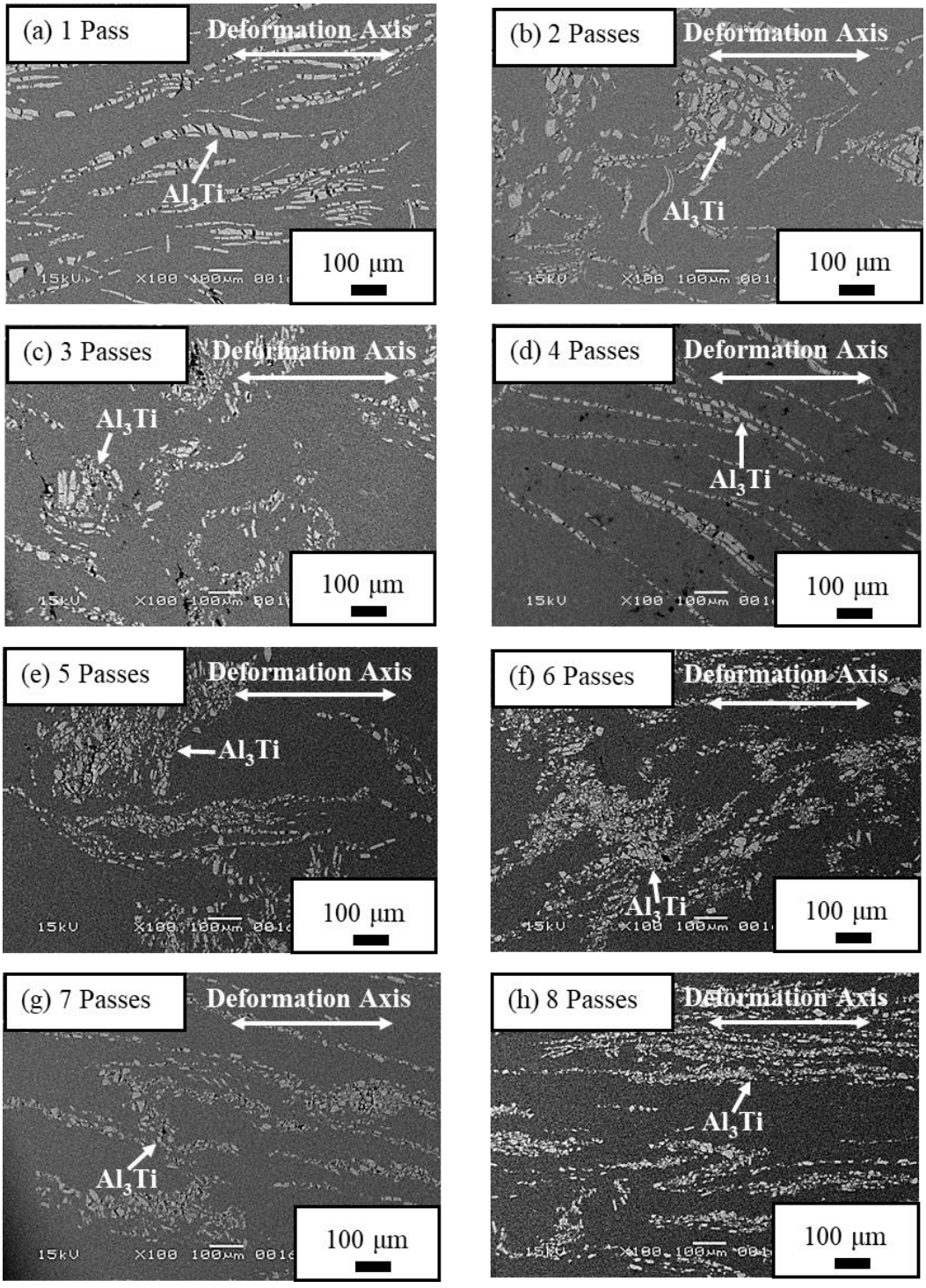

Fig. 3.9. SEM photographs showing the microstructures of Al-Al_3Ti composites by ECAP under route B_c (a) 1 pass, (b) 2 passes, (c) 3 passes, (d) 4 passes, (e) 5 passes, (f) 6 passes, (g) 7 passes and (h) 8 passes.

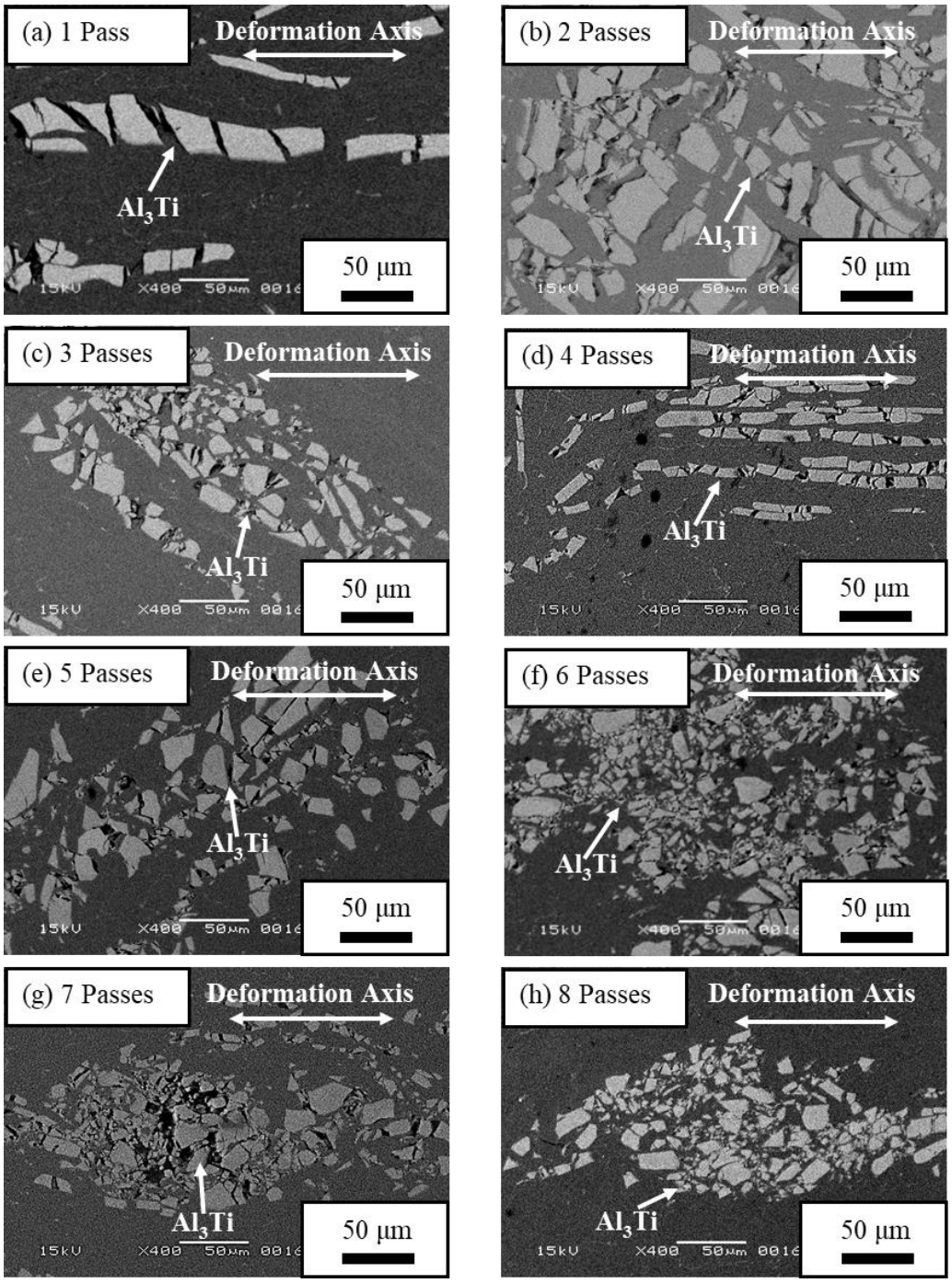

Fig. 3.10. High-magnification SEM photographs showing the microstructure of Al-Al_3Ti composites by ECAP under route B_c (a) 1 pass, (b) 2 passes, (c) 3 passes, (d) 4 passes, (e) 5 passes, (f) 6 passes, (g) 7 passes and (h) 8 passes.

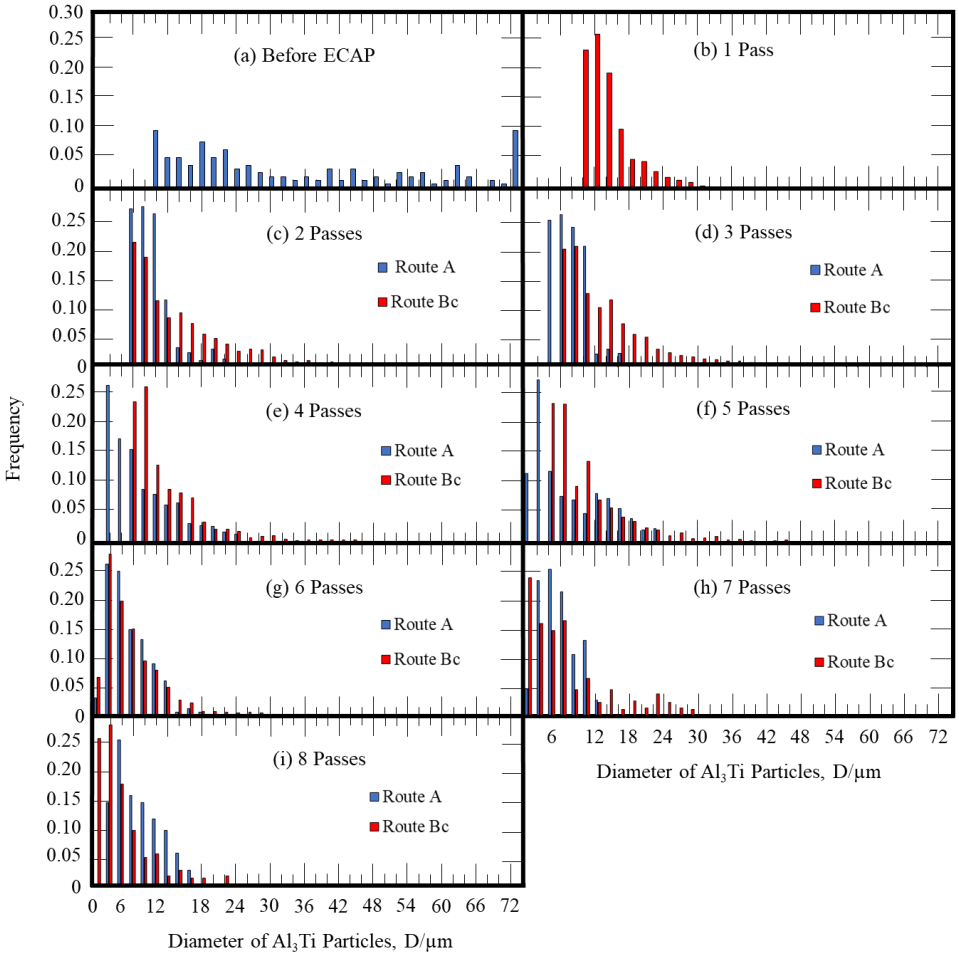

Fig. 3.11. Histograms of Al_3Ti particles diameters in Al-Al_3Ti composites by ECAP under routes A and B_c: (a) before ECAP, (b) 1 pass, (c) 2 passes, (d) 3 passes, (e) 4 passes, (f) 5 passes, (g) 6 passes, (h) 7 passes and (i) 8 passes. In addition, these diameters were calculated assuming that the Al_3Ti particles were circular.

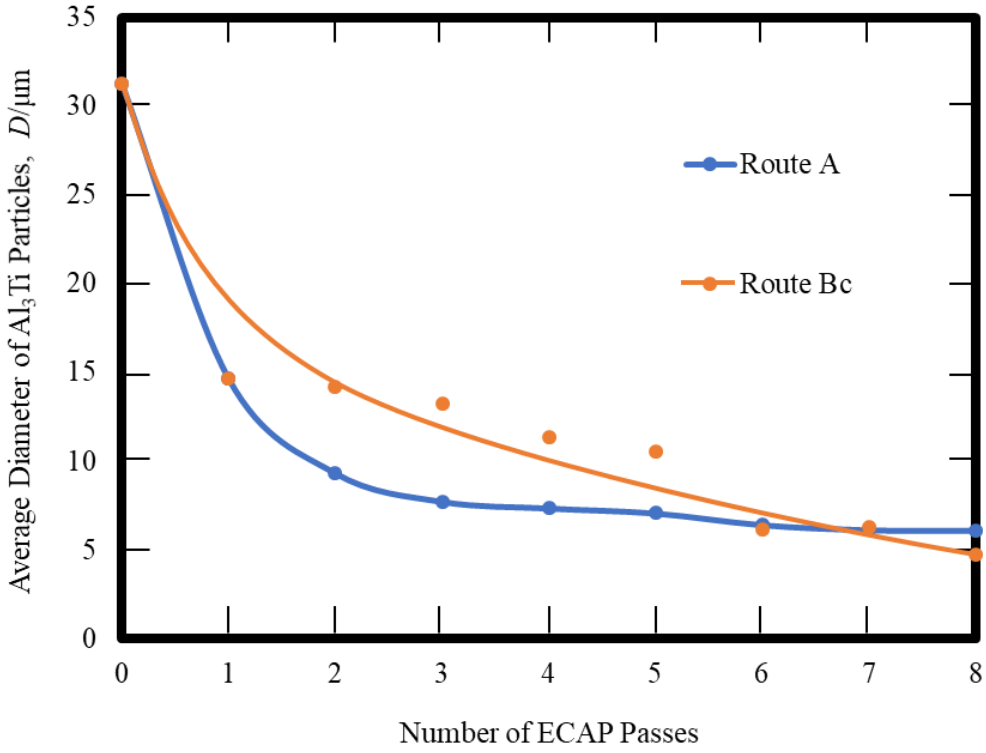

Fig. 3.12. The measured average diameters of Al_3Ti particles in Al-Al_3Ti composite by ECAP under routes A and B_c as functions of the number of passes.

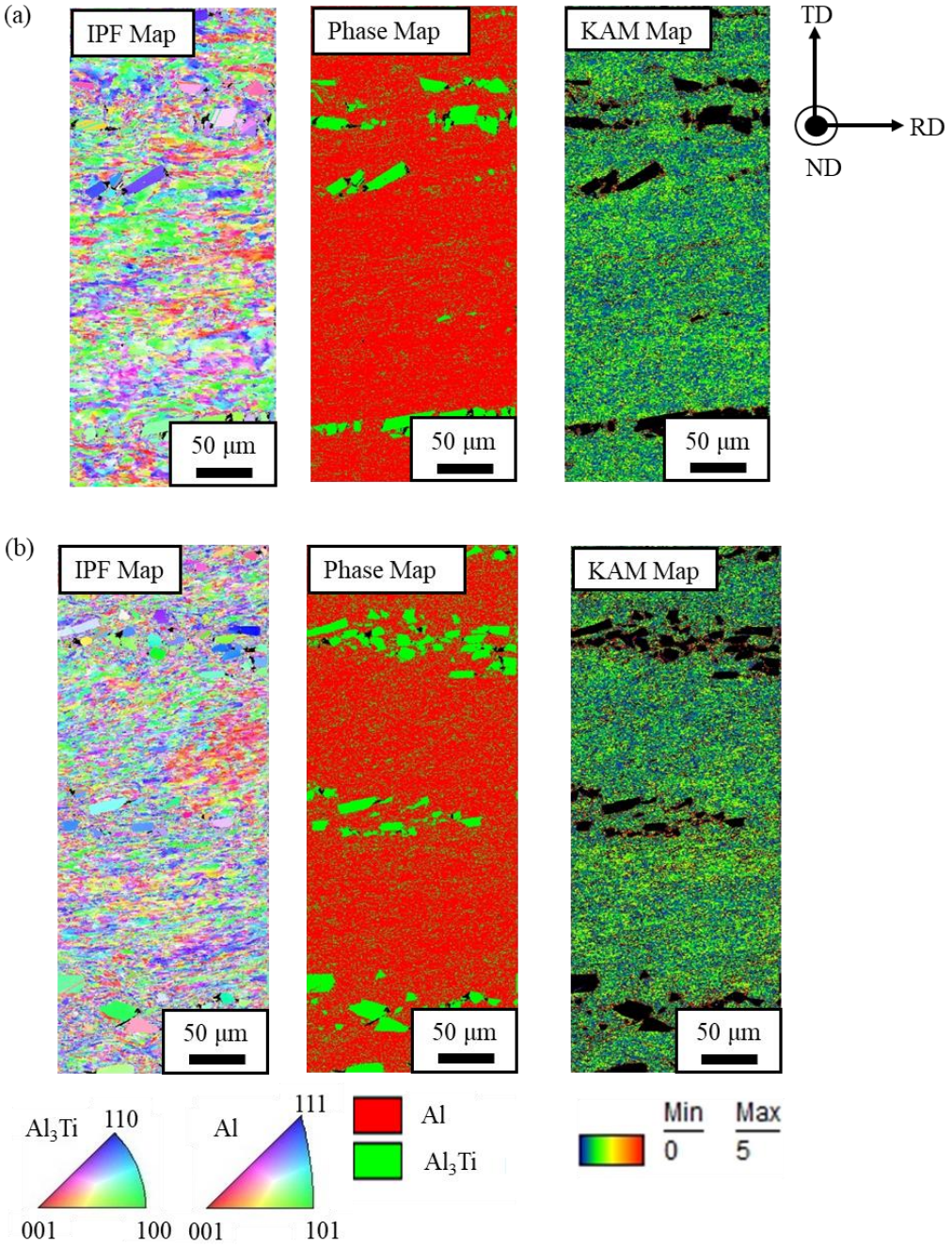

Fig. 3.13. (left) Inverse pole figure (IPF) maps, (center) phase maps and (right) kernel average misorientation (KAM) maps of Al-Al_3Ti composites after 8 passes of ECAP under routes (a) A and (b) B_c.

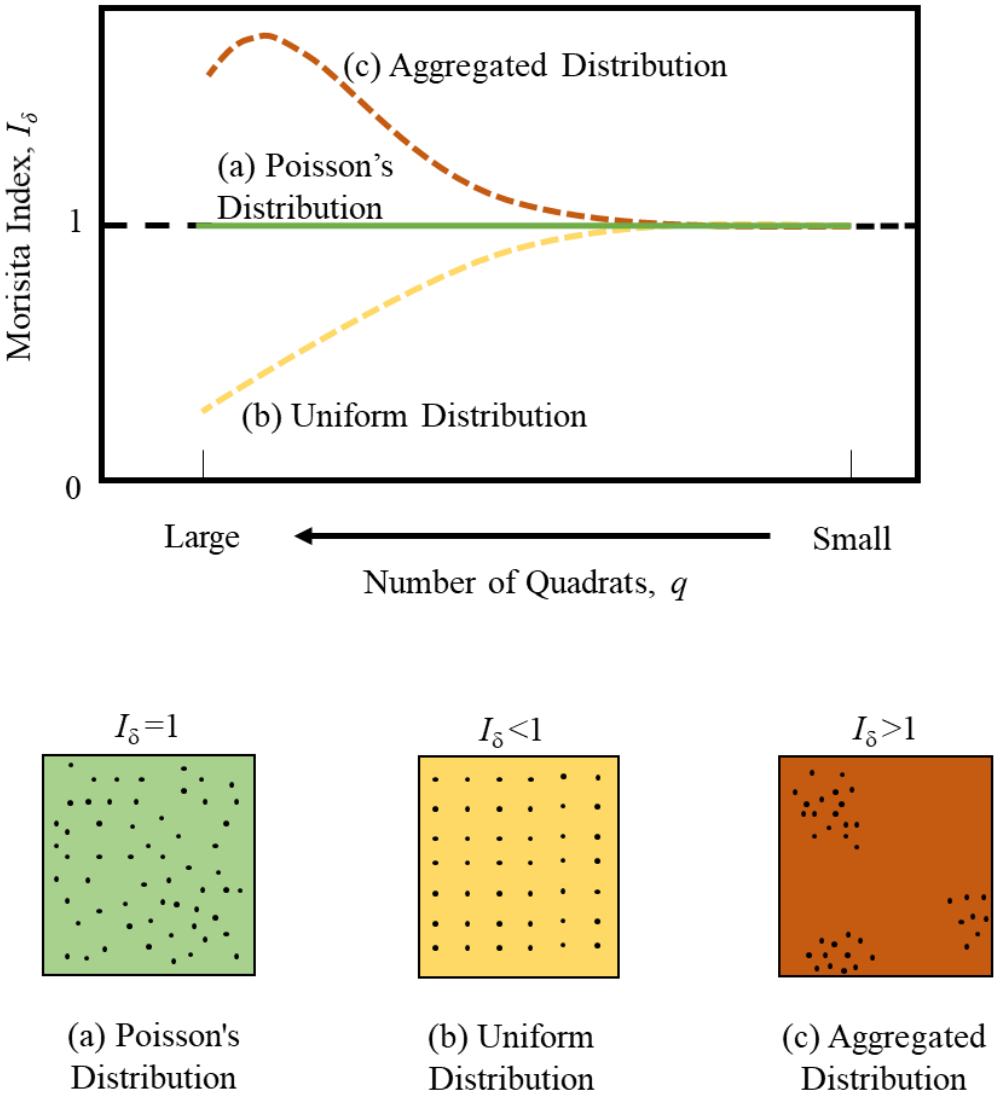

Fig. 3.14. A schematic representation showing variations in I_δ, as a function of the number of quadrats for the spatial distribution of particles (the straight horizontal line indicates a value of 1. The spatial distributions of particles for different I_δ values: (a) Poisson's, (b) uniform, and (c-f) aggregated distribution.

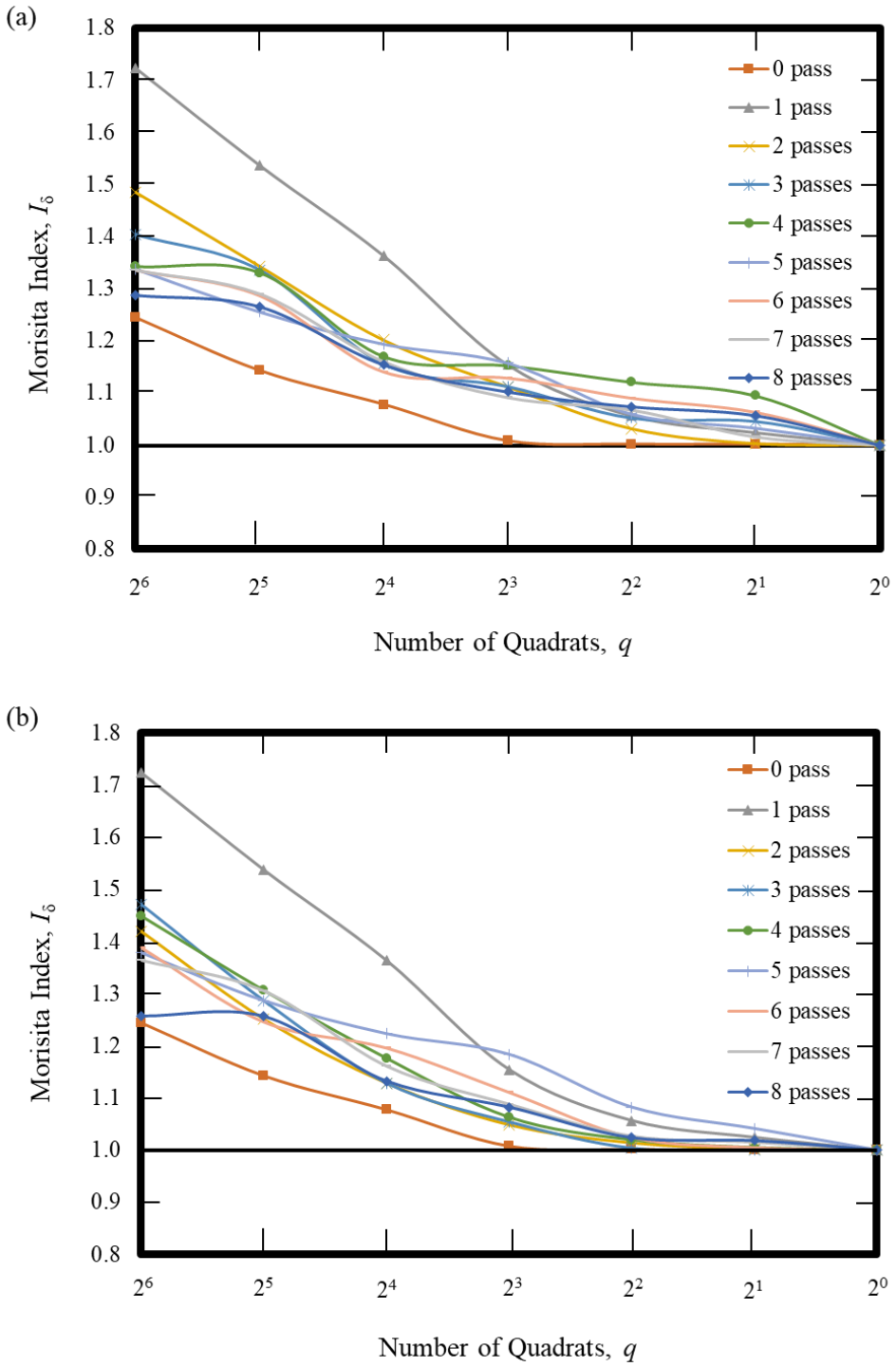

Fig. 3.15. I_δ values as functions of the number of quadrats for Al-Al_3Ti composite by ECAP under routes (a) A and (b) B_c.

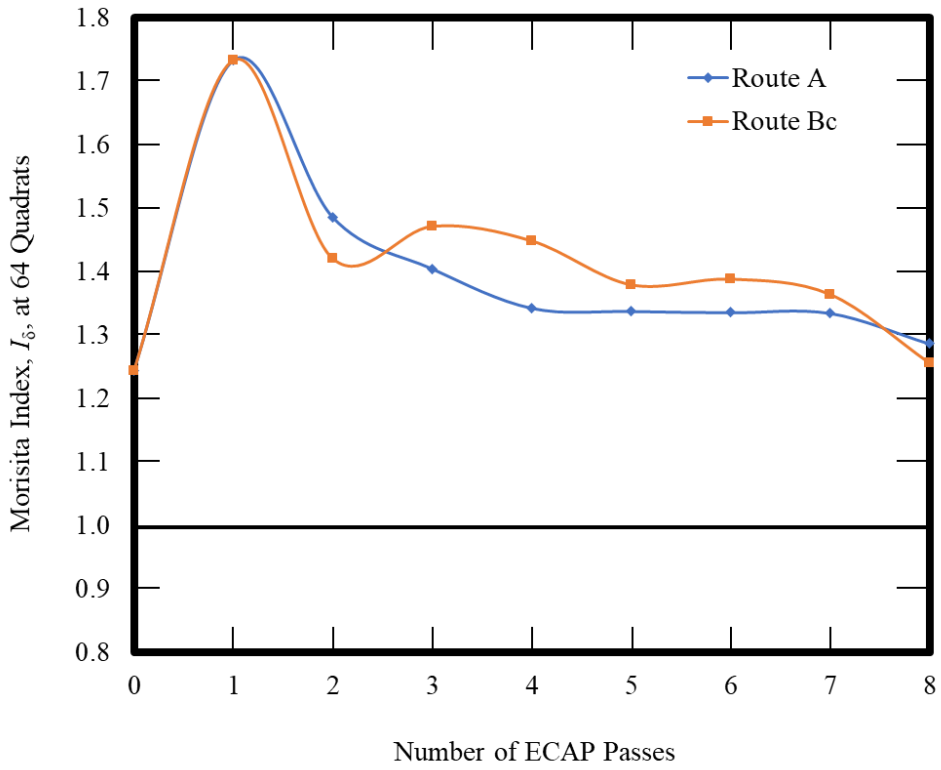

Fig. 3.16. I_δ values as functions of the number of ECAP passes for Al-Al_3Ti composites under routes A and B_c as determined using 64 quadrats.

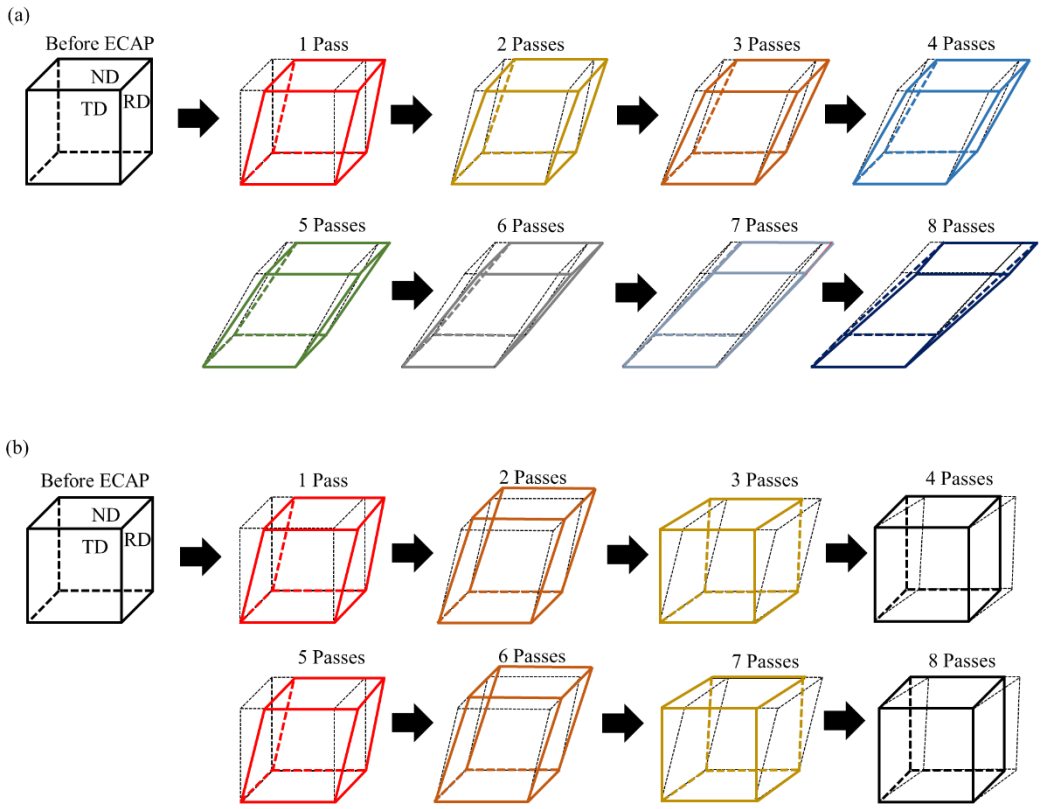

Fig. 3.17. Schematic representation of shearing applied to cubic elements during ECAP under routes (a) A and (b) B_c. Broken black lines indicates the shape of the cubic element formed by the previous passage. The three orthogonal planes of observation are RD, TD and ND.

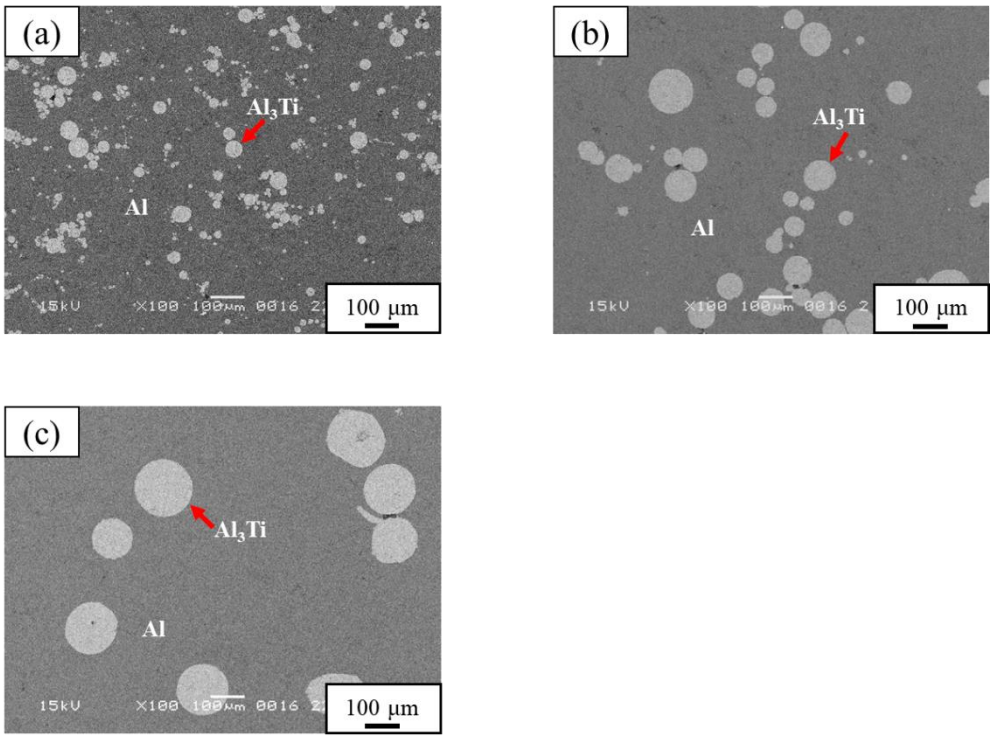

Fig. 3.18. SEM micrographs of an Al-Al_3Ti composites containing spherical shape Al_3Ti particles (a) below 75 μm Al_3Ti particles (b) 75-150 μm Al_3Ti particles and (c) 150-250 μm Al_3Ti particles.

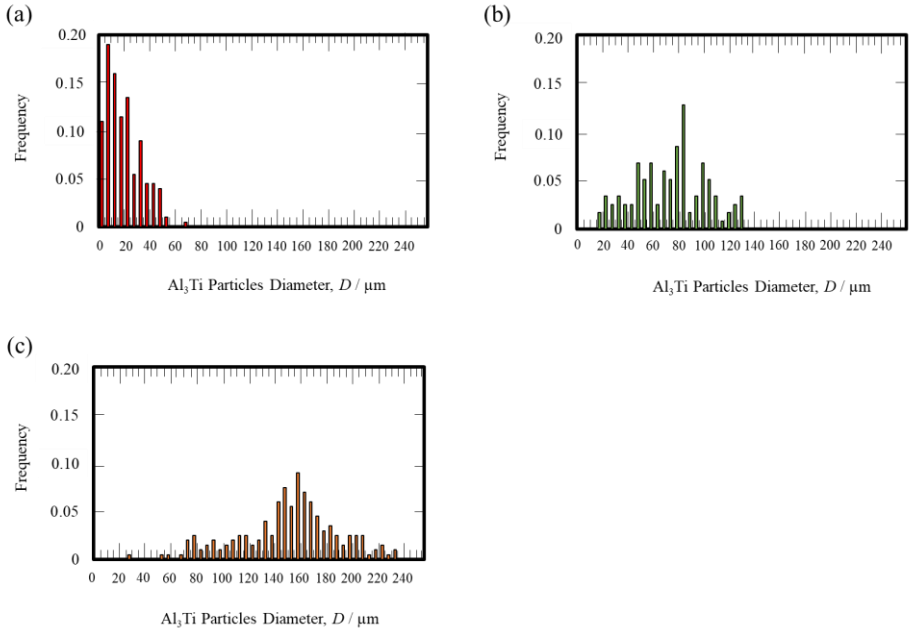

Fig. 3.19. Histograms summarizing the diameter distributions of spherical Al_3Ti particles in Al-Al_3Ti composites (a) below 75 μm Al_3Ti particles (b) 75-150 μm Al_3Ti particles and (c) 150-250 μm Al_3Ti particles.

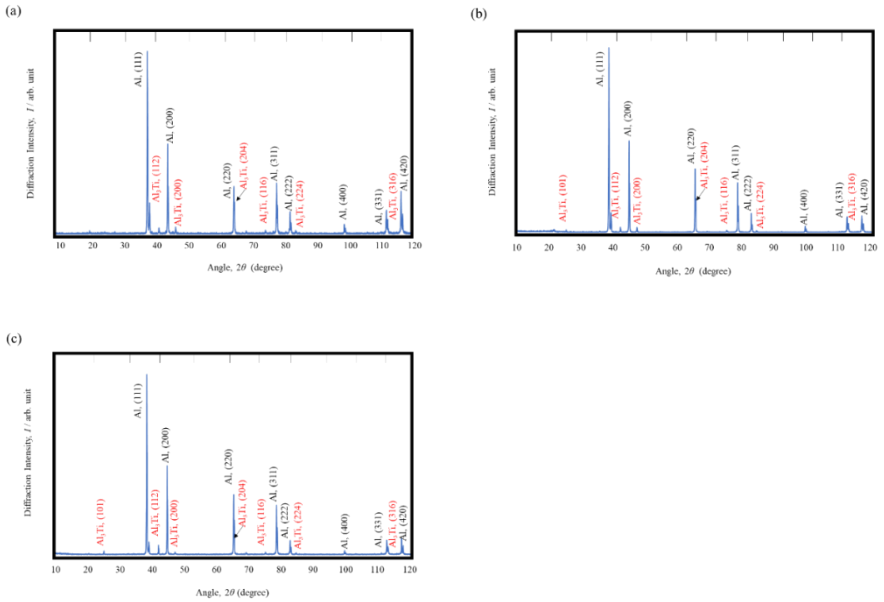

Fig. 3.20. XRD patterns for the Al-Al_3Ti composites contains spherical Al_3Ti particles (a) below 75 µm Al_3Ti particles (b) 75-150 µm Al_3Ti particles and (c) 150-250 µm Al_3Ti particles.

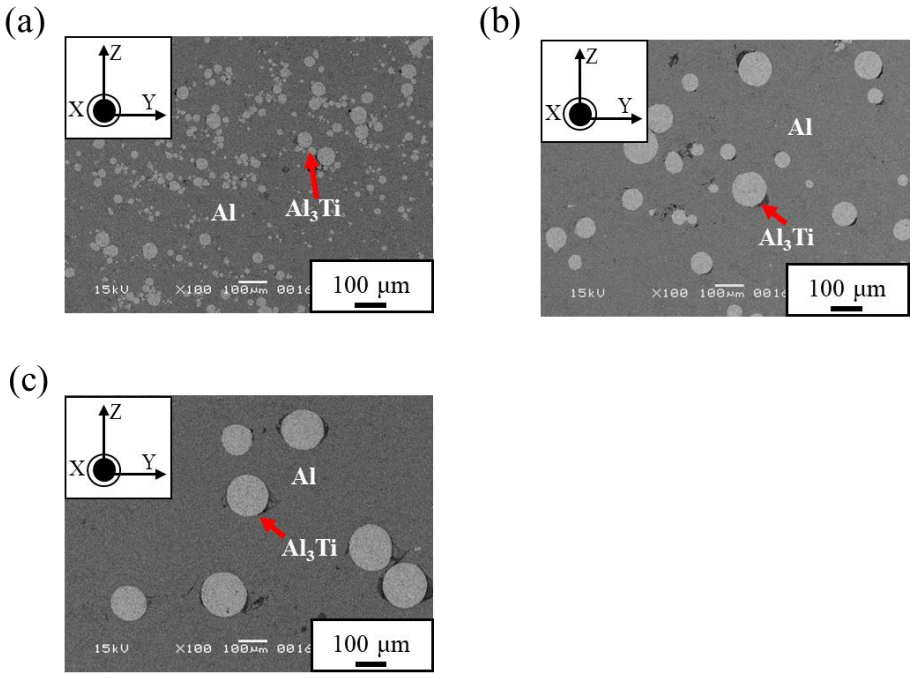

Fig. 3.21. SEM micrographs of Al-Al_3Ti composites after 1 pass of ECAP: (a) below 75 µm Al_3Ti particles, (b) 75-150 µm Al_3Ti particles and (c) 150-250 µm Al_3Ti particles.

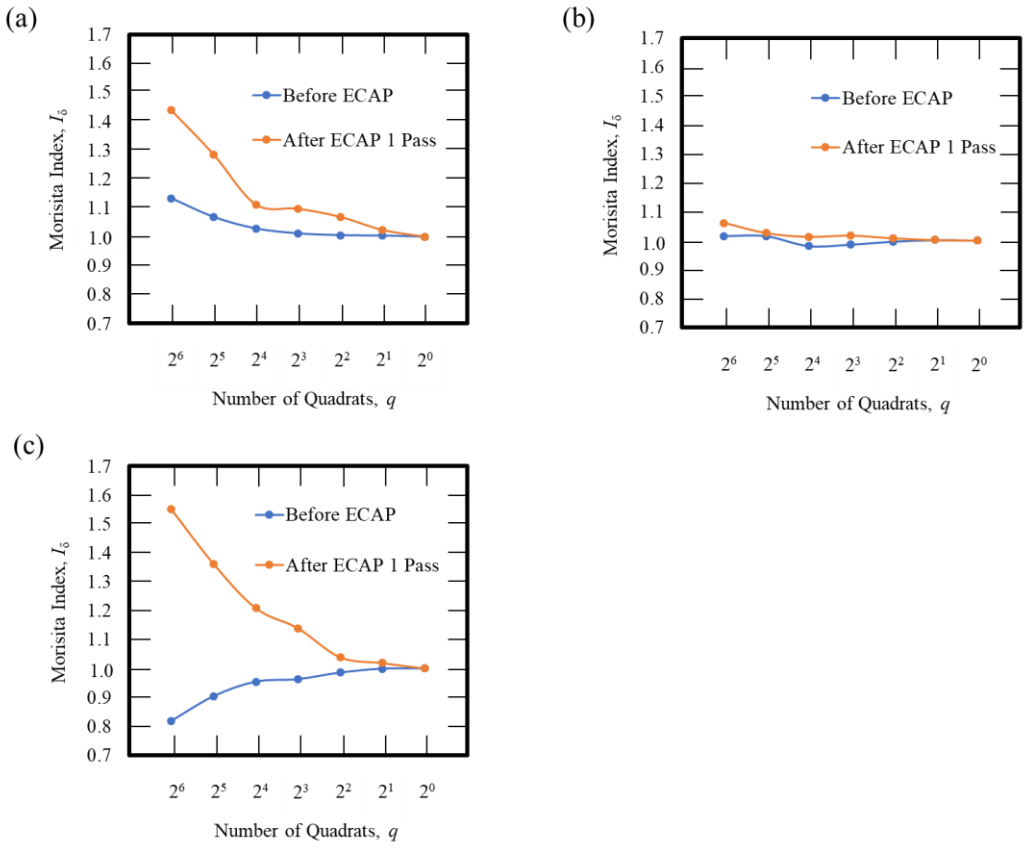

Fig. 3.22. I_δ values as functions of the number of quadrats for Al-Al_3Ti specimens contains spherical Al_3Ti particles processed by (a) ECAP below 75 µm Al_3Ti particles, (b) ECAP of 75-150 µm Al_3Ti particles and (c) ECAP of 150-250 µm Al_3Ti particles.

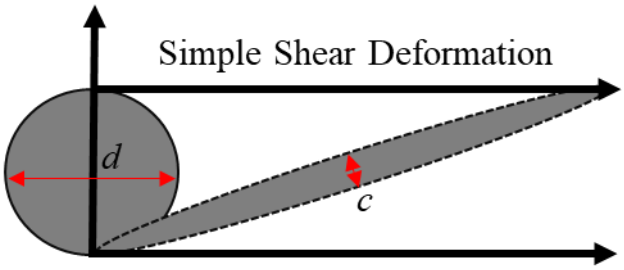

Fig. 3.23. Schematic illustrations of shape changes caused by simple shear deformation.

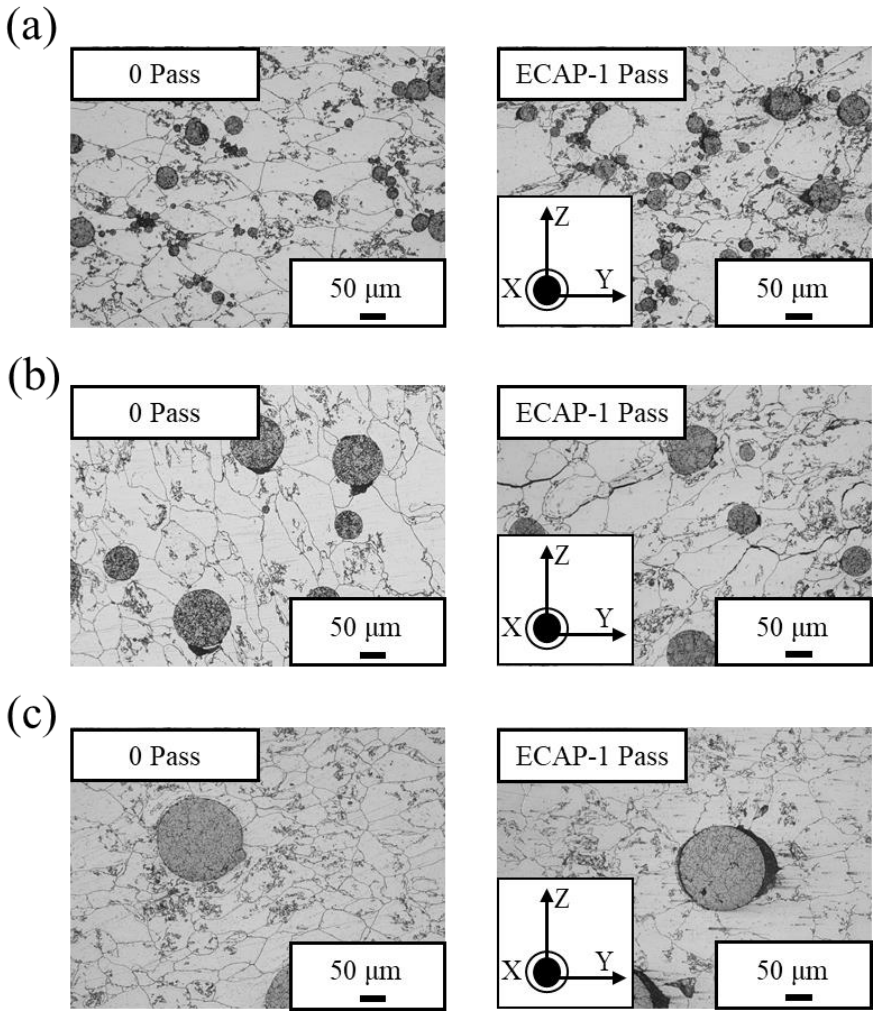

Fig. 3.24. OM photographs of Al-Al_3Ti composites contains spherical Al_3Ti particles (a) below 75 µm Al_3Ti particles (b) 75-150 µm Al_3Ti particles and (c) 150-250 µm Al_3Ti particles.

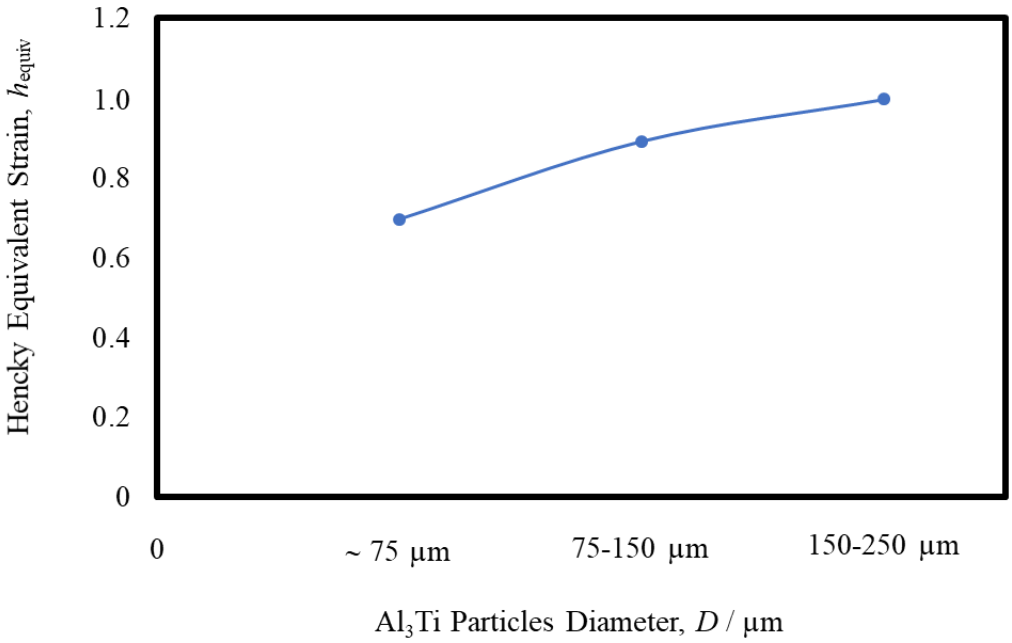

Fig. 3.25. Distribution of Henchy equivalent strain as a function of Al_3Ti particles size in the deformed Al- Al_3Ti composite by after ECAP 1 pass

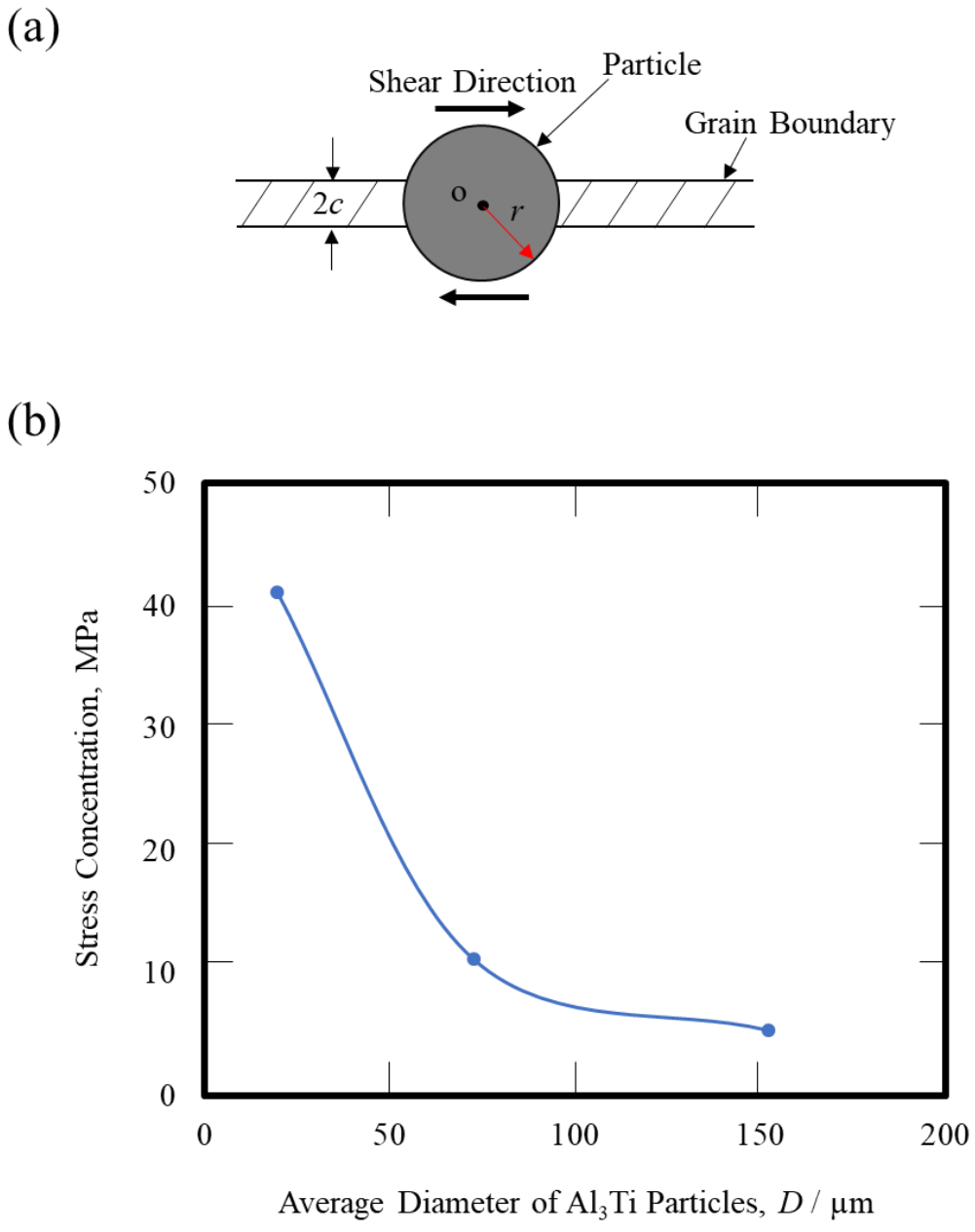

Fig. 3.26. (a) A spherical particle of radius r on the grain boundary thickness 2*c* and (b) schematic representation of stress concentration as a function of particle size

Chapter 4

Effects of spherical, polyhedral and granular shape Al_3Ti particles in fragmentation behavior of Al-based composite by equal-channel angular pressing

4.1 Introduction

In recent years, high strength and lightweight materials have attracted much attention in academic and industrial field applications. The Al-Al_3Ti composite is one of the metal matrix composite (MMC) contains a greater potential for aerospace and other structural application because of their superior properties such as high specific strength and low density [1-3]. The Al-Al_3Ti composite contains Al_3Ti intermetallic particles in Al matrix and this intermetallic particle is very attractive due to higher melting point and relatively low density [1-4]. One of the most important goals is to fabricate the Al-Al_3Ti composite with a homogenous distribution of Al_3Ti particles in the Al matrix. Distribution of Al_3Ti particles will affects the physical and mechanical properties of the Al-Al_3Ti composite. In order to achieve excellent quality Al-Al_3Ti composite, it is important to identify the relevant parameters affecting the uniformity of Al_3Ti particles distribution in the Al matrix. However, studies concerning the homogenous distribution of Al_3Ti particles in the Al-Al_3Ti composite is limited.

Several different techniques have been developed to fabricate MMCs [1-11]. Especially, Ryu *et al.* have investigated that sintering technique can produce more uniform grain distribution Al_3Ti particles in the Al-Al_3Ti composite compared with conventional consolidation methods [6]. In addition, they have reported that sintering pressure and the temperature had large effects on the final

density of particles. On the other hand, Tan and Zhang have proposed a size difference effect of matrix powder and reinforcement particles to obtain a uniform distribution using Al-2.54Li-1.49Cu-0.91Mg-0.13%Zr alloy powders and SiC particles [11]. It is found that the uniform distribution of SiC particles could be expected only when the SiC particles size is not less than a critical size. Secondary deformation processing can enhance the homogenous distribution of SiC particles. Therefore, it is important to understand the selection of particles size, shape and processing technique to obtain homogenous distribution in powder metallurgy MMCs.

Spark plasma sintering (SPS) is a technique developed for sintering ceramics and composite materials [6,9, 12-15]. Watanabe *et al.* have studied that grain refining performance of Al-Al_3Ti composite manufactured by SPS [14]. Furthermore, it is found that Al_3Ti particles act as an effective heterogeneous nucleation site particle for solidification of as-cast Al. This is because of the Al_3Ti particles has good lattice matching with Al. In previous studies, the grain refining performance of Al- Al_3Ti composite [16-18] before and after severe plastic deformation (SPD) by equal channel angular pressing (ECAP) is investigated [19-24].

Sato and Watanabe have studied the spatial distribution of the platelet Al_3Ti particles in the Al-Al_3Ti composite by ECAP processing routes A, B_c and C [24]. Their results show that the change in the spatial distribution of the fragmented Al_3Ti particles depends on material flow of α-Al matrix during ECAP. However, the spatial distribution of Al_3Ti particle in the Al-Al_3Ti composite by ECAP is not investigated quantitatively. On the other hand, the spatial distribution of the fragmented platelet Al_3Ti particles in the Al-Al_3Ti composite by multi-directional

forging (MDF) [25-27] have been evaluated quantitatively using the Morisita index, I_δ [27]. It results that I_δ [28-31] is an effective method to examine the spatial distribution of the Al_3Ti particles quantitatively. However, the spatial distribution changes polyhedral and granular Al_3Ti particle in the SPDed Al-Al_3Ti composite is unknown. Because the deformation of the Al_3Ti particles in the Al-Al_3Ti composite depends on the particle shape, the spatial distribution change of the Al_3Ti particles in the composite with polyhedral or granular Al_3Ti particles would be different from the platelet Al_3Ti particles. Therefore, it is important to evaluate the distribution, size difference and shape of Al_3Ti particles in the SPDed Al-Al_3Ti composite.

In this study, fragmentation behavior and spatial distribution of spherical or polyhedral or granular shape Al_3Ti particles in the Al-Al_3Ti composite during ECAP have been investigated. This spatial distribution of Al_3Ti particles in the Al-Al_3Ti composite is quantitatively evaluated using I_δ. In order to investigate the effect of the particle size and shape effects, the Al-Al_3Ti composite with two different sizes of spherical or polyhedral or granular particles is used. In addition, the Hencky equivalent strain is calculated to describe the severe strain caused by ECAP [33-39]. Based on the obtained results, the fragmentation behavior, spatial distribution and effects of Al_3Ti particle shape in the Al-Al_3Ti composite during ECAP were discussed.

4.2 Experimental procedure

4.2.1 *Preparation of Al-Al_3Ti composites*

At first, the Al_3Ti particles with $D0_{22}$ structure were prepared by gas atomization or arc melting. The spherical and polyhedral Al_3Ti particles prepared

by gas atomization were shown in **Fig. 4.1.** On the other, granular Al_3Ti particles was prepared by arc melting and this Al_3Ti particles was prepared by arc melting of pure Al and pure Ti under an argon atmosphere as shown in **Fig. 4.2**. Subsequently, the prepared Al_3Ti particles was homogenization at 1100 °C for 4 h. After that, the gas-atomized polyhedral Al_3Ti particles and arc melted granular Al_3Ti particles were sieved to obtain the Al_3Ti particles diameters in the range of below 75 μm and 75-150 μm. The sieved Al_3Ti particles were mixed with Al particles (99.9%, 106-180 μm) by using three-dimensional motion mixer (turbula mixer). In this study, the volume fraction of the Al_3Ti particles was 11 vol%. These mixed-powders were sintered using SPS at 550 °C for 15 min under the applied pressure of 45 MPa. Finally, four kinds of Al-Al_3Ti composites containing Al_3Ti particles with two different particles diameter were obtained. Specimen 1 which contains below 75 μm polyhedral Al_3Ti particles in the Al-Al_3Ti composite, specimen 2 contains 75-150 μm polyhedral Al_3Ti particles, specimen 3 contains below 75 μm granular Al_3Ti particles and specimen 4 contain 75-150 μm granular Al_3Ti particles in the Al-Al_3Ti composites. In addition, Al-Al_3Ti composites containing spherical shape Al_3Ti particles were prepared by SPS.

4.2.2 ECAP for the Al-Al_3Ti composites

The required size of ECAP specimens with 10 mm in diameter and 30 mm in length was obtained from machining. In this study, ECAP for the Al-Al_3Ti composite was performed under the pressing speed of 5 mm/min at ambient temperature and ECAP die which can give the nominal equivalent strain of 1.01 per passage. After ECAP specimen was cut at the middle along the deformation axis for microstructural observation.

4.2.3 Microstructural observations of Al-Al_3Ti composites

Microstructure of the Al-Al_3Ti composites before and after ECAP was observed by scanning electron microscope (SEM) and optical microscope (OM). The specimens were mechanically and chemically polished for microstructural observation. The spatial distribution of Al_3Ti particles in the Al-Al_3Ti composites was evaluated by the I_δ [27-31]. The Hencky equivalent strain (h_{equiv}) was a quantitative analysis carried out to evaluate strain distribution around Al/Al_3Ti interface in the Al-Al_3Ti composites deformed by ECAP. The mean size of Al grains was calculated using mean linear intercept. The specimen was etched in 10% hydrofluoric acid solution and observed by OM for grain size determination. The Vickers hardness (*HV*) of the Al-Al_3Ti composites were measured at room temperature under a load of 4.903 N.

4.2.4 Microstructural observations of $L1_2$ intermetallic compound

The spherical and polyhedral shape $L1_2$ structure $Al_{2.7}Fe_{0.3}Ti$ and $Al_{2.5}Cu_{0.5}Ti$ particles were prepared by gas atomization as shown in **Fig 4.14** and **4.15** (a). The $L1_2$ structure particles were mixed with Al particles (99.9%, 106-180 μm) by using three-dimensional motion mixer (Turbula mixer). Where the volume fraction of particles was 11vol%. The mixed powder particles were sintered by SPS.

4.3 Results and discussion

4.3.1 Microstructure of Al-Al_3Ti composites contain spherical or polyhedral Al_3Ti particles by ECAP

Figure 4.3 shows the micrographs of pure Al before and after ECAP. It is found that after 1 pass of ECAP the grain size of pure Al becomes small. In addition, cracks are observed in the specimen after ECAP. SEM micrographs showing microstructure of Al-Al_3Ti composites containing spherical Al_3Ti particles before ECAP as shown in **Fig. 3.18.** It is found that after ECAP there is no deformation in spherical shape Al_3Ti particles in Al-Al_3Ti composites by ECAP as shown in **Fig 3.21**.

SEM micrographs showing microstructure of Al-Al_3Ti composites containing polyhedral Al_3Ti particles before and after ECAP as shown in **Fig. 4.4. Figures 4.4** (a) and (c) are the polyhedral Al_3Ti particles in the Al-Al_3Ti composites in the range of below 75 µm and 75-150 µm. When ECAP is performed, deformation occurs in the polyhedral Al_3Ti particles as shown in **Fig. 4.4** (b) and (d). In previous studies, it is found that cracks generated along with the twin boundary-initiated deformation and crack propagation along with the twin boundary result in the fragmentation of particles in the Al-Al_3Ti composites [24, 10]. As seen in **Fig. 4.5**, the polyhedral Al_3Ti particles are severely fragmented in the Al-Al_3Ti composites. Therefore, the polyhedral Al_3Ti particles in the Al-Al_3Ti composites are severely fragmented by ECAP.

4.3.2 Microstructure of Al-Al_3Ti composites contain granular Al_3Ti particles by ECAP

Figure 4.6 is a SEM photograph showing granular Al_3Ti particles prepared by arc melting. **Figures 4.7** showing the granular Al_3Ti particles in the Al-Al_3Ti composites in the range of below 75 µm and 75-150 µm before and after ECAP. The granular Al_3Ti particles in the Al-Al_3Ti composites are deformed by 1

pass of ECAP as shown in **Fig. 4.7** (b) and (d). It is found that deformation of the granular Al_3Ti particles in the Al-Al_3Ti composite are severely occurs as shown in **Fig 4.8**. It is found that the fragmentation of granular Al_3Ti particles are similar to the fragmentation of platelet Al_3Ti particles. Hence, the fragmentation behavior of Al_3Ti particles in the Al-Al_3Ti composite by ECAP is different depending on the shape and size of Al_3Ti particles.

4.3.3 Spatial distribution of Al_3Ti particles in the Al-Al_3Ti composites by ECAP

Spatial distributions of polyhedral or granular Al_3Ti particles in the Al-Al_3Ti composite deformed by ECAP is quantitatively evaluated using the I_δ. **Figure 3.22** (a) and (b) are the I_δ curves of the Al-Al_3Ti composites containing spherical Al_3Ti particles by ECAP. It is seen that the Al-Al_3Ti composite with relatively higher Al_3Ti particles has homogenous distribution. **Figures 4.9** (a-d) is the I_δ curves of the Al-Al_3Ti composites containing polyhedral or granular Al_3Ti particles deformed by ECAP. From **Fig. 4.9** (a) and (b), before ECAP the I_δ is near to 1 and difference of the I_δ in the polyhedral Al_3Ti particles caused by ECAP is observed. It is seen that the Al-Al_3Ti composite with fragmented Al_3Ti particles has aggregated distribution.

Figures 4.9 (c) and (d) shows the I_δ curves of the granular Al_3Ti particles in Al-Al_3Ti composites by ECAP. Before ECAP process, the granular Al_3Ti particles results the calculated I_δ is near to 1. When ECAP is performed at 1 pass, the Al_3Ti particles in Al-Al_3Ti composite are aggregated in the Al matrix and the I_δ becomes more than 1. Particularly, small size (below 75 μm) of granular Al_3Ti particles in the Al-Al_3Ti composite results the calculated I_δ more than 1compared to large size granular Al_3Ti particles. When the granular particle size is smaller to

the matrix size the spatial distribution becomes aggregated distribution after ECAP. However, when the particle shape is similar, the spatial distribution changes depends on the particle size. Therefore, the change in the spatial distribution of spherical or polyhedral or granular Al_3Ti particles in the Al-Al_3Ti composites depends on the particle size. The spatial distribution of the spherical or polyhedral or granular Al_3Ti particles in the deformed Al-Al_3Ti composite is controlled by the material flow of the matrix by ECAP.

4.3.4 Distribution of the Hencky equivalent strain in the Al-Al_3Ti composites by ECAP

It is found that the change in the spatial distribution of polyhedral or granular Al_3Ti particles in the Al-Al_3Ti composites depends on the particle size. Strain distribution around polyhedral or granular Al_3Ti particles in the Al-Al_3Ti composite deformed by ECAP is evaluated quantitatively using Hencky equivalent strain [32-38]. The mean grain size the Al-Al_3Ti composite which contain polyhedral or granular Al_3Ti particles are calculated using mean linear intercept form **Figs. 4.10** and **4.11.** The calculated mean grain size is presented in the **Table 4.1**. the distribution of h_{equiv} as a function of Al_3Ti particles diameter. The measured thickness values for the Al-Al_3Ti composites contain polyhedral below 75 μm Al_3Ti particles and 75-150 μm Al_3Ti particles are 34.1 μm and 26.4 μm, respectively. In addition, the measured thickness values for the Al-Al_3Ti composites contain granular below 75 μm Al_3Ti particles and 75-150 μm Al_3Ti particles are 36.9 μm and 38.6 μm, respectively. It is found that the h_{equiv} distribution of the Al-Al_3Ti composites contains polyhedral or granular below 75 μm Al_3Ti particles is less compare to other the Al-Al_3Ti composites which contain

large size Al_3Ti particles as shown in **Fig 4.12**. However, h_{equiv} distribution of the Al-Al_3Ti composites increases with the increase in polyhedral or granular Al_3Ti particles size. Moreover, the polyhedral Al_3Ti particles in the Al-Al_3Ti composites results more Hencky equivalent strain compared to granular Al_3Ti particles in the Al-Al_3Ti composites. As a possible reason for this Hencky equicalent strain is the stress concentration around the polyhedral Al_3Ti particles different from granular Al_3Ti particles. It is concluded that large deformation of polyhedral or granular Al_3Ti particles in the Al-Al_3Ti composites occurs when the specimen has larger particle size.

4.3.5 The Vickers hardness distribution of Al-Al_3Ti composites by ECAP

The distribution of Vickers hardness across the Al-Al_3Ti composites before and after by ECAP is calculated as shown in **Fig 4.13**. In all the specimens, it is found Vickers hardness values show the clear trend of improvement after ECAP. This is because of the grain size of the Al matrix decreases with increasing SPD. From this result, it should be noted that SPD by ECAP have a string impact on the hardness of the Al-Al_3Ti composite as well as its grain size.

4.3.6 Microstructure of composites by ECAP

Figures 4.14 and **4.15** (b) shows the microstructure of fabricated composite using SPS. It can be observed that $Al_{2.7}Fe_{0.3}Ti$ and $Al_{2.5}Cu_{0.5}Ti$ particles are dispersed in the Al matrix before ECAP, respectively. Using this composites ECAP was carried out up to 1 pass. It is found that there is no deformation in the spherical shape $L1_2$ structure $Al_{2.7}Fe_{0.3}Ti$ particles in the Al-11vol%$Al_{2.7}Fe_{0.3}Ti$ composite as shown in **Fig 4.14**. In addition, this result has agreement with spherical shape $D0_{22}$ structure $Al_{.3}Ti$ particles in the Al-$Al_{.3}Ti$ composite.

Furthermore, when ECAP is performed Al-11vol%$Al_{2.5}Cu_{0.5}Ti$ composite. It is found that the polyhedral shape $L1_2$ structure $Al_{2.5}Cu_{0.5}Ti$ particles in the Al-11vol%$Al_{2.5}Cu_{0.5}Ti$ composite deformed by ECAP as shown in **Fig 4.15**. Especially, cracks are clearly visible in the specimen after ECAP. It is concluded that deformation of particles in the composites depends on the particle shape.

4.4 Conclusions

Microstructure and spatial distributions of spherical or polyhedral or granular Al_3Ti particles in the Al-Al_3Ti composite by equal-channel angular pressing (ECAP) is investigated. One kind of spherical or polyhedral shape Al_3Ti particles with two different size was prepared by gas atomization and other kind of granular shape Al_3Ti particles with two different size was prepared by arc melting. Using these composites, the shape and size effect of polyhedral or granular Al_3Ti particles on the spatial distributions in Al-Al_3Ti composite were studied. The obtained conclusions were as follows,

(1) ECAP was performed in the Al-Al_3Ti composite, the spherical or polyhedral or granular Al_3Ti particles were fragmented by ECAP. It is found that fragmentation behavior depends on the Al_3Ti particles shape by ECAP.

(2) Spatial distributions of spherical or polyhedral or granular Al_3Ti particles in the Al- Al_3Ti composite deformed by ECAP results the aggregated distribution. The change in spatial distributions of spherical Al_3Ti particles depends on the particle size. Therefore, the spatial distribution of Al_3Ti particles can be explained by the material flow of the Al matrix by SPD.

(3) Distribution of Hencky equivalent strain, h_{equiv}, indicates that larger particles size was deformed more compare to the specimens which have smaller particle size.

References

[1] R. Lerf and D. G. Morris, Mechanical alloying of Al-Ti alloys, Mater. Sci. Eng. A, **128** (1990) 119-127.
[2] K-M. Lee and I-H. Moon, High temperature performance of dispersion-strengthed Al-Ti alloys prepared by mechanical alloying, Mater. Sci. Eng. A, **185** (1994) 165-171.
[3] C. J. Hsu, C. Y. Chang, P. W. Kao, N. J. Ho and C. P. Chang, Al-Al_3Ti nanocomposite produced in situ by friction stir processing, Acta Mater., **54** (2006) 5241-5249.
[4] R. A. Varin, Intermetallic-reinforced light-metal matrix in-situ composites, Metall. Mater. Trans. A, **33A** (2002) 193-201.
[5] S. Srinivasan, S. R. Chen and R. B. Schwarz, Synthesis of Al/Al_3Ti two-phase alloys by mechanical alloying, High temperature aluminides and intermetallic, Bull. Mater. Sci., **19** (1992) 691-695.
[6] J. R. Ryu, K. I. Moon and K. S. Lee, Microstructure and mechanical properties of nanocrystalline Al-Ti alloys consolidate by plasma activated sintering, J. Alloy. Compd., **296** (2000) 157-165.
[7] L. M. Peng, H. Li and J. H. Wang, Processing and mechanical behavior of laminated titanium-titanium tri-aluminide (Ti-Al_3Ti) composites, Mater. Sci. Eng. A, **406** (2005) 309-318.
[8] V. A. Chianeh, H. R. M. Hosseini and M. Nofar, Micro structural features and mechanical properties of Al-Al_3Ti composite fabricated by in-suit powder metallurgy route, J. Alloy. Compd., **473** (2009) 127-132.
[9] K. Park, D. Kim, K. Kim, S. Cho and H. Kwon, Behavior of intermetallic compound of Al-Ti composite manufactured by spark plasma sintering, Materials, **12** (2019) 1-14.
[10] S. B. Duraisamy, H. Sato, T. Chiba and Y. Watanabe, Fragmentation process of platelet Al_3Ti particles in compressed Al-Al_3Ti alloy observed by serial sectioning and EBSD analysis, Mater. Res. Express, **6** (2019) 096575 1-8.
[11] M. J. Tan and X. Zhang, Powder metal matrix composites: selection and processing, Mater. Sci. Eng. A, **244** (1998) 80-85.
[12] S. S. Nayak, S. K. Pabi, D. H. Kim and B. S. Murty, Microstructure-hardness relationship of Al-($L1_2$) Al_3Ti nanocomposites prepared by rapid solidification processing, Intermetallics, **18** (2009) 1-6.
[13] A. Eldesouky, M. Johnsson, H. Svengren, M.M. Attallah and H.G. Salem, Effect of grain size reduction of AA2124 aluminum alloy powder compacted by spark plasma sintering, J. Alloy. Compd., **609** (2014) 215-221.
[14] Y. Watanabe, T. Hirako, T. Chiba and H. Sato, Grain refinement performance of aluminum cast by addition of spherical Al_3Ti particles fabricated by gas atomization method, J. J. I. L. M., **67** (2017) 208-213 (in Japanese).
[15] Y. Watanabe, R. Yamazaki, K. Yamanaka and H. Sato, Grain refinement of pure Al using $Al_{2.5}Cu_{0.5}Ti$ particles with an $L1_2$ structure, J. Mater. Proces. Technol., **255** (2018) 400-410.
[16] Z. Zhang, Y. Watanabe, I. S. Kim, X. Liu and X. Bian, Microstructure and refining performance of an Al-5Ti-0.25C refiner before and after equal-channel angular pressing, Metall. Mater. Trans. A, **36A** (2005) 837-844.
[17] Z. Zhang, S. Hosoda, I. S. Kim and Y. Watanabe, Grain refining performance for Al and Al-Si alloy casts by addition of equal-channel angular pressed Al-5mass%Ti alloy, Mater. Sci. Eng. A, **425** (2006) 55-63.

[18] W. Wei, R. Y. Mao, K. X. Wei, I. V. alexandrov and J. Hu, Effect of equal channel angular pressing on microstructure and grain refining performance of Al-5%Ti master alloy, Mater. Sci. Eng. A, **564** (2013) 92-96.
[19] S-Y. Chang, K-S. Lee, S. K. Ryu, K. T. Park and D. H. Shin, Effect of equal channel angular pressing on the distribution of reinforcements in the discontinuous metal matrix composites, Mater. Trans., **43** (2002) 757-761.
[20] I. Sabirov, O. Kolednik and R. Pippan, Homogenization of metal matrix composites by high-pressure torsion, Metall. Mater. Trans. A, **36A** (2005) 2861-2870.
[21] C. Xu, M. Furukawa, Z. Horita and T. G. Langdon, The evolution of homogeneity and grain refinement during equal-channel angular pressing: a model for grain refinement in ECAP, Mater. Sci. Eng. A, **398** (2005) 66-76.
[22] I. Sabirov, O. Keolednik, R. Z. Valiev and R. Pippan, Equal channel angular pressing of metal matrix composites: effect on particle distribution and fracture toughness, Acta Mater., **53** (2005) 4919-4930.
[23] M. Howeyze, H. Arabi, A. R. Eivani and H. R. Jafarian, Strengthening of AA5052 aluminum alloy by equal channel angular pressing followed by softening at room temperature, Mater. Sci. Eng. A, **720** (2018) 160-168.
[24] H. Sato and Y. Watanabe, Three-dimensional microstructural analysis of fragmentation behavior of platelet Al_3Ti particles in Al-Al_3Ti composite deformed by equal-channel angular pressing, Mater. Charact., **144** (2018) 305-315.
[25] K.B. Nie, K.K. Deng, X.J. Wang, W.M. Gan, F.J. Xu, K. Wu and M.Y. Zheng, Microstructures and mechanical properties of SiCp/AZ91 magnesium matrix nanocomposites processed by multidirectional forging, J. Alloy. Compd., **622** (2015) 1018-1026.
[26] M. R. Jandaghi, H. Pouraliakbar, M. K. G. Shiran, G. Khalaj and M. Shirazi, On the effect of non-isothermal annealing and mulit-directional forging on the microstructural evolutions and correlated mechanical and electrical characteristics of hot-deformed Al-Mg alloy, Mater. Sci. Eng. A, **657** (2016) 431-440.
[27] H. Sato, F. Teshima and Y. Watanabe, Effects of forging temperature on Al3Ti particle distribution in Al-Al_3Ti multi-phase materials deformed by multi-directional forging, J. J. I. L. M., **68** (2018) 2-8 (in Japanese).
[28] M. Morisita, Measuring of the dispersion and analysis of distribution patterns, Mem. Fac. Kyushu Univ., E **2**, (1959) 215-235.
[29] M. Morisita, I_δ-index, A measure of dispersion of individuals, Res. Popul. Ecol., **4** (1962) 1-7.
[30] M. Morisita, Composition of the I_δ-index, Res. Popul. Ecol., **13** (1971) 1-27.
[31] M. K. Amaral, S. N. Pellico, C. Lingnau and A. F. Figueiredo, Evaluation of the morisita index for determination of the spatial distribution of species in a fragment of aracuaria forest, Appl. Ecol. Envir. Res., **13** (2014) 361-371.
[32] H. Hencky, Z. Tech. Phys., **9** (1928) 214-247 (in German).
[33] J. H. Dautzenberg and J. H. Zaat, Quantitative determination of deformation by sliding wear, Wear, **23** (1973) 9-19.
[34] S. Onaka, Equivalent strain in simple shear deformation described by using the Hencky strain, Philos. Mag. Lett., **90** (2010) 633-639.
[35] S. Onaka, Appropriateness of the Hencky equivalent strain as the quantity to represent the degree of severe plastic deformation, Mater. Trans., **53** (2012) 1547-1548.
[36] V. M. Segal, Equivalent and effective strains during severe plastic deformation (SPD), Philos. Mag. Lett., **98** (2019) 511-520.

Table 4.1. Mean grain size of the Al-Al_3Ti composites.

Specimen (Al-Al_3Ti composite contains)	Mean grain size of polyhedral particles	Mean grain size
Below 75 μm Al_3Ti particles	44.1 μm	44.3 μm
75-150 μm Al_3Ti particles	47.7 μm	43.3 μm

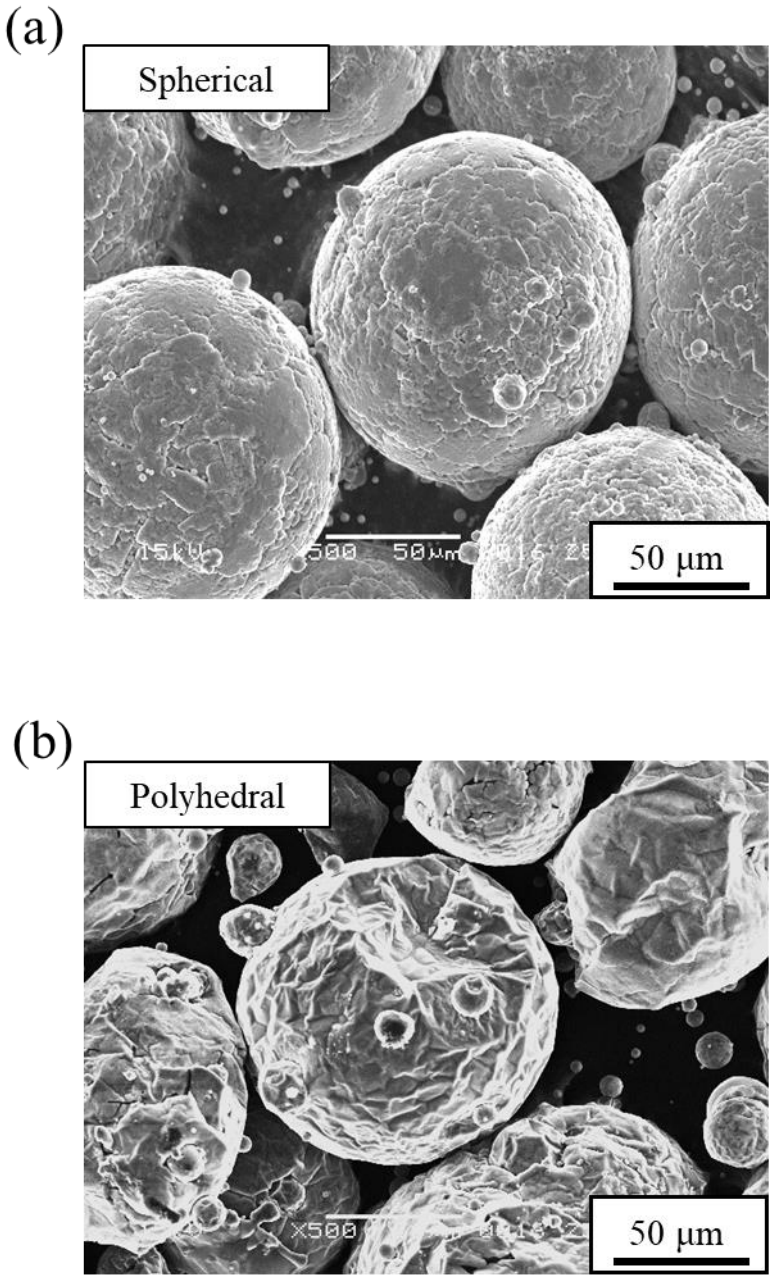

Fig. 4.1. SEM photograph of Al_3Ti particles fabricated by gas atomization: (a) spherical and (b) polyhedral.

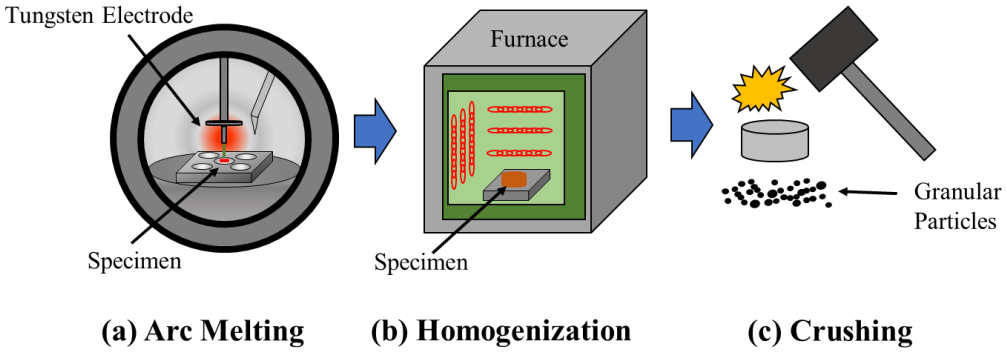

Fig. 4.2. Flow diagram for the fabrication of granular Al_3Ti particles.

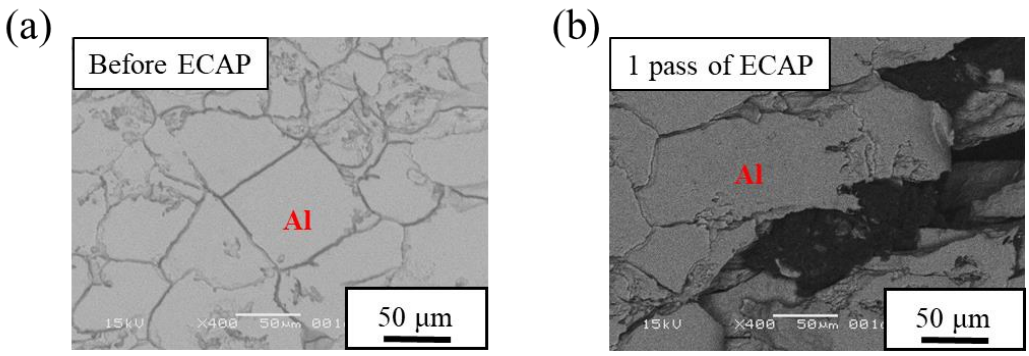

Fig. 4.3. OM of pure Al: (a) before ECAP and (b) 1 pass of ECAP.

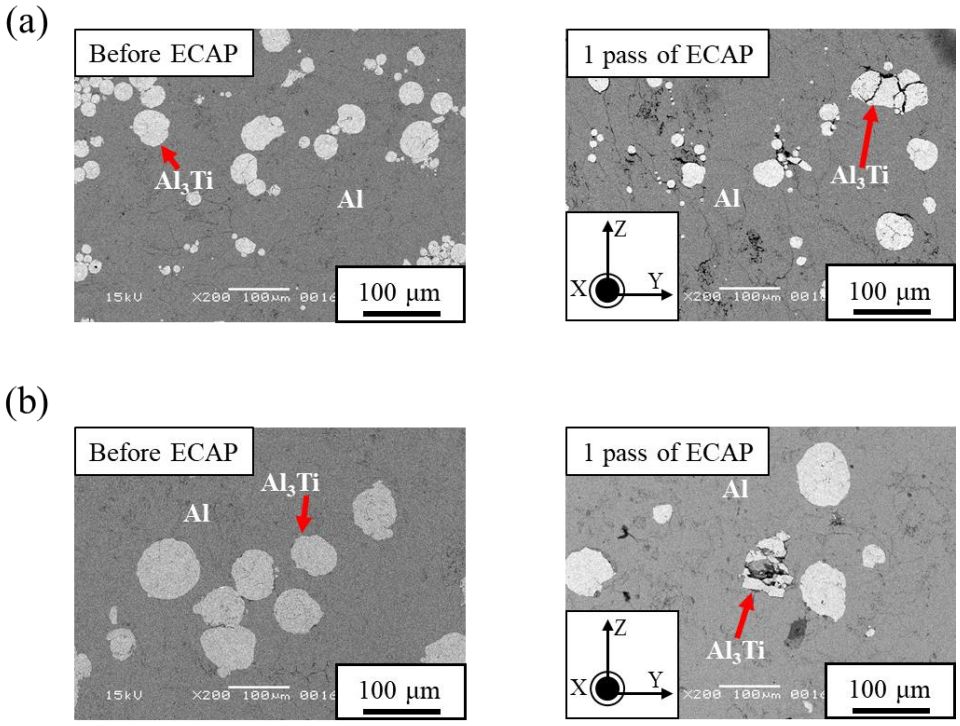

Fig. 4.4. SEM micrograph of Al-Al_3Ti composites contains polyhedral Al_3Ti particles in the range of (a) below 75 µm and (b) 75-150 µm.

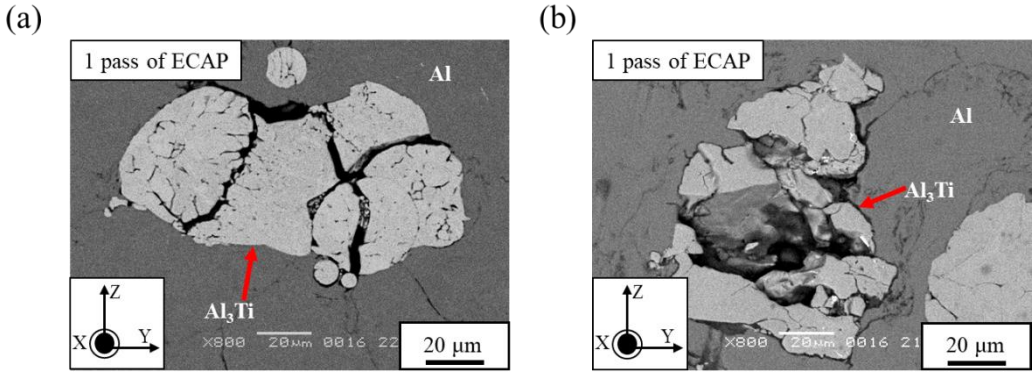

Fig. 4.5. High magnified SEM micrograph of Al-Al_3Ti composites contains polyhedral Al_3Ti particles after 1 pass of ECAP: (a) below 75 µm and (b) 75-150 µm.

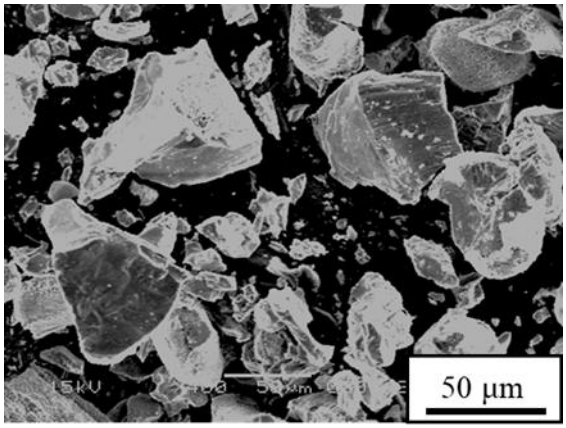

Fig. 4.6. SEM photograph of granular Al_3Ti particles fabricated by arc melting.

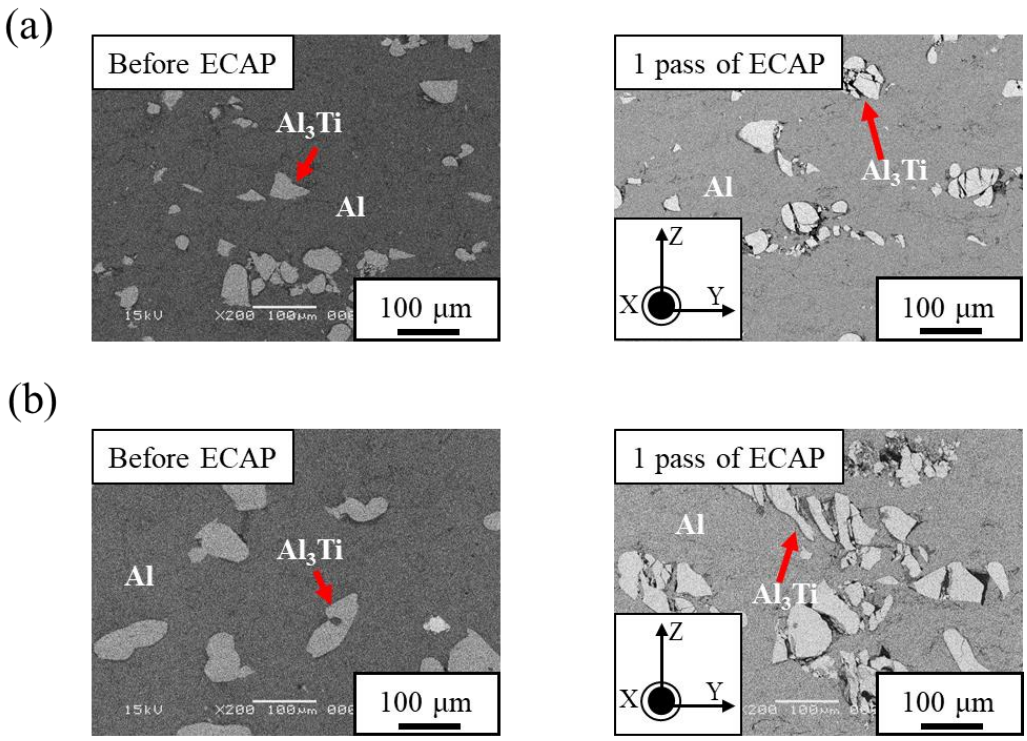

Fig. 4.7. SEM micrograph of Al-Al_3Ti composites contains granular Al_3Ti particles in the range of (a) below 75 µm and (b) 75-150 µm.

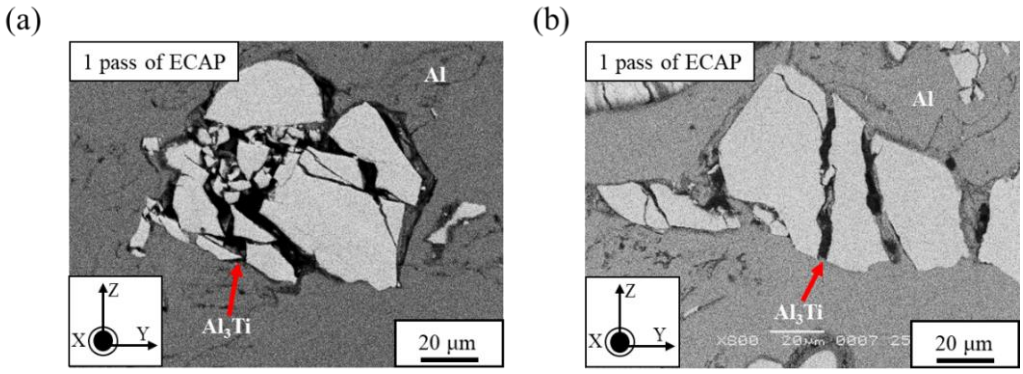

Fig. 4.8. High magnified SEM micrograph of Al-Al_3Ti composites contains granular Al_3Ti particles after 1 pass of ECAP: (a) below 75 μm and (b) 75-150 μm.

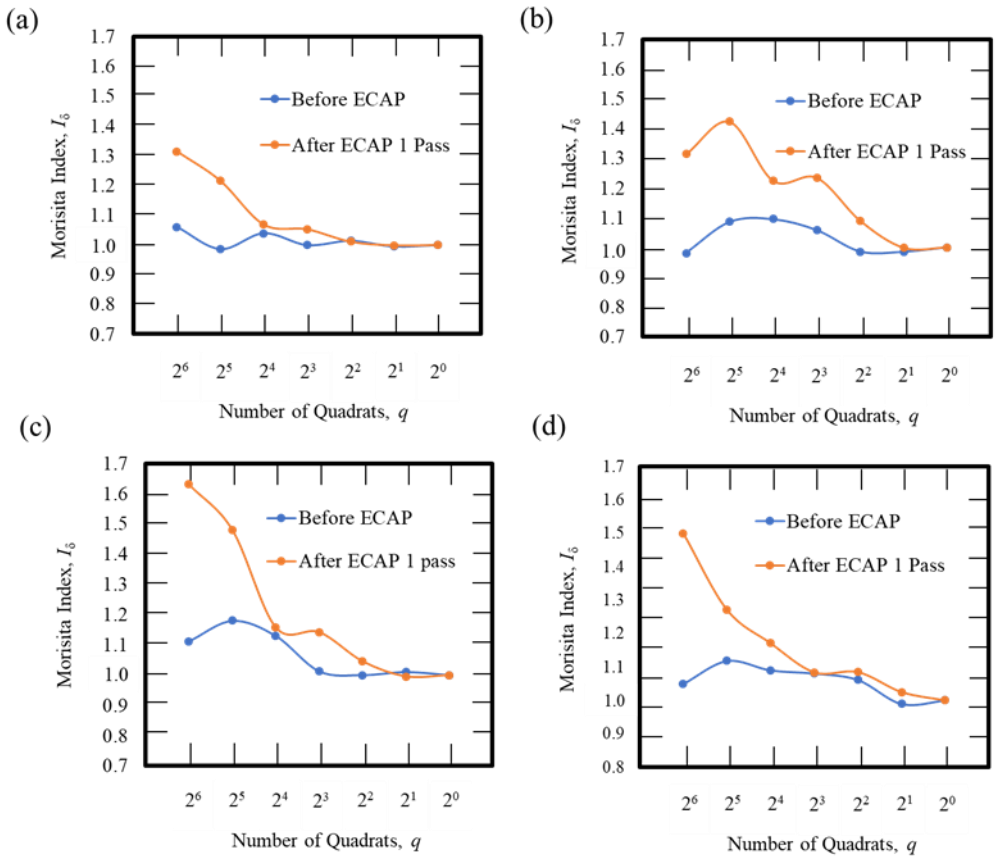

Fig. 4.9. I_δ and number of quadrats relations of the deformed Al-Al_3Ti composites contains polyhedral or granular Al_3Ti particles in the range of: (a) polyhedral below 75 μm Al_3Ti particles and (b) polyhedral 75-150 μm Al_3Ti particles, (c) granular below 75 μm Al_3Ti particles and (d) granular 75-150 μm Al_3Ti particles.

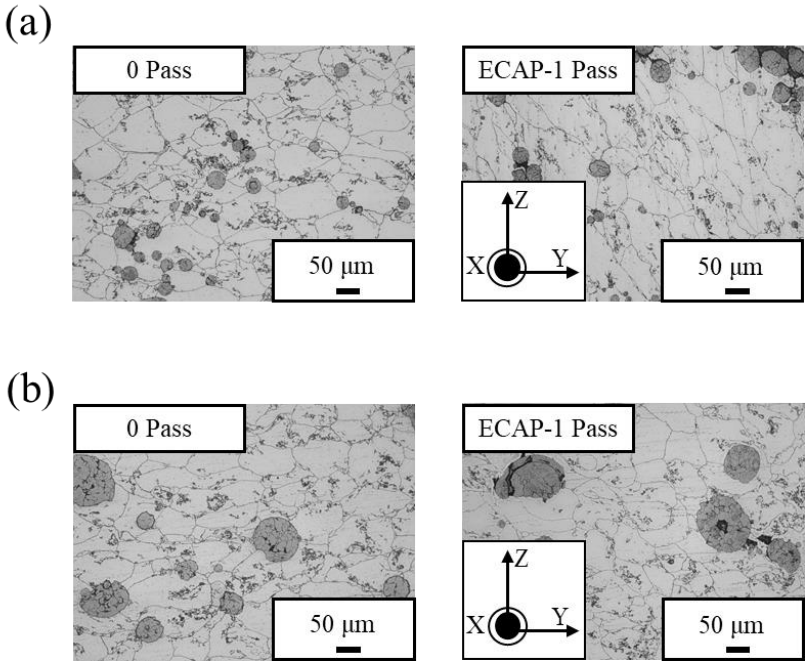

Fig. 4.10. OM photographs of Al-Al_3Ti composites contains polyhedral Al_3Ti particles in the range of (a) below 75 µm and (b) 75-150 µm.

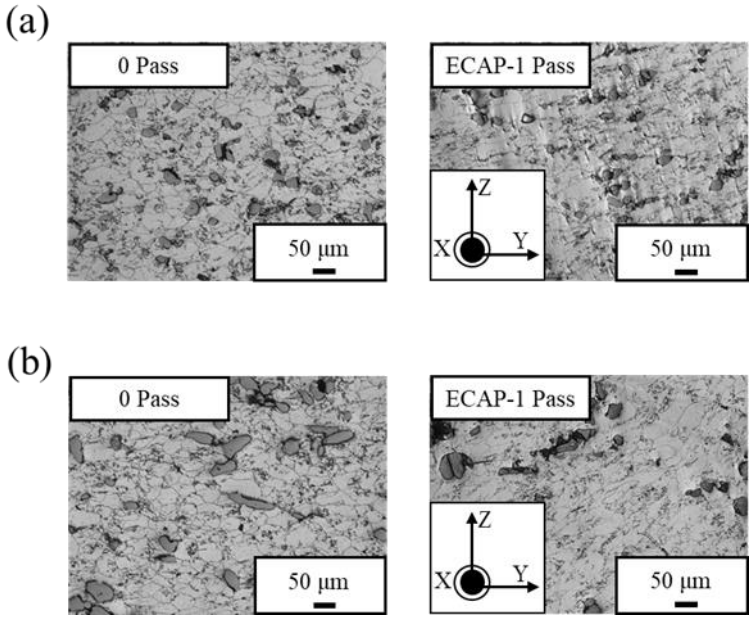

Fig. 4.11. OM photographs of Al-Al_3Ti composites contains granular Al_3Ti particles in the range of (a) below 75 µm and (b) 75-150 µm.

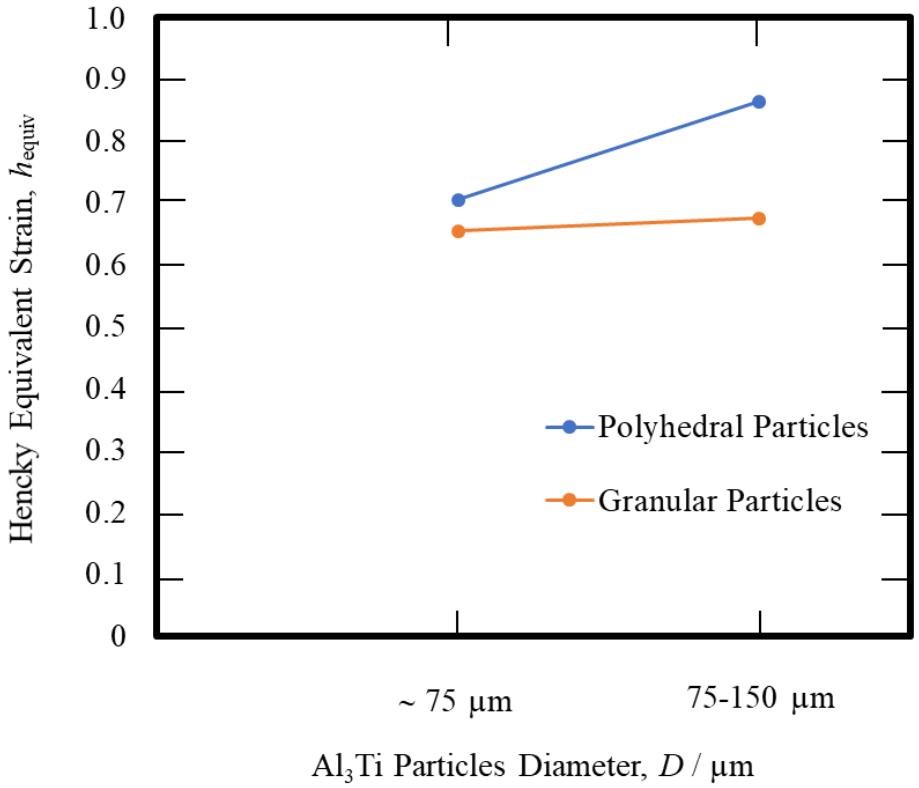

Fig. 4.12. Distribution of Henchy equivalent strain as a function of Al_3Ti particles size in the deformed Al- Al_3Ti composite by 1 pass of ECAP.

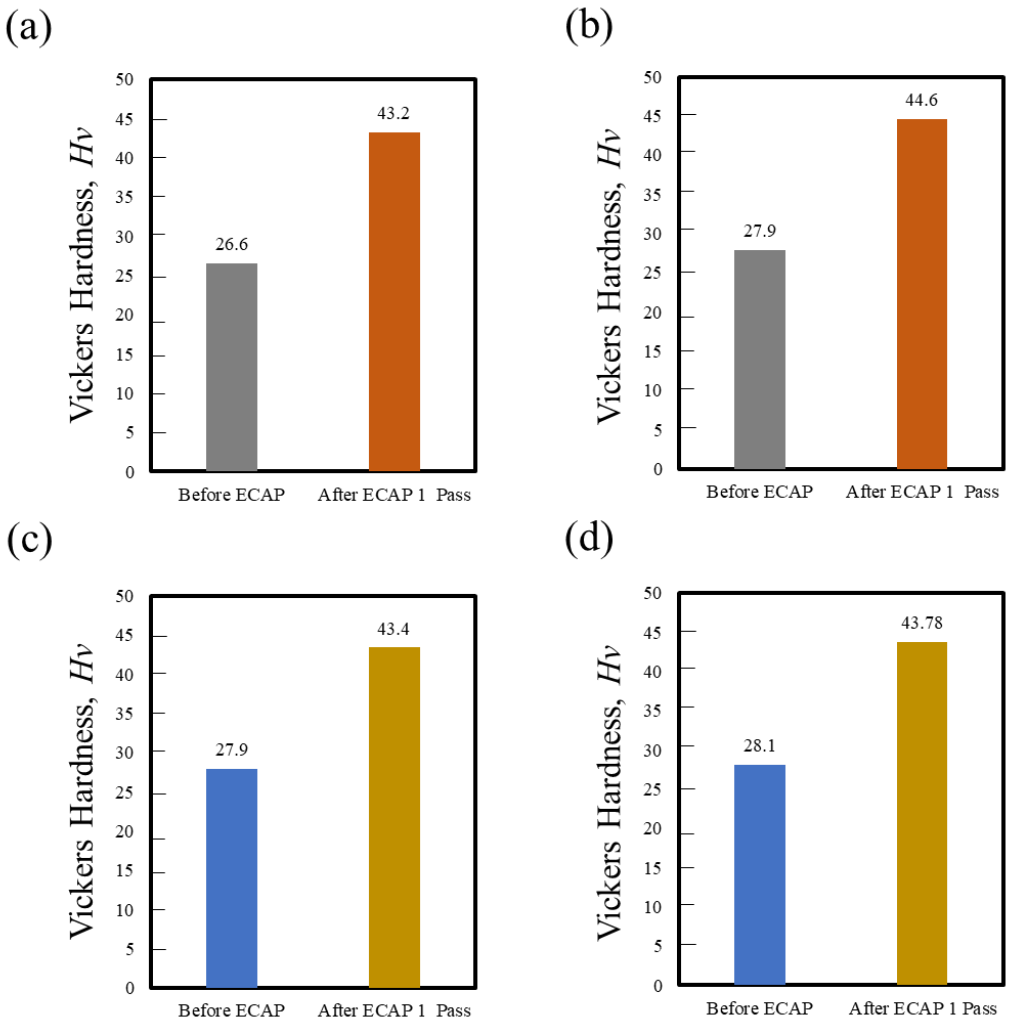

Fig. 4.13. Distribution of Vickers hardness in the Al-Al_3Ti composite contain polyhedral or granular Al_3Ti by ECAP: (a) below 75 µm polyhedral Al_3Ti particles, (b) 75-150 µm polyhedral Al_3Ti particles, (c) below 75 µm granular Al_3Ti particles and (d) 75-150 µm granular Al_3Ti particles.

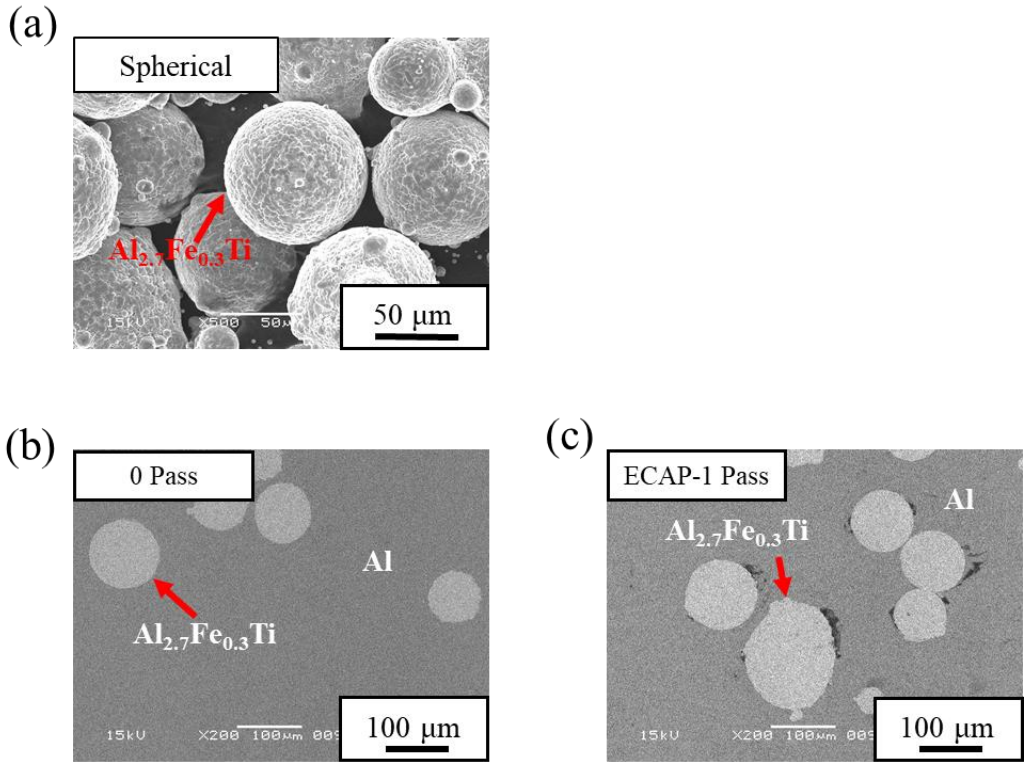

Fig. 4.14. SEM photograph of: (a) spherical $Al_{2.7}Fe_{0.3}Ti$ particles fabricated by gas atomization, Al-11vol%$Al_{2.7}Fe_{0.3}Ti$ composite (b) before and (c) after ECAP.

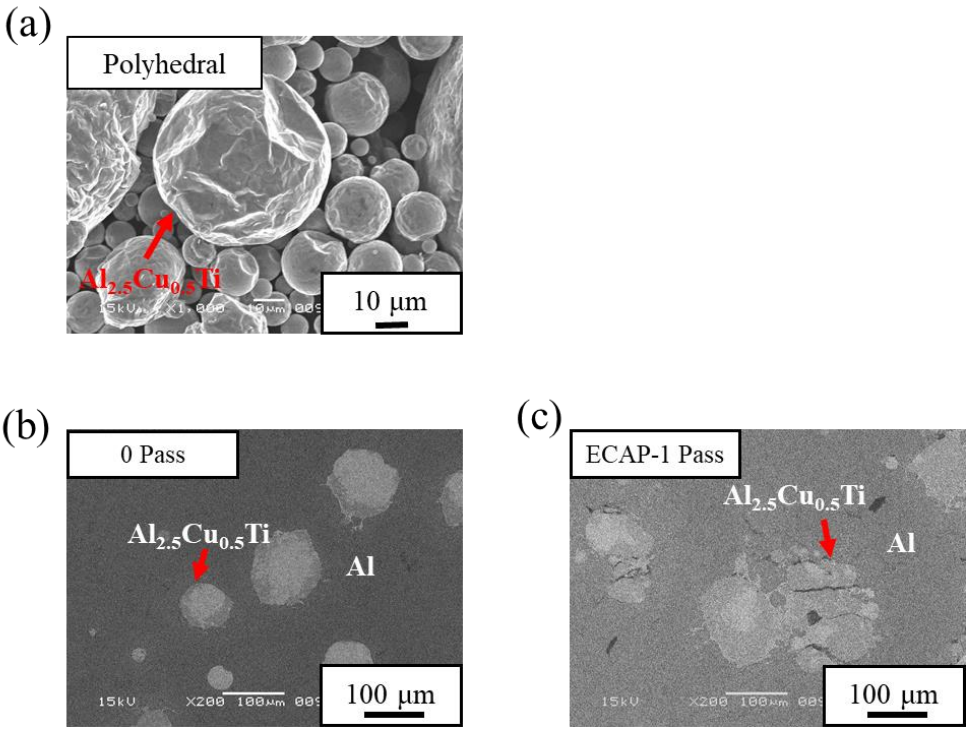

Fig. 4.15. SEM photograph of: (a) polyhedral $Al_{2.5}Cu_{0.5}Ti$ particles fabricated by gas atomization, Al-11vol%$Al_{2.5}Cu_{0.5}Ti$ composite (b) before and (c) after ECAP.

Chapter 5

Fragmentation of platelet Al_3Ti particles in Al-based composite by severe plastic deformation

5.1 Introduction

Adding Al-Al_3Ti composite containing platelet Al_3Ti particles can refine the size of α-Al grains in as-cast Al [1-8]. As a possible reason effective grain reefing because of Al_3Ti has good lattice registry with Al and this intermetallic particles in the Al-Al_3Ti composite plays a role of heterogeneous nucleation site for the α-Al [1]. It is found that the addition of the Al-Al_3Ti composite into the Al melt can promote the as-cast Al having equiaxed and fine α-Al grains.

Grain refinement ability of the Al-Al_3Ti composite for the as-cast Al by severe plastic deformation was investigated in the previous study [5]. This severe plastic deformation for the Al-Al_3Ti composite have made by equal channel angular pressing (ECAP) and its grain refinement ability was studied. It is found that the platelet Al_3Ti particles in the Al-Al_3Ti composite are severely fragmented by ECAP. In addition, the ECAPed Al-Al_3Ti composite has higher grain refinement ability than the undeformed Al-Al_3Ti composite. According to their study, effect grain refinement ability of the Al-Al_3Ti composite comes from the increases in the number of the Al_3Ti particles by ECAP which act as effective nuclei for the α-Al. In previous studies, the plane disregistry between Al_3Ti and Al have calculated and the results suggests that the $\{112\}_{Al3Ti}$ plane of the Al_3Ti is the most effective nucleation site for Al because this crystal plane of the Al_3Ti can have the smallest plane disregistry with Al [6]. Furthermore, Sato and Watanabe have found that the platelet Al_3Ti particles are preferentially fragmented along

twin boundary plane of $\{112\}_{Al3Ti}$ from 3-dimensional observation and crystallographic analysis for the fragmented Al_3Ti particles in the ECAPed Al-Al_3Ti composite [8]. Therefore, it is result that the enhancement of the grain refinement ability of the Al-Al_3Ti composite by ECAP is caused by the increment in the number of the Al_3Ti particles and the exposure of $\{112\}_{Al3Ti}$ plane on fragmented surface.

In previous studies, Sato *et al.* have investigated effects of symmetric rolling (SR) for the Al-Al_3Ti composite on its grain refinement ability and this rolling can performed large specimen size compare to the small specimen size of ECAP [5]. It is reported that the SR for the Al-Al_3Ti composite fragments the platelet Al_3Ti particles and the number of the Al_3Ti particles increases in the Al-Al_3Ti composite. According to theirs study, they have suggested that the SR for the Al-Al_3Ti composite can enhance its grain refinement ability for the as-cast Al as well as ECAP. However, the problem of this technique is the particle size reduction becomes saturated at reduction ratio of 45 %. This is because that the fragmentation of the Al_3Ti particles hardly occurs since the longitudinal direction of the platelet Al_3Ti particles are oriented parallel to the rolling direction. In order to obtain severe fragmentation of the Al_3Ti particle, it is necessary to induce larger shear strain for the Al_3Ti particles.

In recent years, the industries used to induce larger shear strain by asymmetric rolling (ASR) and multi-directional forging (MDF) techniques. ASR technique, which the circumferential velocities of the top and bottom rolls are different [9-14]. The ASR can give larger shear strain uniformly throughout the sheet thickness. Moreover, the ASR would be able to fragment the Al_3Ti particles in the Al-Al_3Ti composite finer comparing with the SR. However, the distribution

change of the platelet Al_3Ti particles in the Al-Al_3Ti composite by the ASR is still unclear. On the other hand, Sato *et al.* reported that spatial distribution of Al_3Ti particles in the Al-Al_3Ti composite during MDF [15] and it is expected that MDF can also fragment the Al_3Ti particles in the Al-Al_3Ti composite.

In this study, the fragmentation behavior of the platelet Al_3Ti particles in the Al-Al_3Ti composite by MDF or SR or ASR are investigated. Especially, microstructure of the fragmented Al_3Ti particles in the Al-Al_3Ti composite deformed by MDF or SR or ASR are observed. In addition, these severe plastic deformation processes can be applied easily as industrial processing comparing with ECAP. Based on the obtained results, the efficiency of MDF or SR or ASR in fragmenting the platelet Al_3Ti particles in the Al-Al_3Ti composite is discussed.

5.2 Experimental procedure

5.2.1 Preparation of Al-Al_3Ti composites for MDF, SR and ASR

Specimens for MDF, SR and ASR were fabricated from a commercial Al-5mass%Ti alloy ingot. This ingot contains platelet Al_3Ti particles with volume fraction of 11% in an α-Al matrix and this ingot was cast at 800 °C using a graphite crucible. At first, the specimen with dimensions of 10 × 14 × 19.5 mm^3 (aspect ratio of 1.00: 1.40: 1.95) in rectangular shape were cut mechanically from this ingot. Using this specimen MDF was carried out.

After that, the Al-Al_3Ti composite with 200 mm × 60 mm × 10 mm in plate shape were mechanically cut from as-cast ingot. These obtained specimens were used for the SR or ASR.

5.2.2 MDF, SR and ASR for the Al-Al_3Ti composites

The MDF was performed on the Al-Al_3Ti composite up to 3 passes at the strain rate of 6.7×10^{-3} 1/s using an Instron-type compression machine. The logarithmic strain induced by MDF one pass was 0.67 at room temperature. The schematic illustration of die and plunger for MDF was shown in **Fig 5.1**. The forging axis for MDF was changed by 90° pass-by-pass. In addition, the plunger and die were used to keep the MDF specimen shape constant.

Furthermore, the SR and ASR were subjected on the Al-Al_3Ti composites up to 10 passes at room temperature. Reduction ratio for 1 pass is 10% or 20%. The circumferential velocity of the rolls for the SR is 2 m /min. In case of the ASR, the circumferential velocity of the upper roll is 2 m /min and that of the lower roll is 1.54 m / min. Therefore, asymmetrical ratio of the ASR used in this study is 130%. The conditions of the ASR and SR are summarized in **Table 5.1**.

5.2.3 Microstructural observation of the Al-Al_3Ti composites

2-dimensional (2D) microstructural observations of the Al-Al_3Ti composites after SPD were carried out by scanning electron microscopy (SEM). **Figure 5.2** shows specimen coordinate system for microstructural observation of MDFed Al-Al_3Ti composites. In addition, microstructures of the ASRed or SRed Al-Al_3Ti composites were observed from TD as shown in **Fig 5.3**.

5.3 Results and discussion

5.3.1 Initial microstructure of Al-Al_3Ti composites contain platelet Al_3Ti particles

SEM micrographs showing microstructure of the Al-Al_3Ti composites comprises platelet Al_3Ti particles before MDF and SR or ASR processes as shown in **Fig. 5.4** (a) and **Fig 5.5** (a), respectively. The SEM micrograph of the Al-Al_3Ti composites before SPD shows the coarse platelet Al_3Ti particles are distributed in the α-Al matrix. In addition, longitudinal direction of the platelet Al_3Ti particles are randomly oriented. This microstructure observed is similar with the microstructure of the non-deformed Al-Al_3Ti composite reported in the previous studies [6,7].

5.3.2 Microstructure of Al-Al_3Ti composites contain platelet Al_3Ti particles by MDF

Figures. 5.4 (b) through (d) show the microstructures of the Al-Al_3Ti composites after MDF up to 3 passes. It is observed that the platelet Al_3Ti particles are fragmented by MDF. When 1 pass of MDF is subjected to the Al-Al_3Ti composite, several cracks are observed in the platelet Al_3Ti particles as shown in **Fig 5.4** (b). Moreover, increasing the number of MDF passes, the cracks in the Al_3Ti particles also increase. In previous studies, it is found that cracks generated along with the twin boundary-initiated deformation and crack propagation along with the twin boundary result in the fragmentation of Al_3Ti particles in the Al-Al_3Ti composites by ECAP and compression [8, 16]. Therefore, the platelet Al_3Ti particles in the Al-Al_3Ti composites are severely fragmented by MDF.

5.3.3 Microstructure of Al-Al_3Ti composites contain platelet Al_3Ti particles by SR or ASR

Figures 5.5 (b) through (d) show that the platelet Al_3Ti particles in the Al-Al_3Ti composites are fragmented by ASR or SR. It is observed that some Al_3Ti particles are remained without fragmentation although large amount of the Al_3Ti particles are fragmented by SR10 **Fig 5.5** (b). Moreover, these fragmented Al_3Ti particles are weakly oriented to RD. Meanwhile, the Al_3Ti particles in the ASR10 and the ASR20 are severely fragmented and the fragmented Al_3Ti particles are strongly aligned to RD. From these results, it is seen that the ASR can induce larger shear strain comparing with the SR.

Figures 5.6 (a) and (b) are graphs of the mean size and the aspect ratio of the Al_3Ti particles as a function of total reduction ratio, respectively. The mean size of the Al_3Ti particles are reduced as increasing total reduction ratio by ASR or SR as shown in **Fig 5.6**. Comparing the mean sizes of the Al_3Ti particles in the SR10, ASR10 and ASR20, the size of the Al_3Ti particles in the SR10 is the largest under the same total reduction ratio. This result suggests that the ASR can induce larger shear strain than the SR under the same reduction ratio. In addition, the mean sizes of the Al_3Ti particles in the ASR10 and the ASR20 are saturated at total reduction ratio of more than 60% while the mean size of the Al_3Ti particles in the SR10 does not change anymore around total reduction ratio of 50%. Sato *et al.* reported that the size of Al_3Ti particles are saturated at reduction ratio of 45% when Al-Al_3Ti composite is symmetric rolled at room temperature [6]. The result of the SR10 in this present study is good agreement with that previous study. Therefore, it is found from the saturation behavior of the Al_3Ti particle size that the shear strain induced by ASR is larger comparing with the SR.

The aspect ratio of the Al_3Ti particle in the SR10 is larger than those in the ASR10 and the ASR20 as shown in **Fig 5.6** (b). This means that the ASR can fragment the Al_3Ti particles more severely and make more granular shaped Al_3Ti particles. Hence, the ASR is more effective processing to fragment the Al_3Ti particles in the Al-Al_3Ti composite.

5.3.4 Fragmentation process of the Al_3Ti particles in the Al-Al_3Ti composites by SPD

At first, during MDF is performed to the Al-Al_3Ti composite, the cubic elements undergo continuous change as shown in **Fig. 5.7**. Al_3Ti particles are fragmented by shear deformation of the α-Al matrix during MDF 1 pass. When the number of MDF passes increases the cubic elements undergo deformation in all three planes as shown in **Fig 5.7**.

Figure 5.8 is schematic illustration showing fragment process of the platelet Al_3Ti particle in the Al-Al_3Ti composite during the rolling process. **Figure 5.8** (a) shows the undeformed Al-Al_3Ti composite comprises coarse platelet Al_3Ti particles before SR or ASR. When the SR or ASR are subjected to the Al-Al_3Ti composite, the platelet Al_3Ti particles are fragmented due to shear deformation by the rolling as shown in **Fig. 5.6** (b). It is found that the crack generated at the fragmentation of the Al_3Ti particle propagates to its thickness direction and this crack in the Al_3Ti particle propagates to TD as well as its thickness direction. This is because of the plain strain deformation during SR or ASR [17, 18]. Moreover, the fragmented Al_3Ti particles are oriented to shear direction and the plane normal direction becomes close to ND. **Figure 5.8** (c) shows that the small platelet Al_3Ti particles with longitudinal direction parallel to TD are aligned to RD. in previous studies, the fragmentation behavior of platelet β-AlFeSi particles in Al–7

mass%Si–1 mass%Fe alloy by ECAP, MDF, ASR and SR were investigated [19]. It is found that the β-AlFeSi particles fragmented by ASR remains platelet shape and crack in these particles propagates to TD and its thickness direction. This fragmentation behavior of the β-AlFeSi particles is agreement with the present results as shown in **Fig. 5.8**.

Considering the efficiency to fragment the platelet Al_3Ti particles in the Al-Al_3Ti composite under the same number of passes, the ASR is more effective than the SR because of its larger shear strain. However, if the plane normal direction of the Al_3Ti particle becomes parallel to ND, the fragmentation of the Al_3Ti particles would not occur anymore even by the ASR. Therefore, it can be concluded that the shear deformation from multiple direction is effective to fragment the platelet Al_3Ti particle in the Al-Al_3Ti composite.

5.4 Conclusions

Microstructure and fragmentation process of the platelet Al_3Ti particles in the Al-Al_3Ti composite by MDF or SR or ASR are investigated. The Al-Al_3Ti composites are deformed by MDF or SR or ASR. The obtained conclusions were as follows,

(1) Platelet Al_3Ti particles in the Al-Al_3Ti composite are fragmented by MDF, SR and ASR. The ASR can fragment the platelet Al_3Ti particles refiner than the SR. This is because that the ASR can induce larger shear strain comparing with the SR.

(2) Increasing the number of SPD processes, the fragmentation of Al_3Ti particle severely occurs in the Al- Al_3Ti composite.

(3) The ASR is more effective to fragment the Al_3Ti particles in the Al-Al_3Ti composite rather than the SR. However, the shear deformation from multiple direction is necessary in order to fragment the Al_3Ti particle refiner.

References

[1] A. Cibula, The mechanism of grain refinement of sand casting in aluminium alloys, J. Inst. Met., **76** (1949-1950) 321-60.
[2] F. A. Crossley and L. F. Mondolfo, Mechanism of grain refinement in aluminum alloys, Trans. AIME, **191** (1951) 1143-48.
[3] P. S. Mohanty and J. E. Gruzleski, Mechanism of grain refinement in aluminium, Acta Metall. Mater., **43** (1995) 2001-2012.
[4] P. Li, E. G. Kandalova and V. I. Nikitin, Grain refining performance of Al-Ti master alloys with different microstructures, Mater. Lett., **59** (2005) 723-727.
[5] Z. Zhang, S. Hosoda, I-S. Kim and Y. Watanabe, Grain refining performance for Al and Al-Si alloy casts by addition of equal-channel angular presses Al-5 mass% Ti alloy, Mater. Sci. Eng. A, **425 (**2006) 55-63.
[6] H. Sato, K. Ota, H. Kato, M. Furukawa, M. Azuma, Y. Watanabe, Z. Zhang and K. Tsuzaki, Grain refinement of as-cast pure Al by cold rolled Al-Ti alloy refiner, Mater. Trans., **54** (2013) 1554-1561.
[7] H. Sato and Y. Watanabe, Three-dimensional microstructural analysis of fragmentation behavior of platelet Al_3Ti particles in Al-Al_3Ti composite deformed by equal channel angular pressing, Mater. Charact., **144** (2018) 305-15.
[8] Y. M. Hwang and G. Y. Tzou, An analytical approach to asymmetrical hot-sheet rolling considering the effects of the shear stress and internal moment at the roll gap, J. Proc. Technol., **52** (1995) 399-424.
[9] Y. M. Hwang and G. Y. Tzou, Analutical and experimental study on asymmetrical sheet rolling, Int. J. Mech. Sci., **39** (1997) 289-303.
[10] K. H. Kim and D. N. Lee, Analysis of deformation textures of asymmetrically rolled aluminum sheets, Acta Mater., **49** (2001) 2583-2595.
[11] J. Sidor, A. Miroux, R. Petrov and L. Kestens, Microstructural and crystallographic aspects of conventional and asymmetric rolling processes, Acta Mater., **56** (2008) 2495-2507.
[12] Y. H. Ji and J. J. Park, Analysis of thermo-mechanical process occurred in magnesium alloy AZ31 sheet during differential speed rolling, Mater. Sci. Eng. A, **485** (2008) 299-304.
[13] S. Wronski and B. Bacroix, Microstructure evolution and grain refinement in asymmetrically rolled aluminium, Acta Mater., **76** (2014) 404-412.
[14] H. Sato, F. Teshima and Y. Watanabe, Effects of forging temperature on Al_3Ti particle distribution in Al-Al_3Ti multi-phase materials deformed by multi-directional forging, J. J. I. L. M., **68** (2018) 2-8 (in Japanese).
[15] S. B. Duraisamy, H. Sato, T. Chiba and Y. Watanabe, Fragmentation process of platelet Al_3Ti particles in compressed Al-Al_3Ti alloy observed by serial sectioning and EBSD analysis, Mater. Res. Express, **6** (2019) 096575 1-8.
[16] P. Juntunen, D. Raabe, P. Karjalainen, T. Kopio and G. Bolle, Optimizing continuous annealing of interstitial-free steels for improving deep drqwability, Metall. Mater. Trans. A, **32A** (2001) 1989-1995.
[17] J.C. Lee, H. K. Seok and J. Y. Suh, Microstructural evolutions of the Al strip prepared by cold rolling and continuous equal channel angular perssing, Acta. Mater., **50** (2002) 4005-4019.
[18] K. Kagimoto, M. Yamada, H. Sato, Y. Watanabe and N. Yamanaka, Fragmentation of platelet-shaped β-AlFeSi intermetallic compound particles in Al-7mass%Si-1mass%Fe alloy by equal-channel angular pressing, multi-directional forging, symmetric rolling and asymmetric rolling, Keikinzoku, **68**

(2018) 673-676.

Table 5.1. The conditions of the ASR and SR for the Al-Al_3Ti composites.

Name of specimen	Type of rolling	Circumferential velocity of rolls	Reduction ratio for 1 pass
ASR10	Asymmetric rolling	Upper roll: 2 m/min Lower roll: 1.54 m/min	10 %
ASR20			20 %
SR10	Symmetric rolling	Upper roll: 2 m/min Lower roll: 2 m/min	10 %

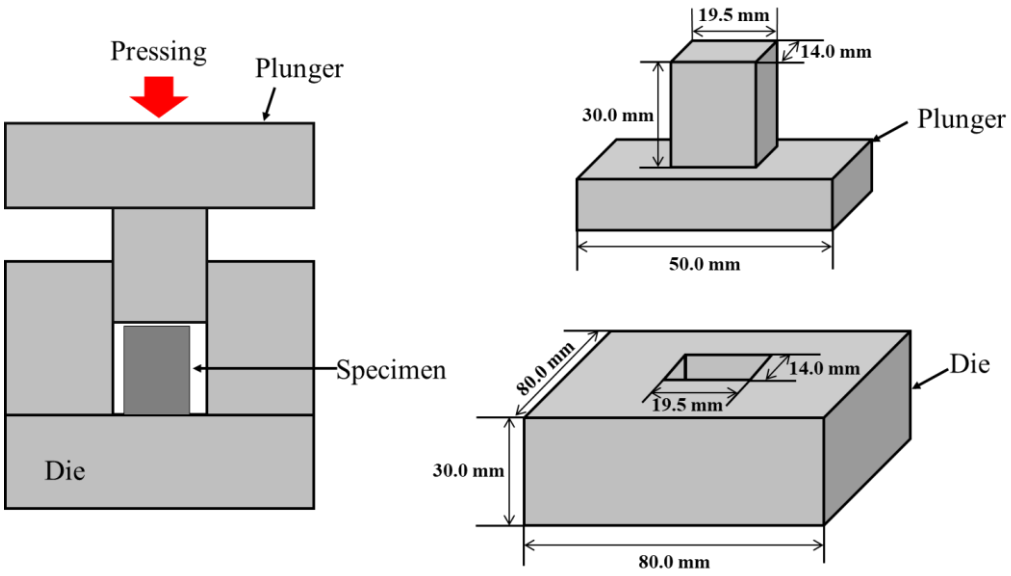

Fig. 5.1. Schematic representations of the MDF process.

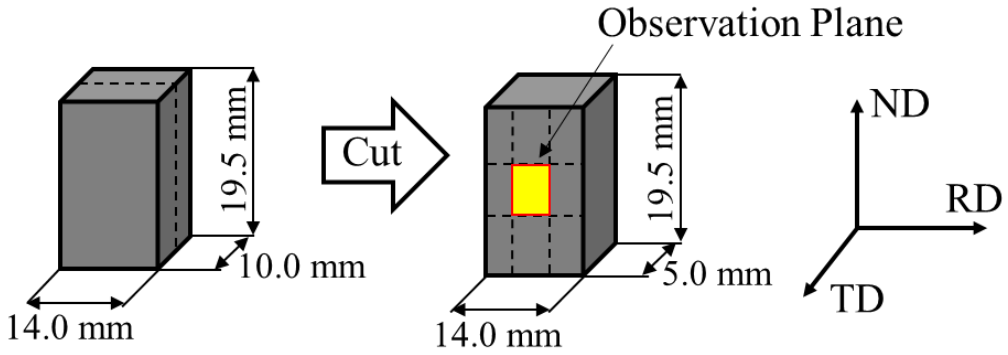

Fig. 5.2. The specimen coordinate system for microstructural observations of the Al-Al_3Ti composites during MDF.

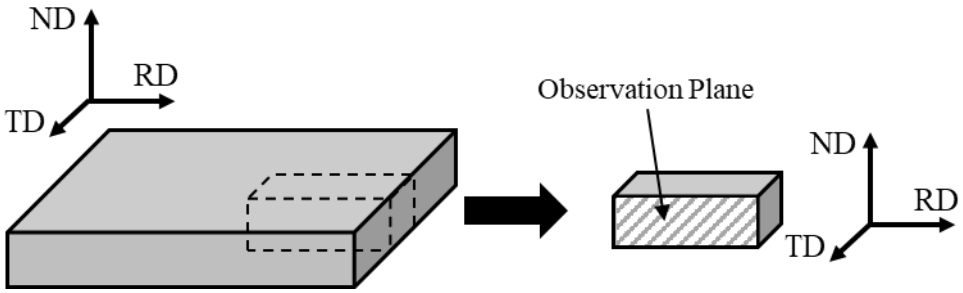

Fig 5.3. The specimen coordinate system for microstructural observation of Al-Al_3Ti composites by ASR and SR.

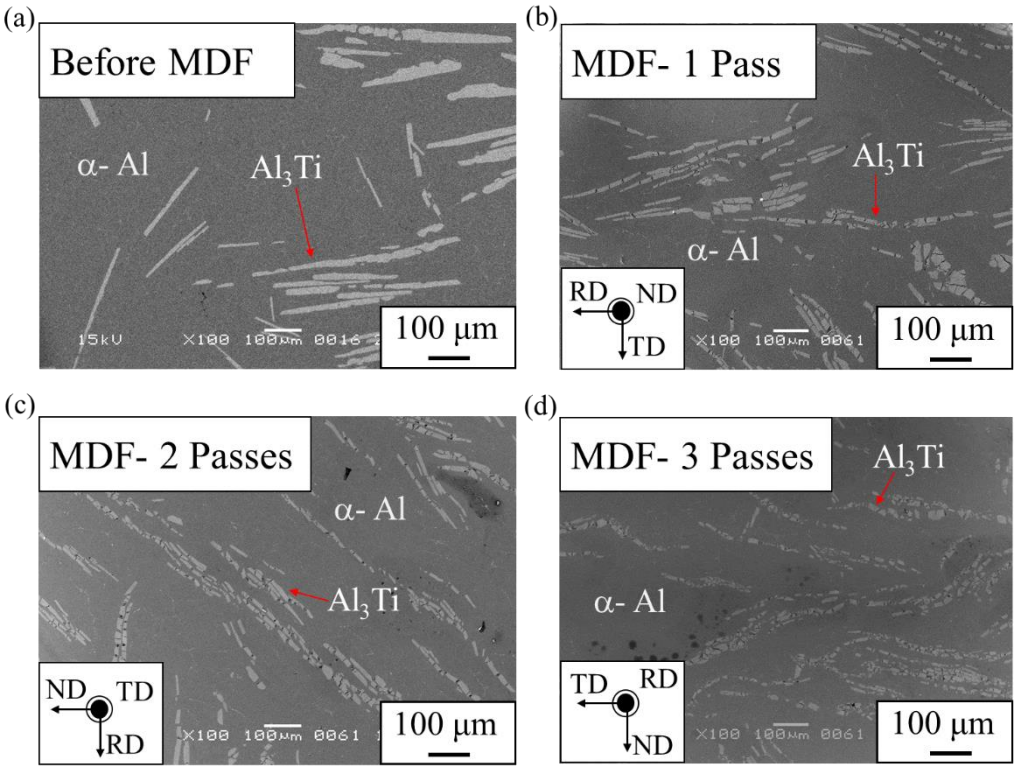

Fig. 5.4. SEM photographs showing the microstructures of Al-Al_3Ti composites by MDF (a) before MDF, (b) MDF-1 pass, (c) MDF-2 passes and (d) MDF-3 passes.

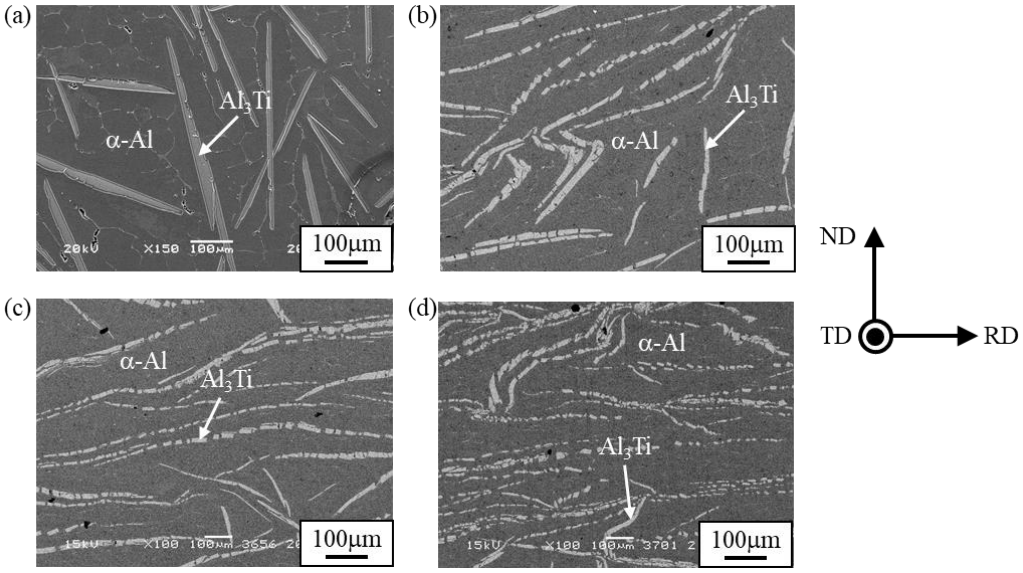

Fig. 5.5. SEM photographs showing microstructures of (a) undeformed Al-Al_3Ti specimen, (b) SR10, (c) ASR10 and (d) ASR20. The SR10, the ASR10 and the ASR20 are the specimens rolled at 5 passes.

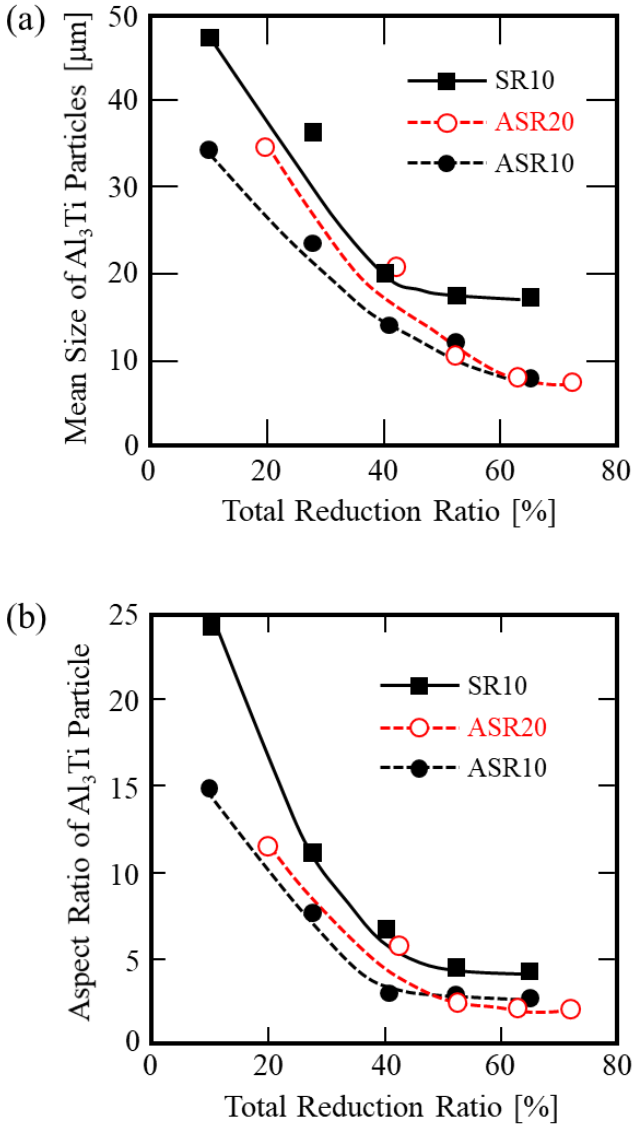

Fig. 5.6. (a) mean size and (b) aspect ratio of Al_3Ti particles in the Al-Al_3Ti specimens as a function of total reduction ratio.

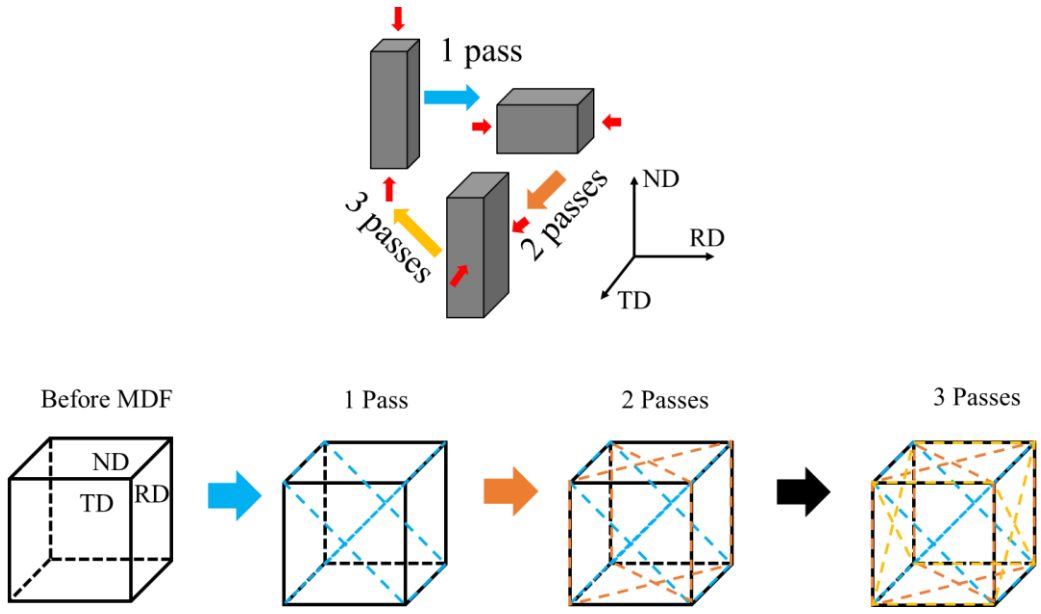

Fig. 5.7. Schematic illustrations showing deformation applied to cubic elements during MDF.

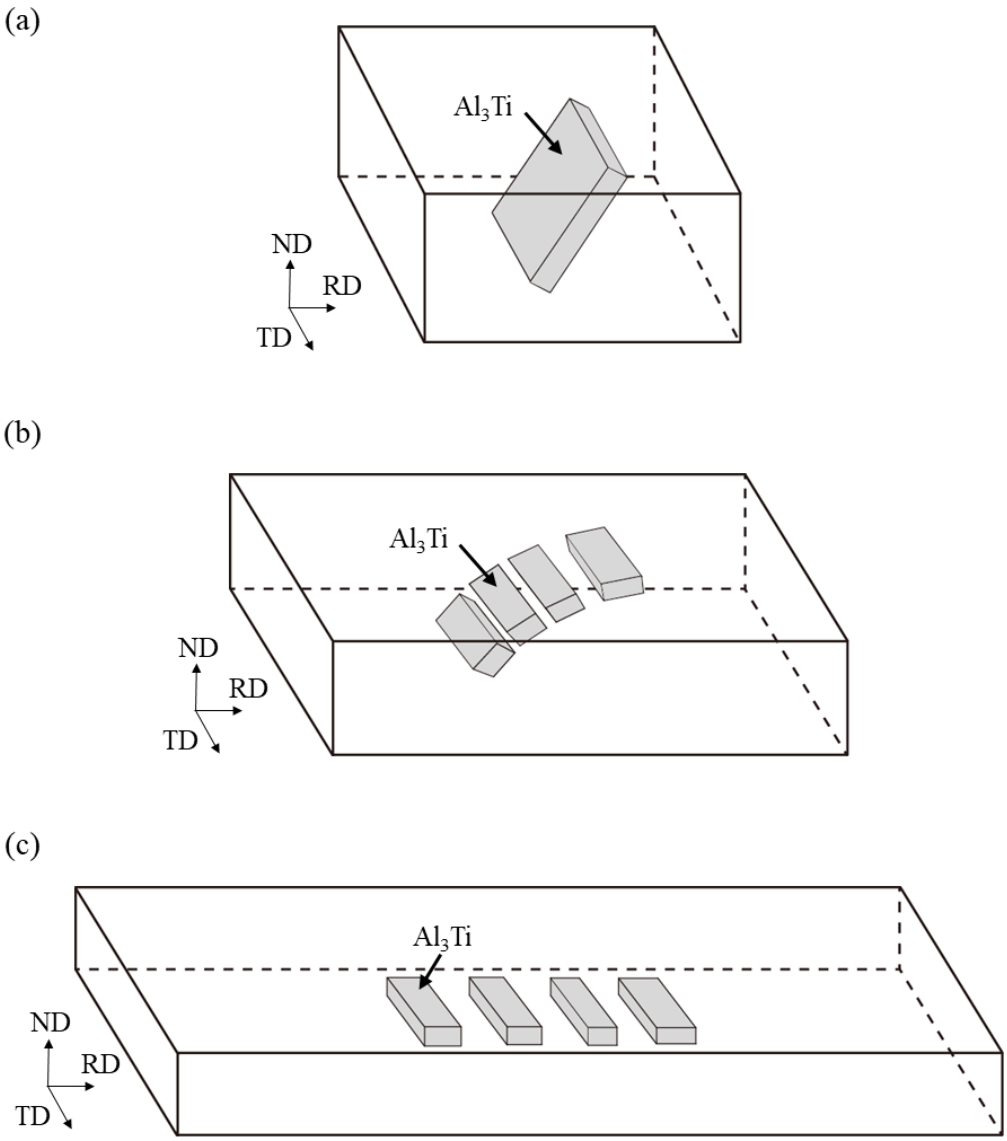

Fig. 5.8. Schematic illustrations showing fragment process of platelet Al_3Ti particle in the Al-Al_3Ti composite during the rolling process: (a) undeformed specimen, (b) specimen rolled with small reduction ratio and (c) specimen with large reduction ratio.

Chapter 6

Grain refinement application of Al-based composite by severe plastic deformation

6.1 Introduction

In recent years, grain refinement of as-cast Al by adding grain refiner has attracted much attention in both academic and industrial field applications [1-13]. When the grain refiner is added into the as-cast Al, it dissolves into the melt and releases the intermetallic particles to act as effective heterogenous nucleation site. The popular grain refiners for as-cast Al are Al-Ti, Al-Ti-B and Al-Ti-C alloys [1-13]. This is because those alloys contain the larger number of intermetallic particles such as Al_3Ti, TiB_2 or TiC particles. These intermetallic particles provide a role of effective heterogeneous nucleation site for the α-Al. As a result, it is found that the addition of the grain refiners into the pure Al melt can promote the as-cast Al having equiaxed and fine α-Al grains during solidification process. The obtained equiaxed grain structure ensures the improved machinability, uniform mechanical properties and various features. In addition, to obtain the equiaxed grain structure of as-cast Al, the number effective heterogeneous nucleation particles in grain refiners plays a major role.

In previous studies, grain refinement ability of the Al-Ti-C composite for the as-cast Al by severe plastic deformation was investigated [6]. This severe plastic deformation for the Al-Ti-C composite have made by equal channel angular pressing (ECAP) and it is found that the number of intermetallic particles increases after fragmentation [6]. In addition, it is reported that the ECAPed grain refiner has better grain refining ability compare to the same refiner before ECAP. On the

other hand, Zhang *et al.* investigated that the grain refinement ability of Al-Al_3Ti composite contains platelet Al_3Ti particles are fragmented by ECAP [8]. According to their study, the ECAPed Al-Al_3Ti composite has better grain refinement ability compare to the Al-Al_3Ti composite before ECAP. In addition, it is reported that the grain refinement ability of Al-Al_3Ti composite by ECAP comes from the increases in the number of intermetallic Al_3Ti particles and these particles can act as effective nuclei for the α-Al. Hence, ECAP is the effective technique to improve the grain refinement ability of the Al-Al_3Ti composite. However, in term of industrial application, the application of ECAP is limited because the specimen obtained by ECAP is relatively small.

In previous studies, Sitdikov *et al.* have suggested the grain refinement by SPD using multi-directional forging (MDF) process [4]. This process can deform relatively large size of the specimen compare to other SPD techniques and it is expected that MDF is suitable for industrial application.

In this study, microstructure evolution and grain refining performance of the Al-Al_3Ti composite comprises the platelet Al_3Ti particles deformed by ECAP and MDF are investigated. Especially, grain refinement ability of the Al-Al_3Ti composite deformed by ECAP and MDF are evaluated. Based on the obtained results, the grain refinement ability of the Al-Al_3Ti composite by ECAP and MDF is discussed.

6.2 Experimental procedure

6.2.1 Preparation of Al-Al_3Ti composites for ECAP and MDF

Specimens for ECAP and MDF were fabricated from a commercial Al-5mass%Ti alloy ingot [14-16]. This ingot was cast at 800 ℃ using a graphite

crucible under argon gas atmosphere and this ingot contains platelet Al_3Ti particles with volume fraction of 11% in an α-Al matrix. From the as-cast ingot, at first, the rod shape Al-Al_3Ti composite with 10 mm in diameter and 60 mm in length was prepared by lathe machining and the prepared Al-Al_3Ti composite was homogenized at 500 °C for 1 h. Using this specimen ECAP was carried out. On the other hand, rectangular shape specimens for the MDF with dimensions of 10 × 14 × 19.5 mm^3 (aspect ratio of 1.00: 1.40: 1.95) were cut mechanically from the cast ingot. Using this specimen MDF was carried out.

6.2.2 ECAP and MDF for the Al-Al_3Ti composites

ECAP was subjected to the Al-Al_3Ti composite up to 1 pass. This ECAP was performed using an Instron-type compression machine at room temperature. The nominal equivalent strain induced to the specimen during 1 pass is about 1.01 with pressing speed of 5 mm/min. On the other hand, MDF was subjected to the Al-Al_3Ti composite up to 3 passes at room temperature. This MDF was performed using an Instron-type compression machine at the strain rate of 6.7×10^{-3} 1/s. The logarithmic strain induced by MDF one pass was 0.67.

Furthermore, microstructures of the Al-Al_3Ti composites after ECAP and MDF were observed by scanning electron microscopy (SEM), electron backscatter diffraction (EBSD) and optical microscopy (OM).

6.2.3 Grain refining performance of the Al-Al_3Ti composites by ECAP and MDF

Grain refining performance of the Al-Al_3Ti composites for pure Al (99.99% purity) was accomplished by a graphite crucible as shown in **Fig 6.1**. At first, pure Al ingot of 148.8 g was melted at 750 °C in argon gas atmosphere. Then, the addition of Al-Al_3Ti composite refiner of 1.2 g into the melt. The melt was stirred for 30 s using the road and kept for 1800 s after the addition of refiners. The

melt was poured into a cylindrical steel mold of 45 mm in inner diameter and 70 mm in outer diameter. The as-cast Al was cut horizontally at 5 mm from the bottom of each specimen. The sectioned surface was mechanically and chemically polished. Etching with a 10% hydrofluoric acid was carried out before observation. The quantitative measurement of the mean α-Al grain size was obtained using mean liner intercept method.

6.3 Results and discussion

6.3.1 Microstructure of Al-Al_3Ti composite refiners

Figure 6.2 is SEM micrographs showing the initial microstructure of Al-Al_3Ti composite comprises platelet Al_3Ti particles. The SEM micrograph of the Al-Al_3Ti composite before SPD shows the coarse platelet Al_3Ti particles are randomly distributed in the α-Al matrix. In addition, inverse pole figure (IPF) and image quality (IQ) maps of the Al-Al_3Ti composite before SPD as shown in **Fig 6.3**. There is no plastic strain observed in the Al-Al_3Ti composite before SPD and this result is agreement with the previous studies [14-17]. Furthermore, the distribution of the length of platelet Al_3Ti particles in the initial specimen is calculated and the calculated value is shown in **Fig 6.5** (a). Length of platelet Al_3Ti particles are calculated from about more than 500 Al_3Ti particles form the SEM micrographs. The calculated mean length of Al_3Ti particles are summarized in **Table 6.1**. It is found that the mean length of platelet Al_3Ti particles in the Al-Al_3Ti composites decreases by ECAP and MDF.

6.3.2 Microstructure of Al-Al_3Ti composites by ECAP and MDF

Figures. 6.4 show the microstructures of the Al-Al_3Ti composites after ECAP 1 pass and MDF up to 3 passes. It is observed that the platelet Al_3Ti particles are fragmented in all of the specimens. When 1 pass of ECAP is subjected to the Al-Al_3Ti composite, several cracks are observed in the platelet Al_3Ti particles as shown in **Fig 6.4** (a). Moreover, the length of Al_3Ti particles also decreases by ECAP with 1 pass. This means that the number of Al_3Ti particles increases in the Al-Al_3Ti composite by ECAP. On the other hand, the platelet Al_3Ti particles are fragmented by MDF up to 3 passes as shown in **Fig 6.4** (b-d). In previous studies, it is reported that the Al_3Ti particles in the Al-Al_3Ti composite fragmented by ECAP and MDF [14, 15]. **Figure 6.5** (b-e) shows that the Al_3Ti particles length decreases after SPD. Therefore, the platelet Al_3Ti particles in the Al-Al_3Ti composites are fragmented by ECAP and MDF. This indicates that after SPD the number density of Al_3Ti particles in the Al-Al_3Ti composite increases after fragmentation. In addition, the Vickers hardness distribution of the Al-Al_3Ti composites are obtained as shown in **Fig 6.5**. In all the specimens, it is found Vickers hardness values show the clear trend of improvement after ECAP and MDF. This clearly indicates that the grain size of the α-Al matrix decreases after ECAP and MDF.

6.3.3 Microstructure of as-cast Al by Al-Al_3Ti composite refiner

Figures 6.6 shows that the microstructure of the as-cast Al without and with addition of Al-Al_3Ti composite refiner. The mean size of the α-Al grain is very large in the as-cast Al without addition Al-Al_3Ti composite refiner as shown in **Fig 6.6** (a). In addition, this as-cast Al contains columnar structure. Furthermore,

when the Al-Al_3Ti composite refiner was added to the as-cast Al, the mean size of the α-Al grain are decreases as shown in **Fig 6.6** (b).

Figure 6.7 is a set of OM photographs showing the as-cast Al with SPDed Al-Al_3Ti composite refiner. When 1 pass ECAPed Al-Al_3Ti composite refiner is added to the as-cast Al and the as-cast Al has smallest equiaxed α-Al grains as shown in **Fig 6.7** (a). This is because of the ECAPed Al-Al_3Ti composite refiner contains the large number of Al_3Ti particles and these particles provide numerous heterogeneous nucleation site for the α-Al grains. On the other hand, MDFed Al-Al_3Ti composite refiner is added to the as-cast Al and the α-Al grains becomes equiaxed. It is found that when the number of MDF passes increases the α-Al grains becomes finer as shown in **Fig 6.8**. In addition, none of the as-cast Al refined by SPDed Al-Al_3Ti composite refiner have columnar structure and all of the as-cast Al indicates the equiaxed structure as shown in **Fig 6.7**. This is because of the fragmented Al_3Ti particles provide numerous heterogeneous nucleation site for the α-Al grains. As a possible reason for the effective grain refinement ability of the Al-Al_3Ti composite refiner depends the number of Al_3Ti particles. ECAP and MDF are effective processes to enhance the grain refining ability of the Al-Al_3Ti composite refiner for the as-cast Al. Therefore, it is found that the Al-Al_3Ti composite refiner deformed by SPD has better grain-refining ability.

6.4 Conclusions

Microstructure evaluation and grain refining performance of the Al-Al_3Ti composite refiner contains platelet Al_3Ti particles deformed by ECAP and MDF

are investigated. The Al-Al_3Ti composites refiner are deformed by ECAP and MDF. The obtained conclusions were as follows,

(1) Platelet Al_3Ti particles in the Al-Al_3Ti composite refiner are fragmented by ECAP and MDF.

(2) Length of the platelet Al_3Ti particles in the Al-Al_3Ti composite refiner decreases by ECAP and MDF. Number of Al_3Ti particle in the Al- Al_3Ti composite increases are increases by ECAP and MDF.

(3) The effective grain refining performance for the as-cast Al was found by the addition of Al-Al_3Ti composite refiner. Fine grained as-cast Al can be obtained using the SPDed Al-Al_3Ti composite refiner. ECAP and MDF were effective processes to enhance the grain refining ability of the Al-Al_3Ti composite refiner for the as-cast Al.

References

[1] A. Cibula, The mechanism of grain refinement of sand casting in aluminium alloys, J. Inst. Met., **76** (1949-1950) 321-60.
[2] F. A. Crossley and L. F. Mondolfo, Mechanism of grain refinement in aluminum alloys, Trans. AIME, **191** (1951) 1143-48.
[3] P. S. Mohanty and J. E. Gruzleski, Mechanism of grain refinement in aluminium, Acta Metall. Mater., **43** (1995) 2001-2012.
[4] O. Sitdikov, T. Sakai, A. Goloborodko, H. Miura and R. Kaibyshev, Effect of pass strain on grain refinement in 7475 Al alloy during hot multidirectional forging, Mater. Trans., **45** (2004) 2232-2238.
[5] P. Li, E. G. Kandalova and V. I. Nikitin, Grain refining performance of Al-Ti master alloys with different microstructures, Mater. Lett., **59**, (2005) 723-727.
[6] Z. Zhang, Y. Watanabe, I. S. Kim, X. Liu and X. Bian, Microstructure and refining performance of an Al-5Ti-0.25C refiner before and after equal-channel angular pressing, Metall. Mater. Trans. A, **36A** (2005) 837-844.
[7] A. Kamio, J. Jpn. Inst. Light Met., **56** (2006) 496-500.
[8] Z. Zhang, S. Hosoda, I-S. Kim and Y. Watanabe, Grain refining performance for Al and Al-Si alloy casts by addition of equal-channel angular presses Al-5 mass% Ti alloy, Mater. Sci. Eng. A, **425 (**2006) 55-63.
[9] H. Sato, K. Ota, H. Kato, M. Furukawa, M. Azuma, Y. Watanabe, Z. Zhang and K. Tsuzaki, Grain refinement of as-cast pure Al by cold rolled Al-Ti alloy refiner, Mater. Trans., **54** (2013) 1554-1561.
[10] Y. Watanabe and H. Sato, Keikinzoku, **64** (2014) 157 [in Japanese].
[11] W. Ding, T. Xia and W. Zhao, Performance comparison of Al-Ti master alloys with different microstructures in grain refinement of commercial purity aluminum, Materials, **7** (2014) 3663-3676.
[12] K. Yamauchi, T. Kunimine, H. Sato and Y. Watanabe, Grain refinement of Al_3Ti dispersed aluminum matrix composites by reaction centrifugal mixed-powder method, Mater. Trans., **56** (2015) 99-107.
[13] Y. Wang, C. M. Fang, L. Zhou, T. Hashimoto, X. Zhou, Q. M. Ramasse and Z. Fan, Mechanism for Zr poisoning of Al-Ti-B based grain refiners, Acta. Mater., **164** (2019) 428-239.
[14] H. Sato and Y. Watanabe, Three-dimensional microstructural analysis of fragmentation behavior of platelet Al3Ti particles in Al-Al3Ti composite deformed by equal channel angular pressing, Mater. Charact., **144** (2018) 305-15.
[15] H. Sato, F. Teshima and Y. Watanabe, Effects of forging temperature on Al3Ti particle distribution in Al-Al3Ti multi-phase materials deformed by multi-directional forging, J. J. I. L. M., **68** (2018) 2-8 (in Japanese).
[16] S. B. Duraisamy, H. Sato, T. Chiba and Y. Watanabe, Fragmentation process of platelet Al_3Ti particles in compressed Al-Al_3Ti alloy observed by serial sectioning and EBSD analysis, Mater. Res. Express, **6** (2019) 096575 1-8.
[17] H. Sato, A. Mori, M. Kitagawa, S. B. Duraisamy, T. Chiba and Y. Watanabe, Three-dimensional analysis of fragmentation process of Al_3Ti platelet particles in Al-Al_3Timultiphase alloy deformed by asymmetric rolling, JOM, **72** (2020) 57-64.

Table 6.1. The mean length of platelet Al_3Ti particles in the Al-Al_3Ti composites.

Specimen	Condition	Mean Length (L/μm)
Initial specimen	0 pass	75.17
ECAP	1 pass	19.97
MDF	1 pass	25.36
	2 passes	13.45
	3 passes	9.96

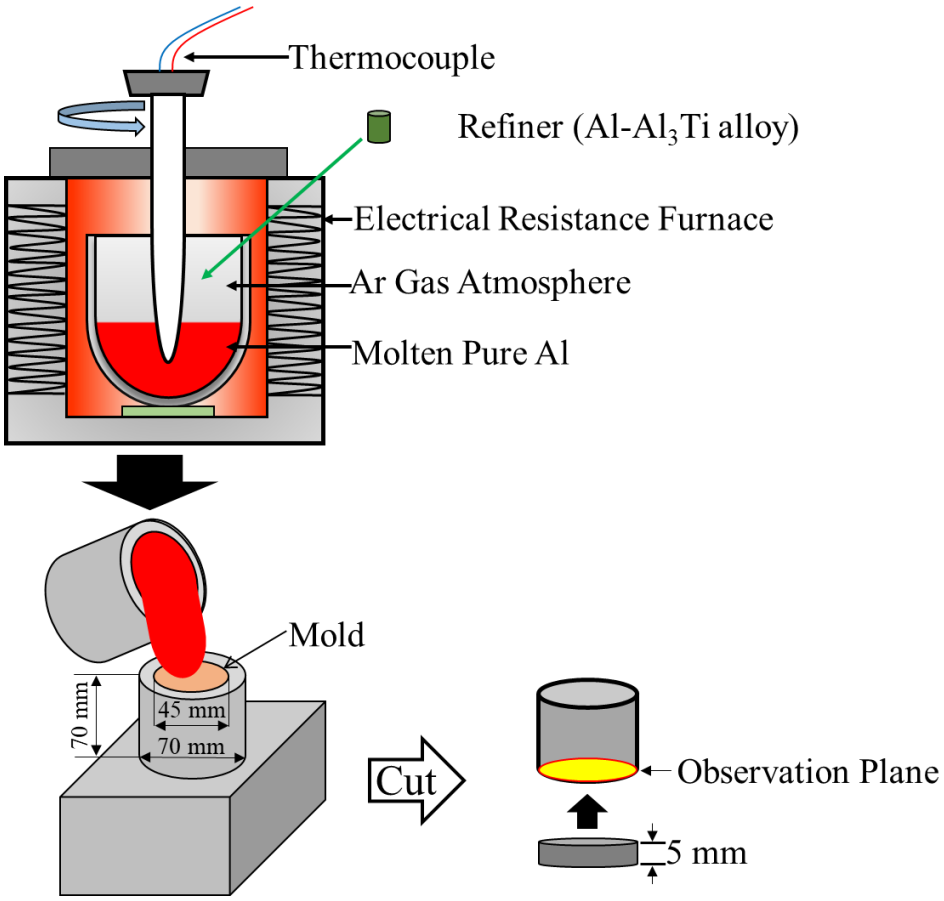

Fig. 6.1. Schematic representations of the casting test.

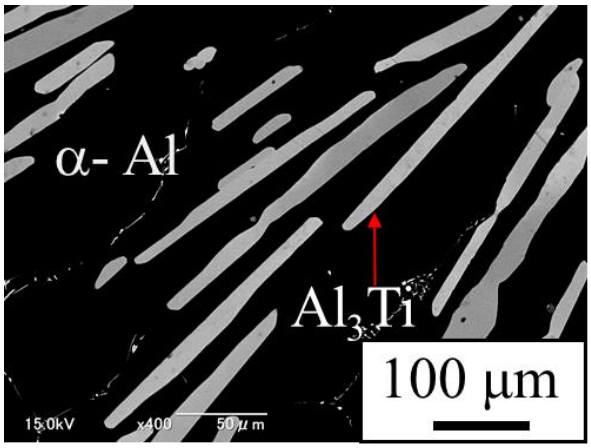

Fig. 6.2. The specimen coordinate system for microstructural observations of the Al-Al_3Ti composites during MDF.

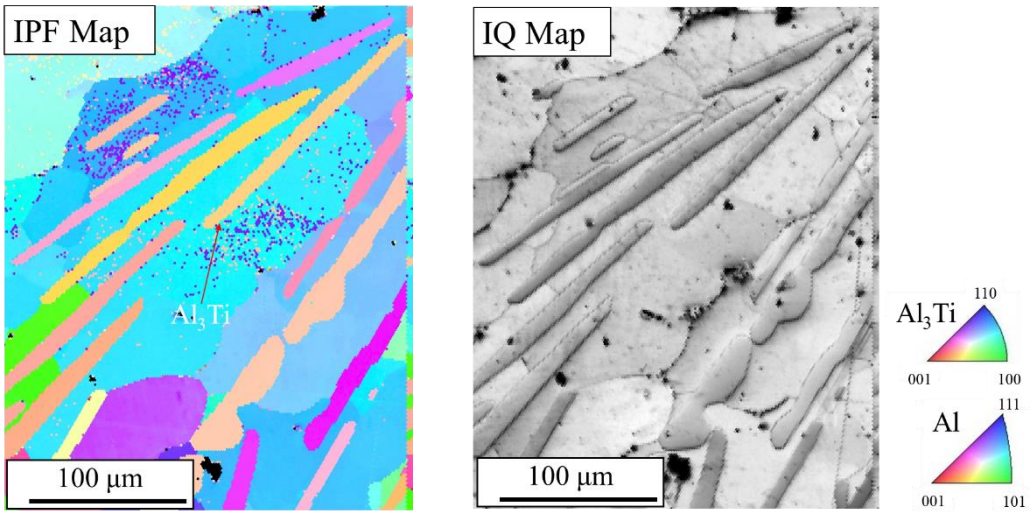

Fig 6.3. IPF (left) and IQ (right) maps of the Al-Al_3Ti composites before SPD.

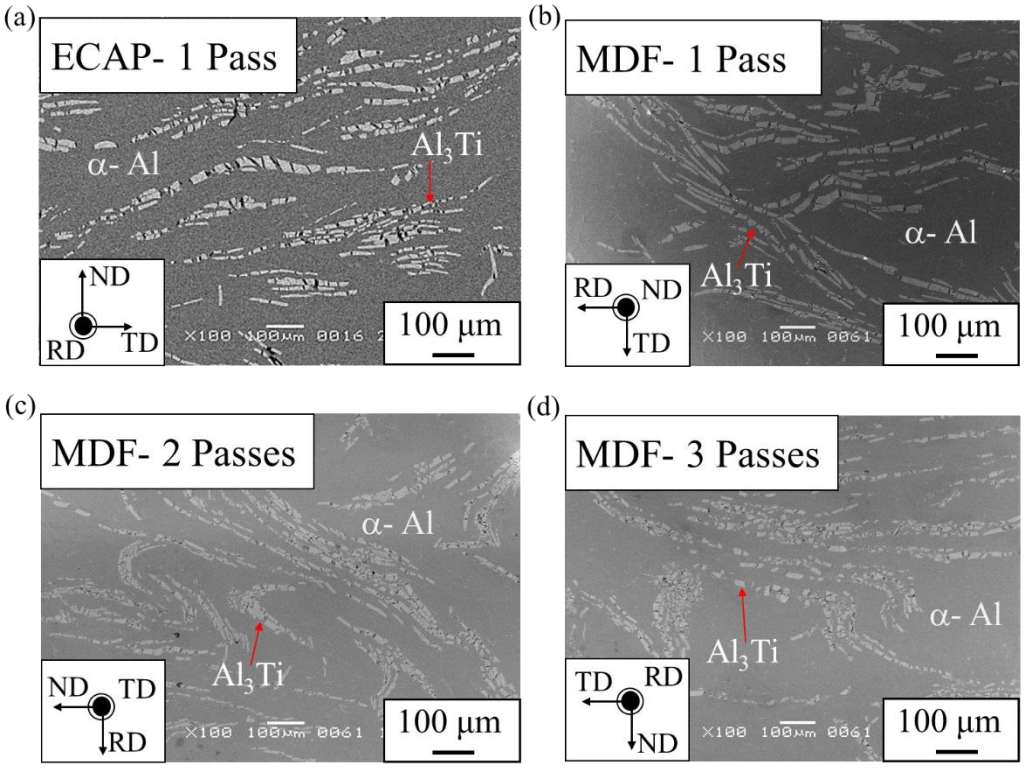

Fig. 6.4. SEM photographs showing the microstructures of Al-Al_3Ti composites after (a) ECAP-1 pass, (b) MDF-1 pass, (c) MDF-2 passes and (d) MDF-3 passes.

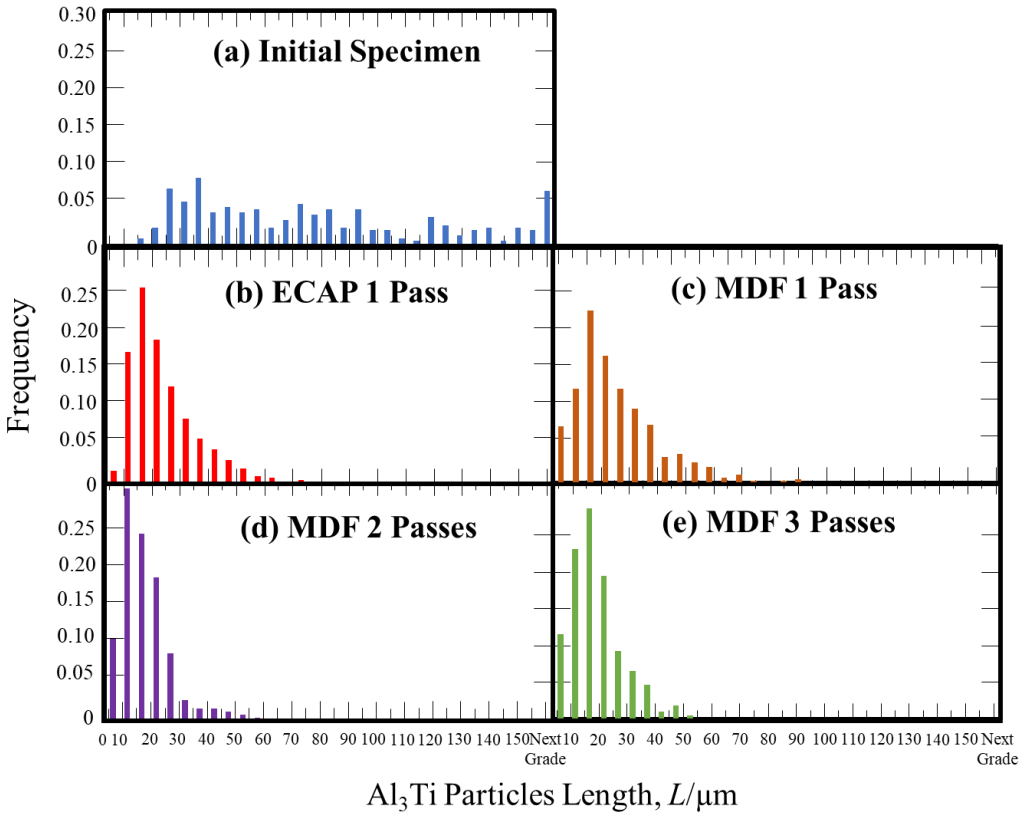

Fig. 6.4. The length of the Al_3Ti particles (a) initial specimen, (b) ECAP-1 pass, (c) MDF-1 pass, (d) MDF-2 passes and (e) MDF-3 passes.

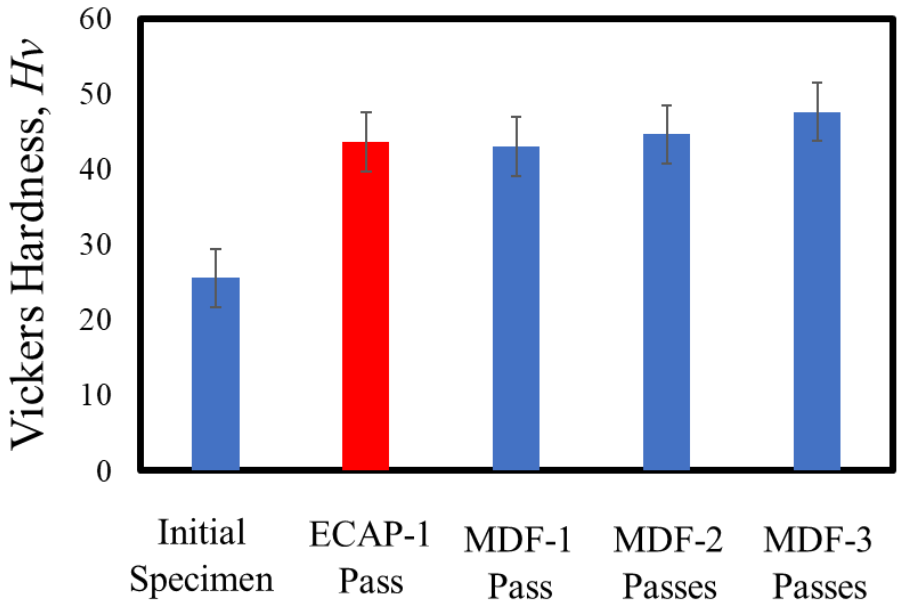

Fig. 6.5. The Vickers hardness distribution in the Al-Al_3Ti composites.

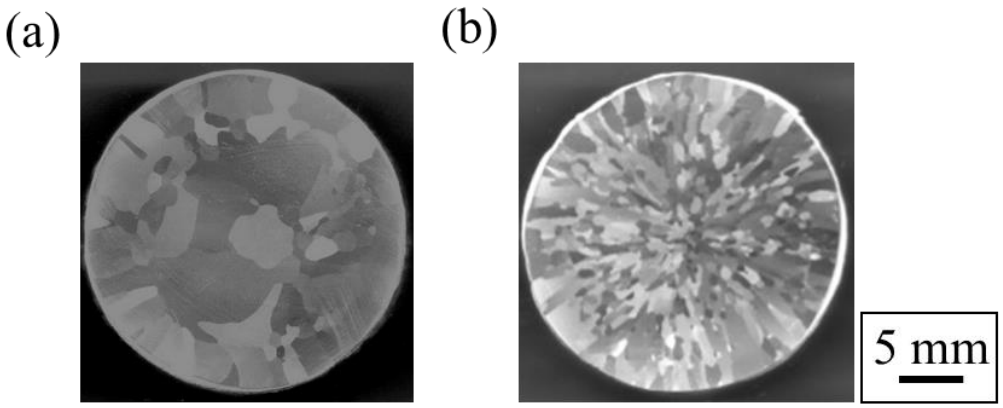

Fig. 6.6. OM photographs of the as-cast Al (a) without refiner and (b) with Al-Al_3Ti composite refiner.

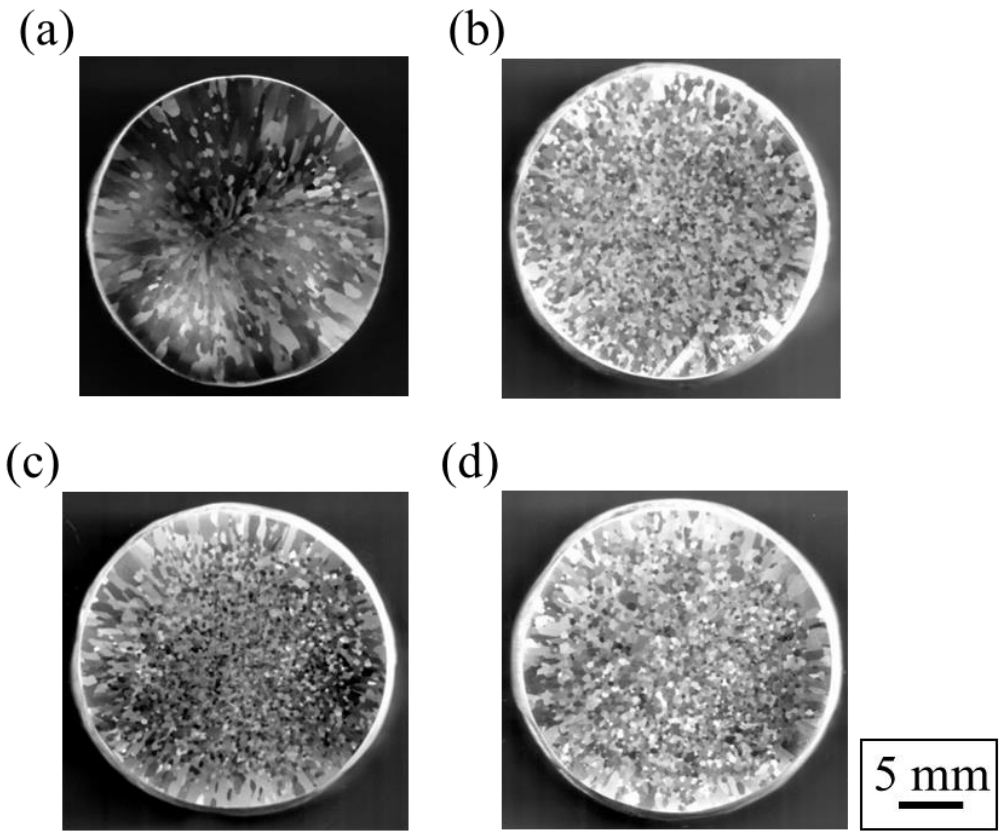

Fig. 6.7. OM photographs of the as-cast Al with (a) 1 pass ECAPed, (b) 1 pass MDFed, (c) 2 passes MDFed and (d) 3 passes MDFed Al-Al_3Ti composites refiner.

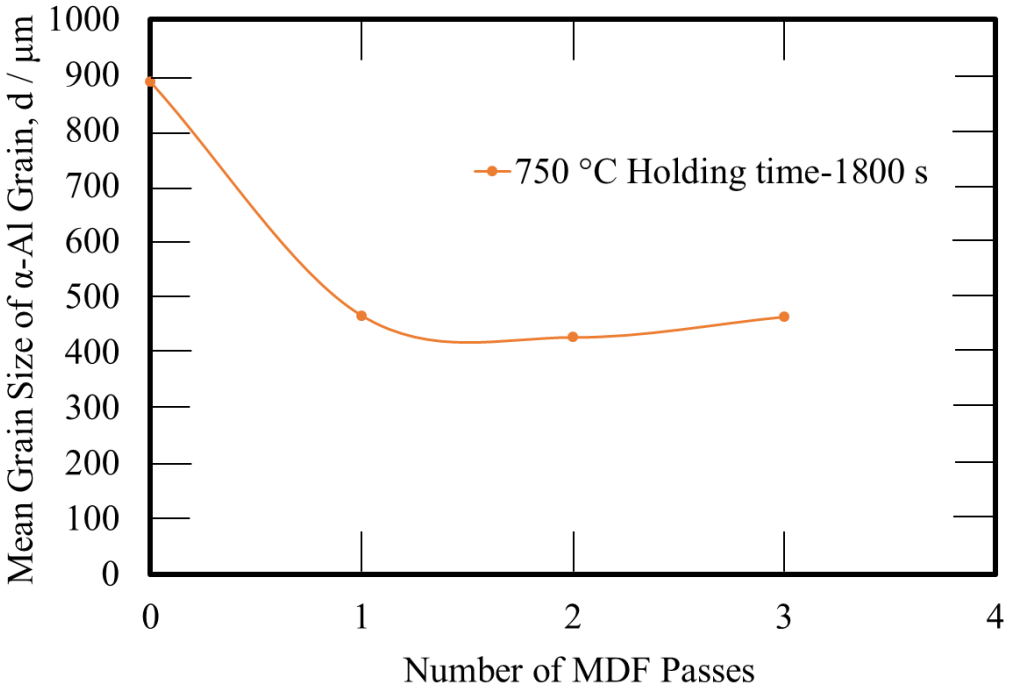

Fig. 6.8. Mean grain size of the α-Al grain in the as-cast Al refined by MDFed Al-Al_3Ti composite refiners as a function of the number of passes.

Chapter 7

Summary and Conclusions

In chapter 1, general introduction of metal matrix composite (MMC) and its properties, applications and fabrication techniques are discussed. Furthermore, previous research concerning with severe plastic deformation (SPD) on the MMC using various techniques are explained.

In chapter 2, fragmentation mechanism of platelet Al_3Ti particles in Al-Al_3Ti composite during compression test was reported using 3-dimensional (3D) microstructural observation and crystallographic analysis. The platelet Al_3Ti particle is first deformed by deformation twinning parallel to a $\{112\}_{Al_3Ti}$ trace. The cracks generated along with the twin boundary-initiated fragmentation in the platelet Al_3Ti particle. The fragmentation of platelet Al_3Ti particles in Al-Al_3Ti composite preferentially occurs at twin boundary after deformation twinning.

In chapter 3, controlling factor for the platelet Al_3Ti particles fragmentation in Al-Al_3Ti composite and effect of Al_3Ti particles size in fragmentation during equal-channel angular pressing (ECAP) were presented. At first, Al-Al_3Ti composite containing large platelet Al_3Ti particles in an α-Al matrix was deformed by ECAP using routes A and B_c up to 8 passes. Moreover, the diameter of Al_3Ti particles gradually decreased as the number of ECAP passes increased. While increasing the number of ECAP passes, the Al_3Ti particle shape changes from platelet to granular and the fragmented particles under routes A and B_c. The particles Al_3Ti were found to have different spatial distributions under routes A and B_c. Quantitative evaluation of the spatial distributions of Al_3Ti particles in the Al-Al_3Ti alloy based on I_δ values showed the aggregate distributions for both routes A and B_c. It is reported that changes in the spatial

distributions of Al_3Ti particles are dependent on the occurrence of material flow of the α-Al matrix during ECAP under routes A and B_c.

The spatial distribution of spherical Al_3Ti particles in the Al-Al_3Ti composite deformed by ECAP results the aggregated distribution. The change in spatial distributions of spherical Al_3Ti particles depends on the particle size. It is reported that the Al-Al_3Ti composite with larger particles size were deformed more compare to the Al-Al_3Ti composites which have smaller particle size.

In chapter 4, microstructure and effects of spherical or polyhedral or granular Al_3Ti particles in fragmentation of Al-Al_3Ti composite during ECAP were examined. It is reported that the fragmentation behavior of Al_3Ti particles in the Al-Al_3Ti composite occurs by stress concentration around the Al_3Ti particles and it depends on the particles shape by ECAP.

In chapter 5, microstructure and fragmentation of platelet Al_3Ti particles in the Al-Al_3Ti composite using SPD techniques such as multi-directional forging (MDF), symmetric rolling (SR) and asymmetric rolling process (ASR) were reported. It is found that the SPD methods can be used to modify the distribution of platelet Al_3Ti particles in the Al-Al_3Ti composite.

In chapter 6, microstructure evaluation and grain refining performance of the Al-Al_3Ti composite containing platelet Al_3Ti particles deformed by ECAP and MDF were examined. Length of the platelet Al_3Ti particles decreases and the number of the Al_3Ti particles in the Al-Al_3Ti composite refiner increases by ECAP and MDF. ECAP and MDF were effective SPD processes to enhance the grain refining ability of the Al-Al_3Ti composite refiner for the pure Al.

Future Work

During this research, deformation mechanism of solid particles in Al-based composite by SPD is investigated. However, phenomena not fully reported in this thesis. Thus, an extensive study would be required to understand the significant influence on the microstructure and thus on the mechanical properties. For future work, it would be interesting to do the following:

Study the effects of solid particles distribution in Al-based composite during SPD using box counting method. The box counting method offers an alternative approach for the investigation of spatial distributions.

Study the fabrication method for Al-based intermetallic compounds, which has a less pore around particles. In addition, advance fabrication method needs for preparation of intermetallic compounds. Arc melting would be a possible method.

Furthermore, grain refinement application of Al-based composite needs more detail study by increasing the number of ECAP passes. ECAP can induce huge strain into the specimen by increasing number of passes. It is expected that ECAP processed Al-based composite could be an effective refiner for commercial cast Al production.

Study the changes in mechanical properties of Al-based composite during SPD. In addition, investigation needs to find the effect of cavity formation in Al-based composite during SPD have an impact on the mechanical properties.

List of Presentations

1. Fragmentation Process of Platelet Al_3Ti Particles in Al-Al_3Ti Composite Deformed by Compression, Sarath Babu Duraisamy, Hisashi Sato, Tadachika Chiba and Yoshimi Watanabe, Frims Symposium, December 2016, Nagoya Institute of Technology (NITech), Japan.

2. Effects of Al_3Ti Particles on The Crystallographic Texture of Al matrix in Al-Al_3Ti Composite Deformed by Equal-Channel Angular Pressing, Sarath Babu Duraisamy, Hisashi Sato, Tadachika Chiba and Yoshimi Watanabe, Frims Symposium, May 2017, Nagoya Institute of Technology, Japan.

3. Change in Spatial Distribution of Platelet Al_3Ti Particles in Al-Al_3Ti Composite by Equal-Channel Angular Pressing, Sarath Babu Duraisamy, Hisashi Sato, Tadachika Chiba and Yoshimi Watanabe, 10th Anniversary International Symposium on Advanced Plasma Science and its Applications for Nitrides and Nanomaterials (ISPlasma 2018), March 2018, Meijo University, Japan.

4. Three-Dimensional Analysis of Distribution Change of Platelet Al_3Ti Particles in Al-Al_3Ti Composite Deformed by Asymmetric Rolling Process, Hisashi Sato, Akihiro Mori, Mariko Kitagawa, Sarath Babu Duraisamy, Tadachika Chiba and Yoshimi Watanabe, 4th International Congress on 3D Materials Science (3DMS 2018), June 2018, Kulturvaerftet Conference Center, Denmark.

5. Al-Ti 微細化剤の微細化能に及ぼす Al_3Ti 粒子形状の影, 渡辺義見, Sarath Babu Duraisamy, 坪内寛仁, 山田素子, 佐藤尚, October 2018, 日本鋳造工学会　第 172 回全国講演大会 (石川県地場産業振興センター), Japan.

6. Effect of Particle Shape on Fragmentation Behavior of Al_3Ti Particles in Al-Al_3Ti Composite Deformed by Multi-Directional Forging, Hisashi Sato, Kohei

Takayama, Sarath Babu Duraisamy, Tadachika Chiba and Yoshimi Watanabe, ISPlasma 2019, March 2019, Nagoya Institute of Technology, Japan.

7. Spatial Distribution Change of Spherical Al_3Ti Particles in Severe Plastic Deformed Al-Al_3Ti Composite Fabricated by Spark Plasma Sintering, Sarath Babu Duraisamy, Hisashi Sato, Tadachika Chiba and Yoshimi Watanabe, ISPlasma 2019, Japan (**ISPlasma 2019- "Best Presentation Award in The Area of Nanomaterials"**).

8. Al-Al_3Ti 複相材料への多軸鍛造に伴う Al_3Ti 粒子破壊挙動に 及ぼす Al_3Ti 粒子形状の影, Hisashi Sato, Kohei Takayama, Sarath Babu Duraisamy, Tadachika Chiba and Yoshimi Watanabe, 日本金属学会 2019 年春期（第 164 回）講演大会, March 2019, Tokyo, Japan.

9. Spatial Distribution of Spherical of Al_3Ti Particles in Al-Al_3Ti Composite by Equal-Channel Angular Pressing and Multi-Directional Forging, Sarath Babu Duraisamy, Hisashi Sato and Yoshimi Watanabe, Material Science and Technology, September 2019, Oregon Convention Center, Portland, Oregon, USA (**MS&T19- "Material Advantage Graduate Student Poster Competition Award Winner"**).

10. Microstructure Evolution and Grain Refining Performance of Al-Al_3Ti Alloy by Equal-Channel Angular Pressing and Multi-Directional Forging, Sarath Babu Duraisamy, Hirohito Tsubouchi, Hisashi Sato and Yoshimi Watanabe, 14th International Aluminium Conference, November 2019, The University of Tokyo, Tokyo, Japan (**INALCO 2019- "Outstanding Poster Presentation Award Bronze Prize"**).

List of Publications

1. Fragmentation Process of Platelet Al_3Ti Particles in Compressed Al-Al_3Ti Alloy Observed by Serial Sectioning and EBSD Analysis, Sarath Babu Duraisamy, Hisashi Sato, Tadachika Chiba and Yoshimi Watanabe, Materials Research Express, 6 (2019) 096575.

2. Three-Dimensional Analysis for Distribution Change of Platelet Al_3Ti Particles in Al-Al_3Ti Composite Deformed by Asymmetric Rolling Process, Hisashi Sato, Akihiro Mori, Mariko Kitagawa, Sarath Babu Duraisamy, Tadachika Chiba and Yoshimi Watanabe, JOM, (2019) 1-8.

3. Microstructure Evolution and Grain Refining Performance of Al-Al_3Ti Alloy by Equal-Channel Angular Pressing and Multi-Directional Forging, Sarath Babu Duraisamy, Hirohito Tsubouchi, Hisashi Sato and Yoshimi Watanabe, Proceedings of 14th INALCO2019 250-251.

4. Changes in the Spatial Distributions of Platelet Al_3Ti Particles in an Al-Al_3Ti Alloy by Equal-Channel Angular Pressing, Sarath Babu Duraisamy, Hisashi Sato and Yoshimi Watanabe, will be published in Materials Characterization, (2020).

5. Spatial Distributions of Spherical Al_3Ti Particles in an Al-Al_3Ti Composite by Equal-Channel Angular Pressing and Multi-Forging, Sarath Babu Duraisamy, Hisashi Sato and Yoshimi Watanabe, will be submitted to Materials Science and Engineering A (2020).

Acknowledgments

First and foremost, I would like to express my deep and sincere gratitude to my mentors Professor Yoshimi Watanabe and Associate Professor Hisashi Sato for the continuous support of my Doctor of Engineering study and research work. They have guided me in all the time of research, writing thesis and helping me to achieve my goals. I want to thank for all of the opportunities I was given to conduct my research in their laboratory. Particularly, my lab seminars and discussion, the professors are engaging with us directly and it helps me to do my research efficiently with continuous improvement day by day. It was a great privilege and honor to work under their guidance. I am extremely grateful for their motivation, patience, enthusiasm and immense knowledge.

I express my deep sense of gratitude to Professor Kitamura Kazuhiko and profound thankfulness to my thesis committee members for their valuable guidance, encouragement, insightful comments and time.

I would like to thank the Assistant Professors Moritani Tomokazu and Tadachika Chiba for all the valuable discussions and encouragement during my research work**.** I am also grateful to my laboratory staffs Ms. Motoko Yamada and Ms. Ryoko Shimizu for their patience and support in overcoming numerous obstacles I have been facing through my research.

It is my pleasure to acknowledge all the past and present members of my research group. My special thanks to my tutors Mr. Takayasu Sugiura and Mr. Ryo Nakanishi for their cooperation and of course friendship. Besides my tutors, I would like to thank my colleagues Mr. Kohei Takayama, Mr. Syusuke Taniai and Mr. Fumiya Nakamura for their help, various instructions about the usage of laboratory equipment related to my research and for all the funs we have had

together. I thank my fellow colleagues Mr. Hirohito Tsubouchi and Mr. Makoto Kikko for their help and cooperation during my study.

I would like to express my deep acknowledgement to the Ministry of Education, Culture, Sports, Science and Technology (MEXT), Japan for recognizing and offering me with the scholarship to pursue my PhD in Japan. I want to thank all of the Nagoya institute of technology staff members. Particularly, I also appreciate international student office Ms. Yamashita who is the care take of MEXT scholarship guided and very supportive during my stay in Japan. This note won't be complete without thanking my friends to Ms. Caroline Vijayakumari, Mr. Raj Matrin Crove, Dr. Manish Singh, Dr. Shrinathan and Ms. Thilagavathi Gurusamy whose friendship and support made my stay delightful.

Finally, I am very much indebted to my father Mr. Ramsamy Duraisamy, my mother Vaithilingam Manimekala, my brothers Mr. Sathesh Raj, Mr. Bala Kumar, Mr. Guru, Mr. Subash, Mr. Muthu Kumar, Mr. Vignesh, my sisters Ms. Sharmila, Ms. Subhasri and all my family members for their love, support, pray and encouragement. Last but not least, I wish to express my gratefulness to all my friends, who were of great support in deliberation over out problems and findings as well as providing happy distraction to rest my mind outside of my research.